2008

Dross formation mechanism and development of wear resistant scraper in aluminum-silicon-zinc coating bath.

Ashok Varadarajan

Dross Formation Mechanism and Development of Wear Resistant Scraper in 55Al-1.5Si-Zn Coating Bath

By
Ashok Varadarajan

Dissertation

Submitted to the
College of Engineering and Mineral Resources
at West Virginia University

In Partial Fulfillment of the Requirements for the
Degree of

Doctor of Philosophy
in
Mechanical Engineering

Bruce Kang, Ph.D., Chair and Advisor
Kenneth Means, Ph.D.
John Loth, Ph.D.
Eric Johnson, Ph.D.
Carl Irwin, Ph.D. (NRCCE)

Department of Mechanical and Aerospace Engineering

Morgantown, West Virginia
2008

Keywords: Zinc, 55Al-Zn, Dross Mechanism, Scraper Wear, Sink Roll

Dross Formation Mechanism and Development of Wear Resistant Scraper in 55Al-1.5Si-Zn Coating Bath

By
Ashok Varadarajan

ABSTRACT

Steel sheet manufacturers across the globe, face a huge loss of production due to the molten metal corrosion of the pot hardware in continuous galvanizing lines. The development of steel sheet with corrosion resistant for more than 30 years using a high aluminum content zinc coating has made an impact in the construction industry. High aluminum content bath (55 wt%) causes severe corrosion of the pot hardware and causes huge repair and replacement cost with frequent stoppages. One of the main reasons for stoppages is the severe dross formation over the submerged hardware (sink roll), which results in poor coating layer over the steel sheet.

Complete understanding of the mechanism of the dross formation over the submerged hardware has not yet been completely achieved. In order to establish the dross formation mechanism, an array of tests was performed. Initial inhibition of Al attack by the silicon rich layer and further formation of Fe_2Al_5 layer hindering the diffusion of the Al into the substrate were observed. Also, the effect of the hydrodynamic motion of the bath ein the dross formation mechanism was established.

A series of tests for efficient removal of the dross formed over the sink roll using high hardness, corrosion resistant materials were conducted at 600^{o}C. After these tests, an efficient scraping process with a potential for energy and cost savings was developed with a better scraper material, resulting in a reduction of 75% in line stoppages.

ACKNOWLEDGEMENTS

Very little work is ever achieved in isolation but more than most, this work of mine, would not have been possible without the input of many individuals who helped shape it.

The person with the most influence on my dissertation work has been Dr. Bruce S Kang, my research advisor, who provided tremendous support, knowledge and encouragement and had the trust in my capability to the conduct the research of this nature.

I appreciate the research funding supplied under the U.S. DOE Grant N0. DE-FC36-04GO14038, under the direction of Dr. Ever Barbero and Dr. Carl Irwin.

I am indebted to my doctoral review committee for providing me insight and guidance throughout my graduate study. I, greatly appreciate the cooperation of Liviu Magean, Adrienne Macleod in the Chemical Engineering Analytical Laboratory for their assistance in performing the SEM/EDS analyses. Thanks to the Industrial partners and especially Mr. Frank Mollica, Operations Manager, Wheeling Nisshin Inc.

All my graduate student colleagues- past and present- have had a hand in my work, albeit some more than others. A special thanks to my brother, John Sakasci, who was with me through out this arduous journey and stood by me, at times, when I felt the entire World was against me. “Thank you John”

Finally, every individual has a core group of supporters who unflinchingly spur them on to achieve higher goals. My family has been that core group for me. First and foremost, my parents, Mr. Varadarajan Raghavan and Mrs. Jayamani Varadarajan, have always looked at the bigger picture while I was muddling along the way. Right blend of humor and stern love while egging me on constantly, especially in the last couple of years, which made me to have the final go is my wife Archana, without whom I would never have completed this journey

Dedicated to

Maatha (Mother)

Pitha (Father)

Guru (Teacher)
&
Daivam (Almighty)

TABLE OF CONTENTS

LIST OF FIGURES

LIST OF TABLES

1. INTRODUCTION

Iron and steel have been most favored and vastly used for a wide range of applications from hairpins to aeroplanes, earth moving systems to earth orbiting systems because of its excellent strength, formability, economics of production and its ability to recycle indefinitely. However it tends to react in the environment in which it is used and form stable compounds such as oxides and salts. The process of reverting to the natural or original state of the steel is known as corrosion. Upon corrosion, the properties for which the steel was preferred gets compromised. Various techniques from simple surface painting till alloying of steel have been developed to overcome the adverse effect of the reaction between the steel and its environment. One of the most economical means of corrosion resisting of steel is by coating zinc (Zn) over iron (Fe) or steel stock or finished products.

Coating of Zn over steel substrates provides corrosion protection through (i) physical barrier, by preventing the steel surface reacting with the corroding atmosphere (ii) galvanic protection, where Zn being lower in the galvanic series (less noble) compared to Fe, acts as the anode and corrodes faster than the cathode (Fe here) and (iii) Zn-healing by which the zinc oxides cover the cut edges or scratches over the coating.

The coating of steel with protective metals such as zinc and aluminum (hot-dip coating) has been proven to be a high quality and highly economical means of corrosion resisting method to protect steel [1]. The hot dipping of steel is one of the most economical processes of mass production. Hot dipping of steel involves the application of molten zinc and/or aluminum over the surface of the steel. The hot-dip can be classified in to two

categories: “Batch Galvanizing” and “Continuous Galvanizing” depending upon the size and shape of the steel to be coated. Types of hot-dip coatings that are standard in today’s steel industry are (i) Galvanize (Zn), (ii) Galfan© (5%Al-Zn) (iii) Galvanneal (10%Fe-Zn) (iv) Galvalume© (55%Al-Zn) (v) Aluminize (8%Si-Al) and (vi) Terne (8%Sn-Pb).

Continuous galvanizing process is much faster in coating steel products which are in coil form (sheets, tubes and wire) and batch galvanizing process is used for steel which are fabricated to the required shape such as fasteners, large diameter pipes and structural beams. Other major factors to be considered to choose the process of batch or continuous galvanizing process are (a) coating thickness (b) coating hardness (c) coating integrity and (d) coating mass.

For steel to retain its leadership as the building material of choice, a lot depends on prolonging the life of the steel by prolonging the life of the protective coating. Steel sheets coated using Galvalume® (GL) are used mainly for structural applications. “Buildings with GL steel sheets have withstood corrosion for more than 25 years with less maintenance under various climatic conditions from areas prone to acid rain, harsh winters and humid coastal areas with salt laden moisture content and also from corrosive elements from the industrial areas” based on the survey conducted by Galvalume Sheet Producers of North America (GSPNA).

In the continuous hot-dip coating process, the pot hardware (bearings, sink roll, stabilizing rolls, corrector rolls and snout) is subjected to severe corrosion attack by the molten bath material. Figure 1.1 shows the schematic diagram of the pot hardware in the hot-dip coating process.

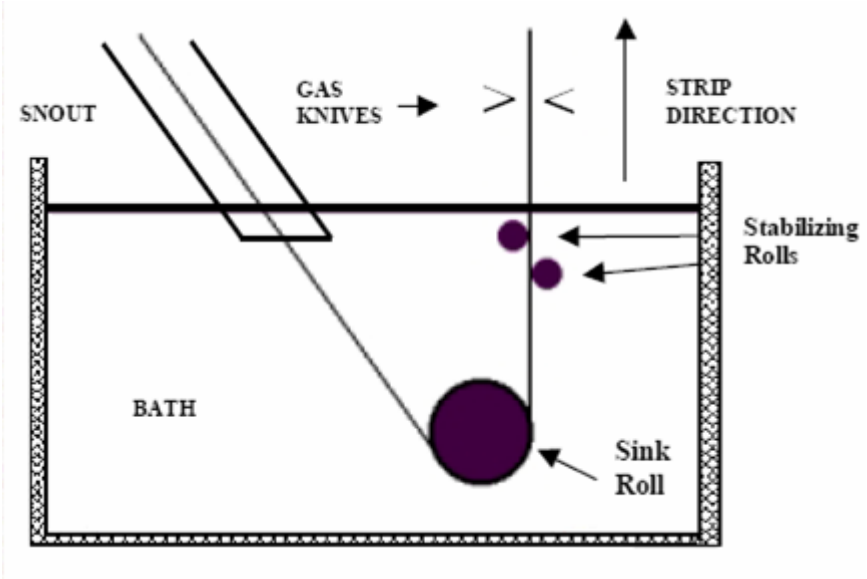

Figure 1-1: Schematic Diagram of Pot Hardware in Continuous Hot-dip line.

In addition to the corrosion, the pot hardware undergoes abrasion and erosion. The degradation of the pot hardware hinders the line operation, reduces the quality of the sheets produced. Thus increasing the maintenance cost and down time for replacement of the pot hardware. One of the main reasons for the failure of the rolls is the build up of dross on the surface of the roll. Average cost of running a galvanizing line is estimated to be around $1000 per hour in addition to this the stoppage of lines results in a great loss of energy and money. As shown in figure 1.1, the steel sheet to be galvanized is guided by the stabilizing rolls and sink rolls in the pot, where the zinc/aluminum alloy is maintained at high temperature. To ensure a smooth coating, the rolls which are in contact with the steel sheet are maintained at good surface quality. As the submerged rotating rolls tend to

pick up the floating dross particles and cause surface degradation, due to which the coating of the steel sheets gets affected. Therefore, the quality and the performance of the submerged rolls correspond to the quality of the sheets produced.

Intermetallic compound (Fe-Al, Fe-Zn, and Fe-Al-Zn) formed due to the reaction between the steel and zinc/aluminum in the molten bath is termed as “Dross” apart from the oxides (ZnO, and/or Al_2O_3). The density of the dross formed depends on the Al content. The particles formed, if rich in Al content floats over the bath surface known as Top Dross”. The Fe-Zn dross particles, due to higher density than the density of the bath, settle down at the bottom of the pot known as “Bottom Dross”. The top dross particles suspend in the bath and stick to the roll surface and agglomerates and tends to grow, when the Al and Fe concentrations in the bath are more than the soluble limits [2] as shown in Figure 1.2. After certain amount of growth over the roll surface, causes coating imperfections [3].

Shutdown of these lines to repair and replace the damages pot hardware is costly because of both loss of production, additional energy loss to restart the lines and the replacement parts cost. Hence the material used in as pot hardware must be carefully selected in order to ensure good quality of the coating and effective operation of the cycle.

Figure 1-2: Sink Roll Surface Degradation Due to the agglomeration of Dross Particles

Research Objectives

The current research is aimed to understand the dross formation mechanism on the pot hardware especially on the sink roll in the Galvalume® (GL) line and to identify a material with good wearing resistance to be used as a scraper to maintain the sink roll surface smooth and to develop a more efficient scraping method to maintain the roll surface. The goal of this research work is to make to the Continuous Hot-dip Galvalume line more productive and energy efficient.

Organization

The dissertation has been organized in several chapters, An in-depth literature review on the reaction mechanism on the kinetics of corrosion and dross build-up in molten zinc-aluminum system with the help of equilibrium diagrams have been explained in Chapter 2. Also, the effects of varying amount of aluminum content in the zinc bath along with the review of dross particles characterization are discussed. However no significant research was found describing the dross build-up mechanism over the rotating roll bodies in the GL bath.

Chapter 3 describes the experimental methodology involved in the study of the dross build-up mechanism over the roll surface in the GL bath. This chapter also discusses about the detailed SEM microstructural analysis of the samples and the dross formation mechanism established, based on the analysis.

Chapter 4 describes the need and use of the scraper system in the GL line with the discussion on the experimental set-up of the lab scale simulation of the actual hot dip galvanizing line. The test procedure for evaluating the wearing rate of various materials for scraping process in actual line conditions and comparison of performance of the tested materials are detailed in the results section. The overall summary and the conclusions inferred from this research project are explained in Chapter 5.

Trademark Notice

The 55%Al-Zn composition is manufactured and sold under different trademarks. For convenience, the author addresses the alloy composition as Galvalume in the upcoming chapters in this report. The 55% Al-Zn coated steel product is manufactured and sold under the **GALVALUME®** trademark by Bethlehem Steel Corp., Dofasco Inc., National Steel Corp., U.S. Steel Group of USX Corp., and Wheeling-Nisshin, Inc. It is also manufactured and sold by Steelscape Inc. under the **ZINCALUME®** trademark, by Industrias Monterrey S.A. under the **ZINTRO-ALUM™** trademark and by Galvak, S.A. de C.V. under the **GALVAL™** trademark.

2. LITERATURE REVIEW

Introduction

Galvanizing is the generic terminology for any of the several techniques for applying thin coatings of zinc (Zn) to steel or iron (Fe) stock or finished components (products) to protect the base metal from corrosion. The two major classification of the galvanizing is (a) Physical barrier protection and (b) Galvanic protection. The effectiveness of coating over steels to protect corrosion is based on the metallurgical bond formed between the base metal (steel) and the molten bath (coating). In the hot dip process the steel which has to be coated is completely immersed in the molten bath maintained at high temperature ($465^{o}C$- $700^{o}C$) depending on the melting point of the coating required based on the application of the end product.

Physical barrier: The formation of a physical barrier by using zinc/aluminum coating to separate the corroding atmosphere from the substrate (steel) by providing a continuous and impervious metallic coating, which is commonly known as barrier protection.

Cathodic protection: Also known as the galvanic protection, based on the galvanic series. Zinc and aluminum are more electro-negative than steel, corrodes preferentially, thus the coating (zinc and/or aluminum) prevents the substrate from corroding.

Depending on the size and shape of the substrate to be coated, the hot dip process can be classified in to two main types (i) *Continuous galvanizing* and (ii) *Batch galvanizing*. Continuous galvanizing is much faster in galvanizing steel products which are in coil

form (sheets, tubes and wire) and batch galvanizing process is used for steel which are fabricated to the required shape such as fasteners, large diameter pipe and structural beams. Apart from the shape factor the other major factors to be considered to choose the process of batch or continuous galvanizing process are (a) coating thickness (b) coating hardness (c) coating integrity and (d) coating mass.

Continuous Hot-Dip Process

In general, galvanization process involves the coating of the steel or iron (Fe) based substrate with zinc alloy depending on the field of application the steel substrate to be used. By immersing of passing the steel substrate in liquid Zn bath maintained at $860^{o}F$ coats the iron or steel substrate with a thin zinc layer over the surface. The layer of zinc formed, reacts with the oxygen in the atmosphere, when exposed forms zinc oxide which further reacts with carbon dioxide (CO_2) and forms zinc carbonate over the zinc layer beneath. This acts as a protective coating by avoiding further reaction of the zinc beneath, which in turn protects the steel substrate. Cross section of a galvanized steel substrate is shown in Figure 2-1.

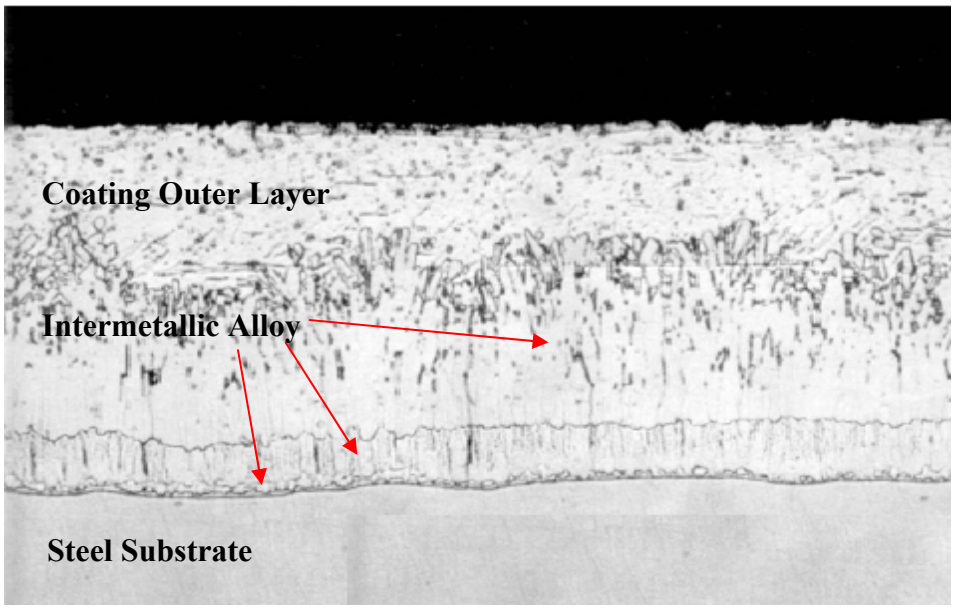

Figure 2-1: Cross- Sectional view of a Galvanized Steel substrate

The hot-dip galvanizing process follows the cold-rolling process. The process overall have several stages before coating the sheets like cleaning, annealing, galvanizing, temper rolling and surface treatment. In order to keep the production continuous, the steel strips are welded together and goes through cleaning procedures such as alkaline cleaning, brush cleaning and electrolytic cleaning to remove all the contaminants such as iron fillings and emulsion residue after the cold-rolling process. After the cleaning stage, the sheets enter the annealing furnace, where it is recrystalized to achieve particular properties depending upon the steel grade. After this stage, the sheets are rapidly cooled and the temperature is maintained close to the bath temperature of 870^{o}F.

After exiting the bath, air knifes with pre-set pressure blows nitrogen or compressed air to control the thickness of the coating. After this stage, the sheets are cooled and passed

through skin pass mill and tension leveler, where the roughness and flatness are achieved. Following this, depending upon the customer request, the sheets go through, chemical passivating, oiling, chromating, phosphating and anti -fingerprint treatments before being packed and shipped. A General galvanizing line process schematic is shown below in the Figure 2-2.

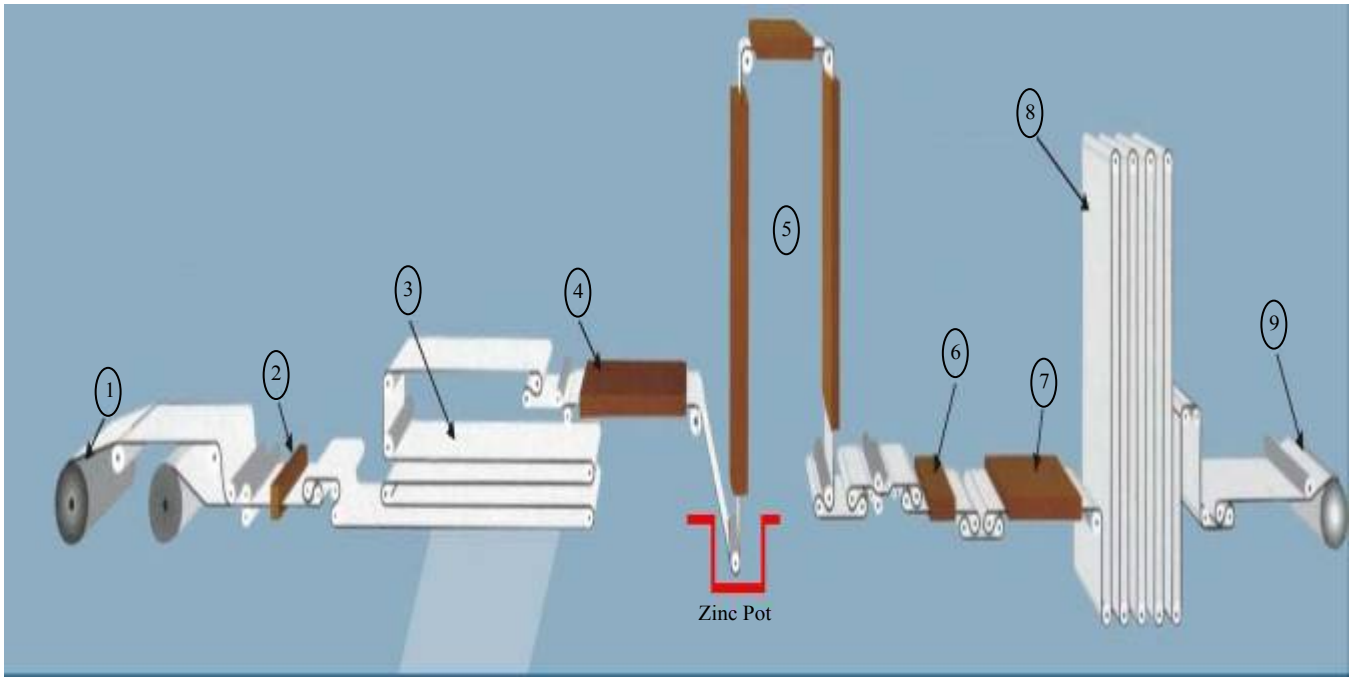

1. Entry Coil Car 2. Welder 3. Entry Accumulator (Cleaning) 4. Furnace 5.Cooling Tower 6. Chemical Coater 7. Dryer 8. Exit Accumulator (Skin Pass) 9. Exit Coil Car

Figure 2-2: Schematic showing the General Galvanizing Process Line.

The most critical part in the entire galvanizing line is the region in which the actual metallurgical bonding between the steel sheet and the bath takes place. The steel sheet enters the melt pot (zinc bath) maintained at 860^{o}F, through the snout. The pot contains

the sink roll and the stabilizing rolls, which are supported by the bearings. The sink roll, stabilizing rolls and the bearings referred as pot hardware (Figure 2-3), are completely submerged in the bath.

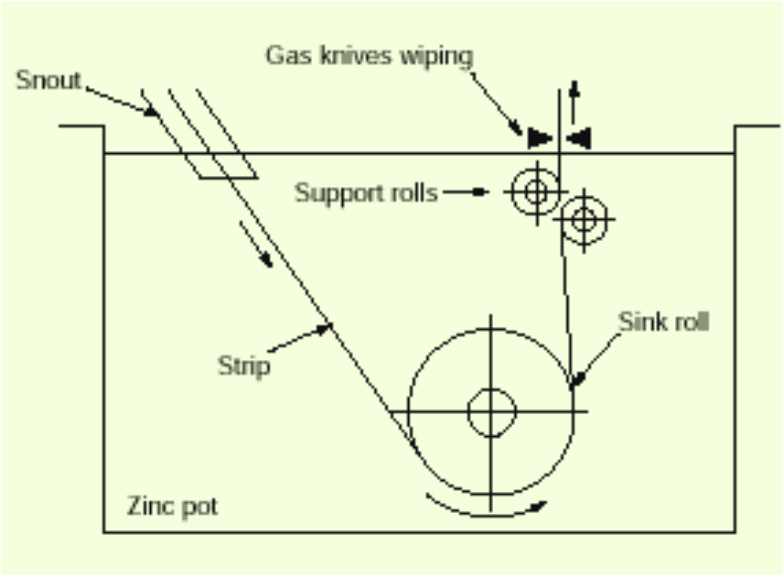

Figure 2-3: Schematic showing the Submerged Pot Hardware.

One of the major problems causing the line stoppages and the productivity loss is the condition of the pot hardware, which may need maintenance repair or replacement, thus selecting the pot hardware material is an important aspect to minimize the line stoppages and improve energy efficiency.

The coating over the steel substrate formed due to the reaction between Fe from the substrate and Zn from the bath, forms a brittle Fe-Zn compound. The zinc coated steel (galvanized steel) offers high strength (determined by the substrate), formability, light weight, corrosion resistant and low cost.

Over the last 3 decades, Aluminum (Al) is added to the zinc bath for various reasons like enhancing the application of zinc to steel, improving formability and improving corrosion resistance. Addition of Al to the zinc bath inhibits the formation of the brittle Fe-Zn intermetallic layer (IMC) by rapidly forming a Fe-Al rich compound which inhibits the diffusion of Fe from the substrate towards the bath and Zn towards the substrate. Currently four main types of Zn-Al alloys are used in hot-dip coatings as standards, in the steel industry [4].

1. Galvanize (GI) (Zn-0.16Al)
2. Galfan® Coating (Zn-5%Al)
3. Galvalume® (GL) (Zn-55%Al)
4. Aluminize (Al-8%Si)

In addition to these four, Galvanneal (GA) (Zn-0.13%Al) is sometimes used in hot-dip continuous coating. The above mentioned Zn-Al alloys are used for coating the steel sheets depending on the application they are intended for.

Table 2-1: Performance of various hot-dip coatings

	Galvanize	Galvanneal	Galfan®	Galvalume®
Corrosion Resistant	6	5	8	10
Galvanic Protection	10	8	9	5
Formability	8	6	10	6
Paintability	8	10	10	8
Weldability	7	10	6	5

It is well established that the hot dip coating process is controlled by

1. High initial dissolution rate at the interface between solidiron and the molten mixture, i.e. outward diffusion of iron in the melt
2. Inward diffusion of Al-Zn to the base metal to form an intermetallic alloyed layer
3. Outward layer is formed upon withdrawal from the bath. [5]

Intermetallics

Intermetallics can be defined as an ordered alloy formed by combination of two or more metal elements. Development of high temperature applications in the recent past have increased research interest in the development of this unique class of materials that have a varied field of applications due to their properties. Iron aluminides have been of interest due to their excellent corrosion resistance.

In order to analyze the nucleation and growth of these intermetallic compounds (dross particles) in the galvanizing lines, it is essential to understand the basic interaction between the different elements involved in the bath composition. Here, we will be discussing about the iron- zinc- aluminum interaction based on the conditions prevailing in the galvanizing lines.

Iron- Zinc (Fe-Zn) Binary Phase Diagram

The various compounds formed due to the reaction between the iron and the zinc that takes place in the galvanizing can be understood from the Fe-Zn binary phase diagram as shown in Figure 2-4.

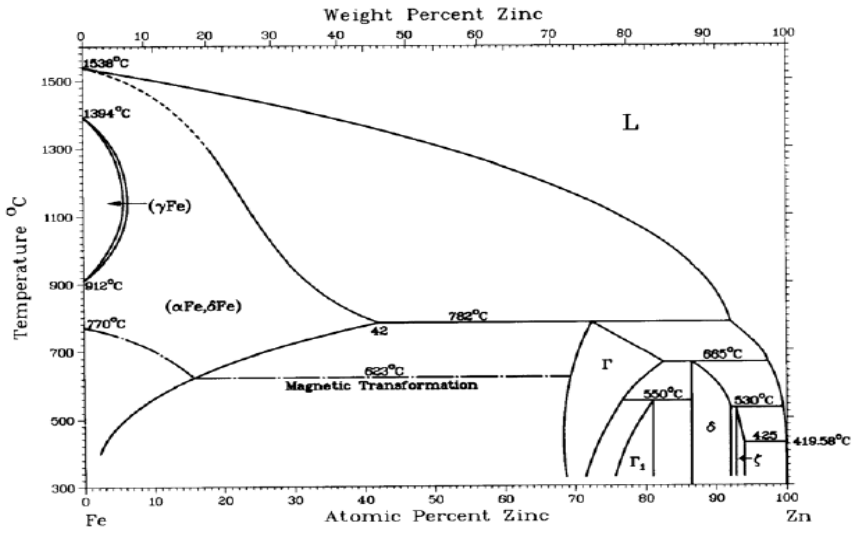

Figure 2-4 : Binary Fe-Zn Equilibrium Diagram [6]

The series of phases viz., ξ (zeta-$FeZn_{13}$), δ (delta-$FeZn_7$), Γ́ (gamma prime-$FeZn_4$) and Γ (gamma-Fe_3Zn_{10}), with Fe content increasing from zeta through gamma phases can be identified in Figure 2-5. Table 2-1 summarizes the phases observed in the relevant portion of the binary Fe-Zn phase diagram [7].

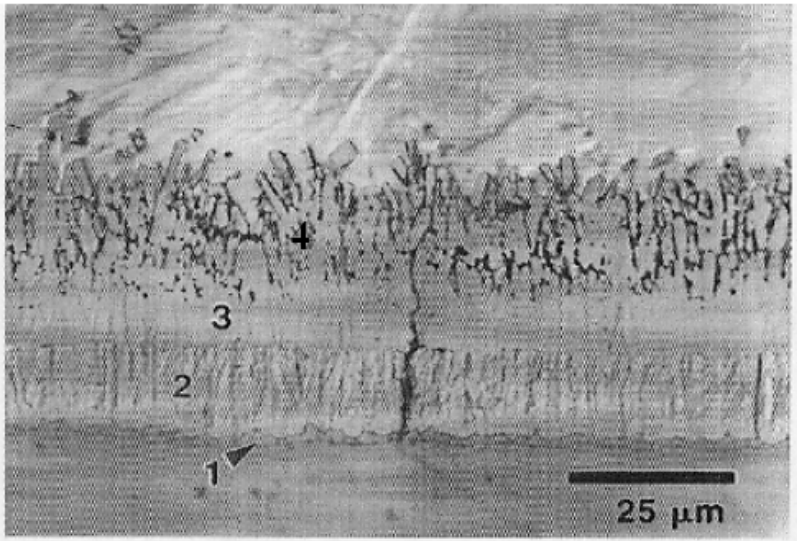

Figure 2-5: Cross sectional microstructure of coating formed in a 450₀C Zn-bath (1) gamma (Γ) (2) delta (δ) (3) zeta (ζ) phases [8]

Table 2-2: Fe-Zn Phase Characteristics [7]

Phases	Formula	Crystal Structure	VHN (25mg)
Fe	Fe(Zn)	BCC	104
Γ	Fe_3Zn_{10}	BCC	326
Γ1	Fe_5Zn_{21}	FCC	505
Δ	$FeZn_{10}$	Hexagonal	358
Z	$FeZn_{13}$	Monoclinic	208
ηZn	Zn(Fe)	HCP	52

Aluminum-Zinc Binary Phase Diagram

Addition of Aluminum to the zinc, from the binary phase diagram (Figure2-6) shows that, up to 5Wt% Al reduces the melting point of Zn to 381^{o}C from 420^{o}C and beyond the 5%, the melting point increases. Table 2-3 shows the phase transformations in the Al-Zn binary system. Three important phase transformations can be observed from the phase diagram

- 5 % Al: Eutectic reaction (Liquid phase to 2 solid phase (98.6 Zn and 83.1 Zn-16.9 Al) at 381^{o}C.
- At 22.3 % Al: Eutectoid reaction (two phases: nearly pure Zn and Zn-22.3% Al) at 277^{o}C.
- Spinodal decomposition at 351^{o}C.

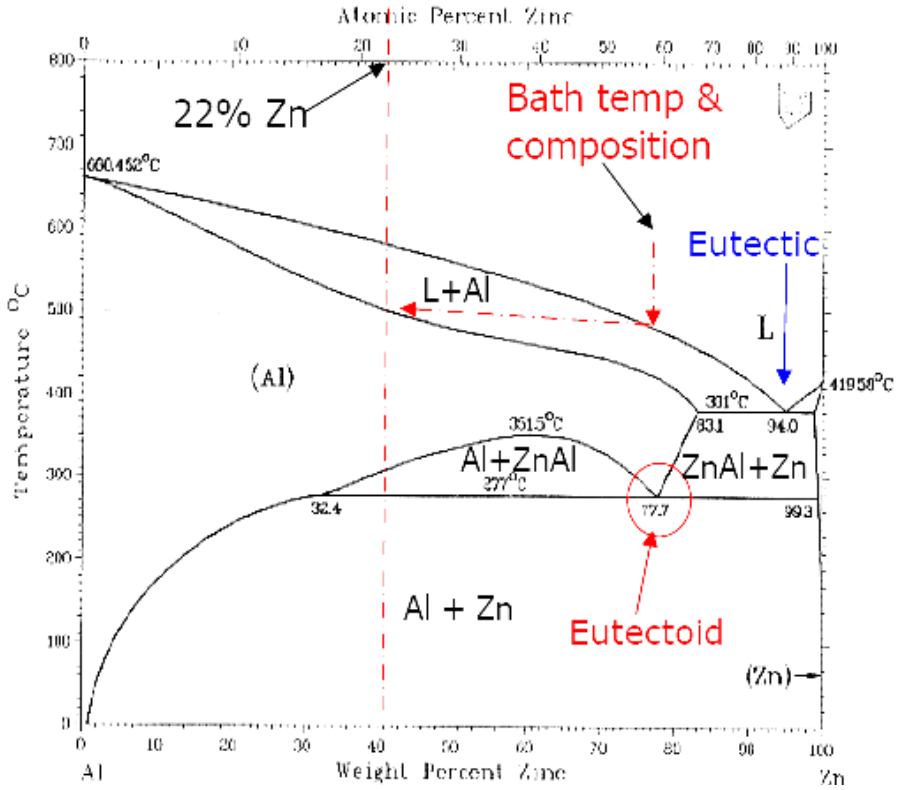

Figure 2-6: Binary Fe-Zn Equilibrium Diagram [6]

Table 2-3: Phase Transformations in the Al-Zn binary system. [7]

Phase Transformation	Composition wt%(at%Zn)	Temperature (°C)	Transportation type
L=β+η	95.0 (88.7)	381	Eutectic
β= β'+ η	77.7 (59.0)	277	Eutectoid
(Al)= β'+ β	61.3(39.5)	351.5	Critical
L=(Al)	0(0)	660.45	Congruent
L+ η	100 (100)	419.58	Congruent

Iron-Aluminum Phase Diagram

The compounds formed due to the reaction between Fe and Al are seen both at the Fe rich and Al rich areas as shown in the equilibrium diagram (Figure 2-7). The Fe rich zone has compound Fe_3Al and the Al rich corner has Fe_2Al_5, $FeAl_3$ and $FeAl_2$ compounds. The compounds at the Al rich area, forms at elevated temperature and are rich in Al content. In the field of galvanizing, Fe_2Al_5 and $FeAl_3$ are more relevant. $FeAl_3$ containing about 60% Al forms at 1157^{o}C and Fe_2Al_5; containing 54-55% Al (weight percent) forms at 1171^{o}C. Table 2-4 shows the characteristics of the Fe-Al compounds.

Table 2-4: Fe-Al Compounds Characteristics

Formula	**Crystal Structure**	***Symbol***
αδFe	BCC(A2)	*αδFe*
γFe	FCC(A1)	*γFe*
Fe_3Al	Cubic, BiF3-type(DO3)	*β 1*
FeAl	Disordered BCC (A2) Ordered BCC (B2)	*β 1* *β 2*
Fe_2Al_3	Cubic, 16 atoms/unit cell	*E*
$FeAl_2$	Triclinic	*Z*
Fe_2Al_5	Orthorhombic	*H*
$FeAl_3$	Monoclinic	*Θ*
Al	*FCC (A1)*	*Al*

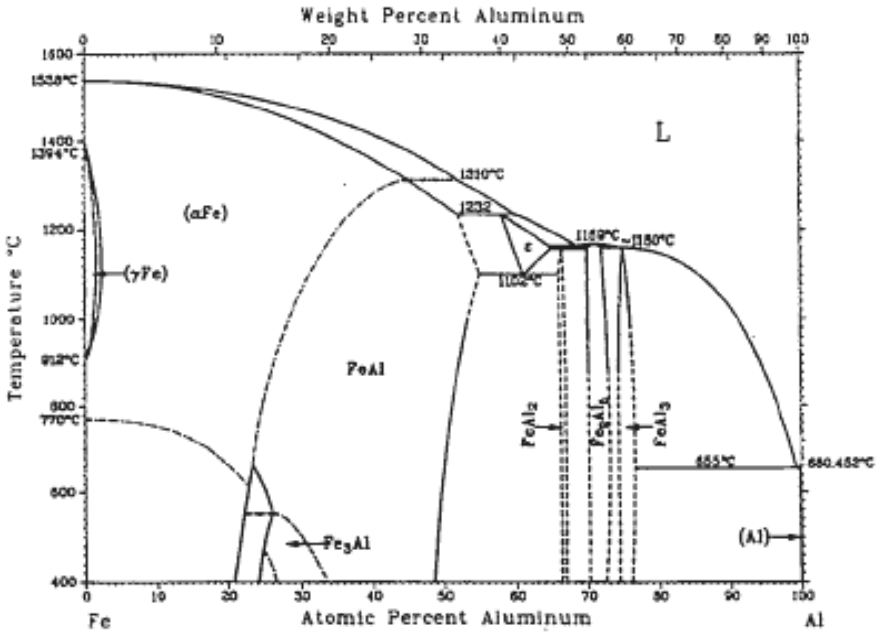

Figure 2-7: Fe- Al Equilibrium Diagram. [6]

Iron-Aluminum-Zinc Phase Diagram

Various research projects conducted over the last 50 years have come to the conclusion that addition of small amounts of aluminum will slow down the unstable reactions between Fe and Zn by forming an inhibition layer. Aluminum compared to zinc has stronger affinity towards iron and starts reacting much faster with iron thus retarding the brittle and unstable products formed due to the reaction between iron and zinc. From the Fe-Al-Zn phase diagram (Figure 2-8) at isothermal 575^{o}C, it can be noticed that Fe-Zn compounds with limited solubility of Al forms at Zn rich corner and Fe-Al compounds with limited solubility of Zn forms at Al rich zone[9]. The Fe_2Al_5 compound can have maximum solubility of 10%, thus the more accurate formula is Fe_2Al_5-xZn_x. Owing to simplicity Fe_2Al_5 is widely accepted [10].

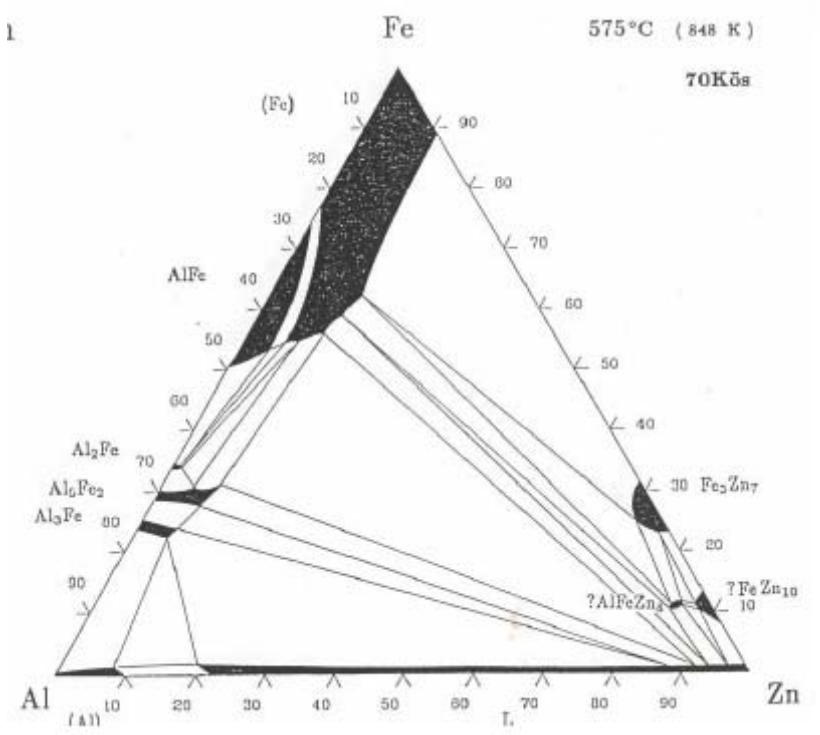

Figure 2-8: Fe-Al-Zn Phase Diagram at 575°C [9]

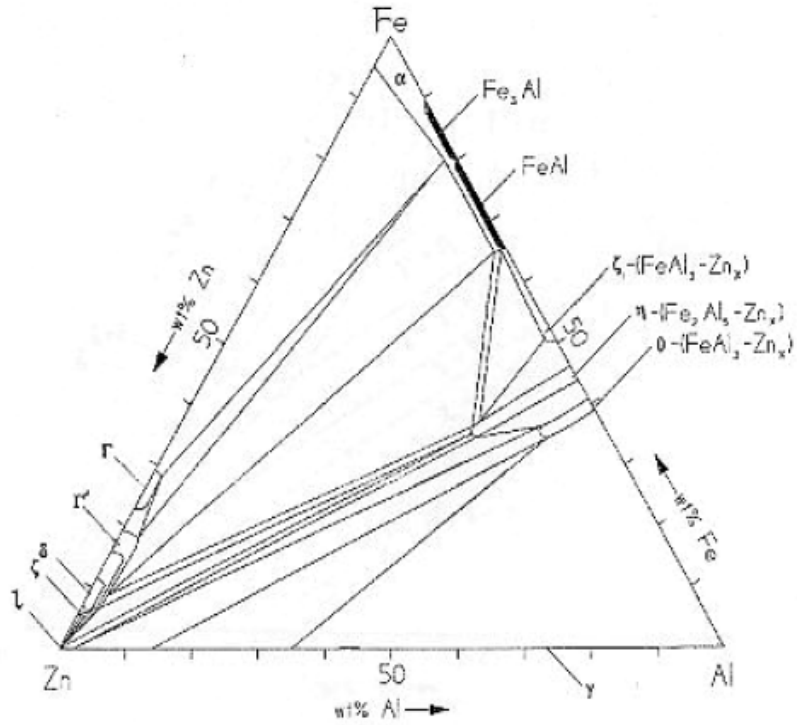

Figure 2-9: Fe-Al-Zn Phase Diagram at 450°C [10]

Effect of Aluminum in Zinc Bath

Zn bath containing Al <1%

Horstmann [11] has proposed that "Variation in Al concentration with time in the neighborhood of the iron surface leads to change in equilibrium condition, which causes the occurrence of various phases". It is assumed that in the initial stages, the Al distribution remains uniform (time = to) as shown in Figure 2-10 At time t1, a higher Al content compound, compared to the bath is formed over the steel (Fe_2Al_5) and due to which depletion of Al results in the melt, causing non-uniformity in the bath. Over the period, time (t=t4), the Al content decreases as the Fe_2Al_5 layer thickness increases. Due to the depletion, Fe_2Al_5 layer changes to "delta" phase as the equilibrium shift in the binary phase of Fe-Al.

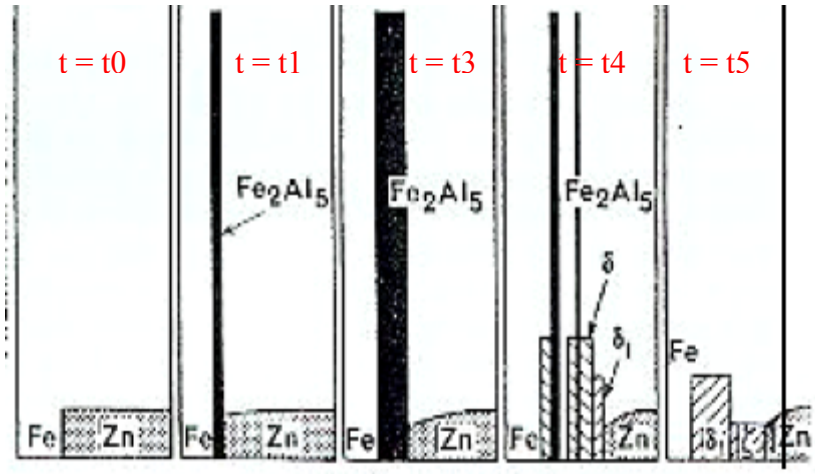

Figure 2-10: Al concentration variation at the Fe surface over time (t)

As the depletion of Al continues as time proceeds, the transformation of "delta" layer to "delta 1" occurs. The process of transformation continues as the compound formed is still rich in Al compared to the bath and the process continues further to form the "zeta"

phase, which has Al content lower than the melt, to bring out the compensation new layers of delta and zeta phase are formed over the steel surface. It was established that the final equilibrium condition between the reaction of Zn-Al (melt) and Fe is situated on a straight line which connects the melt composition with the Fe corner in the ternary diagram. The schematic of the ternary diagram is shown in Figure 2-11.

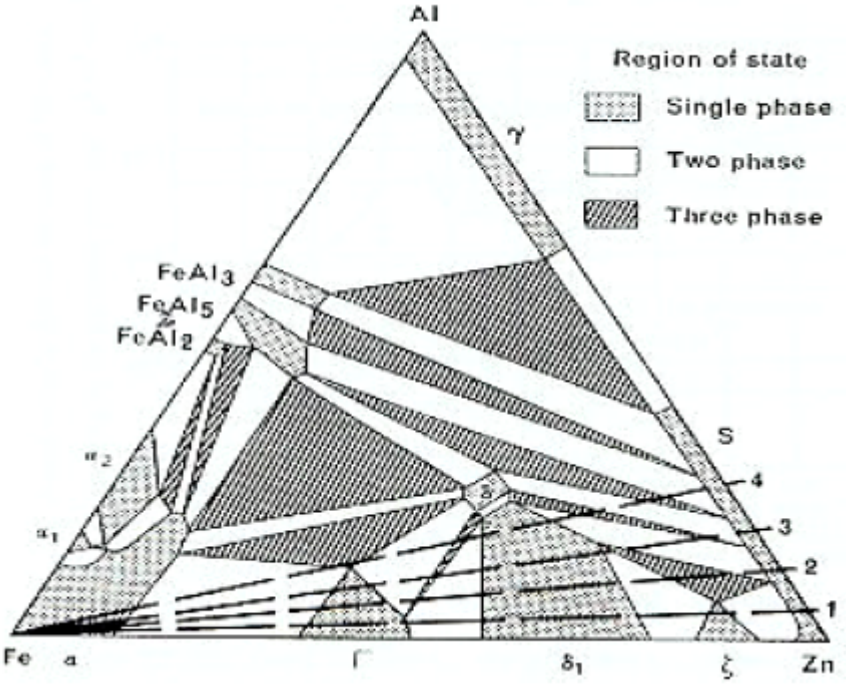

Figure 2-11: Ternary equilibrium diagram with Course of reaction in Zn-melts containing Al [11]

Based on the composition of the melt (depending on the Al content), the straight lines cut through different regions of the equilibrium diagram, which are formed during the reaction of Fe with the melt, implying the sequence of phases formed. From Figure 2-11 (line 1) for melt with very small Al contents, the gamma, $delta_1$ and zeta phases are formed on the iron surface in that particular order, as these phases are intersected by the straight line from the melt composition to the Fe rich corner. As the Al content increases

in the melt, the $delta_1$ layer is formed at 485^{o}C as shown in the Figure 2-11 (line 2). With further increase in the Al content (line 3), delta layer forms first and later converts to delta1 due to the impoverishment of Al. For melt with higher Al content (line 4), the layer formed over the steel substrate is Fe_2Al_5 and later due to the decrease in the Al content locally in the melt, the Fe_2Al_5 phase changes to a three phase region (Fe_2Al_5-delta-melt) in which the delta phases is uniformly distributed in form of crystals. Figure 2-12 shows the schematic representation of the phases formed in 0.20% Al-Zn melt Galvanizing bath. The kinetics of the phase formation in the pure Zn melt [12] and the melt with 0.2 wt% Al [13] have be been studied previously.

Zn bath containing Al 1-20 wt %

Adding Aluminum to the Zn bath up to 0.5 wt % was known to delay the reaction between Fe and Zn and suppress the growth of brittle Fe-Zn phases [3]. With zinc baths containing 1- 20 wt % of Al, the conditions are not favored for the formation of normal galvanizing layers, especially the ζ phase ($FeZn_{13}$). Instead $FeAl_3$ layer adjacent to the steel substrate is formed, which has an isomorphic structure. The reaction products containing zinc are formed in the temperature region 450-490^{o}C. At higher temperatures, the products formed are rich in Al content and low in Zn content. With the increase in the Al content in the bath, conditions are created for relative rapid interaction between iron and liquid Zn-Al as shown in Figure 2-13.

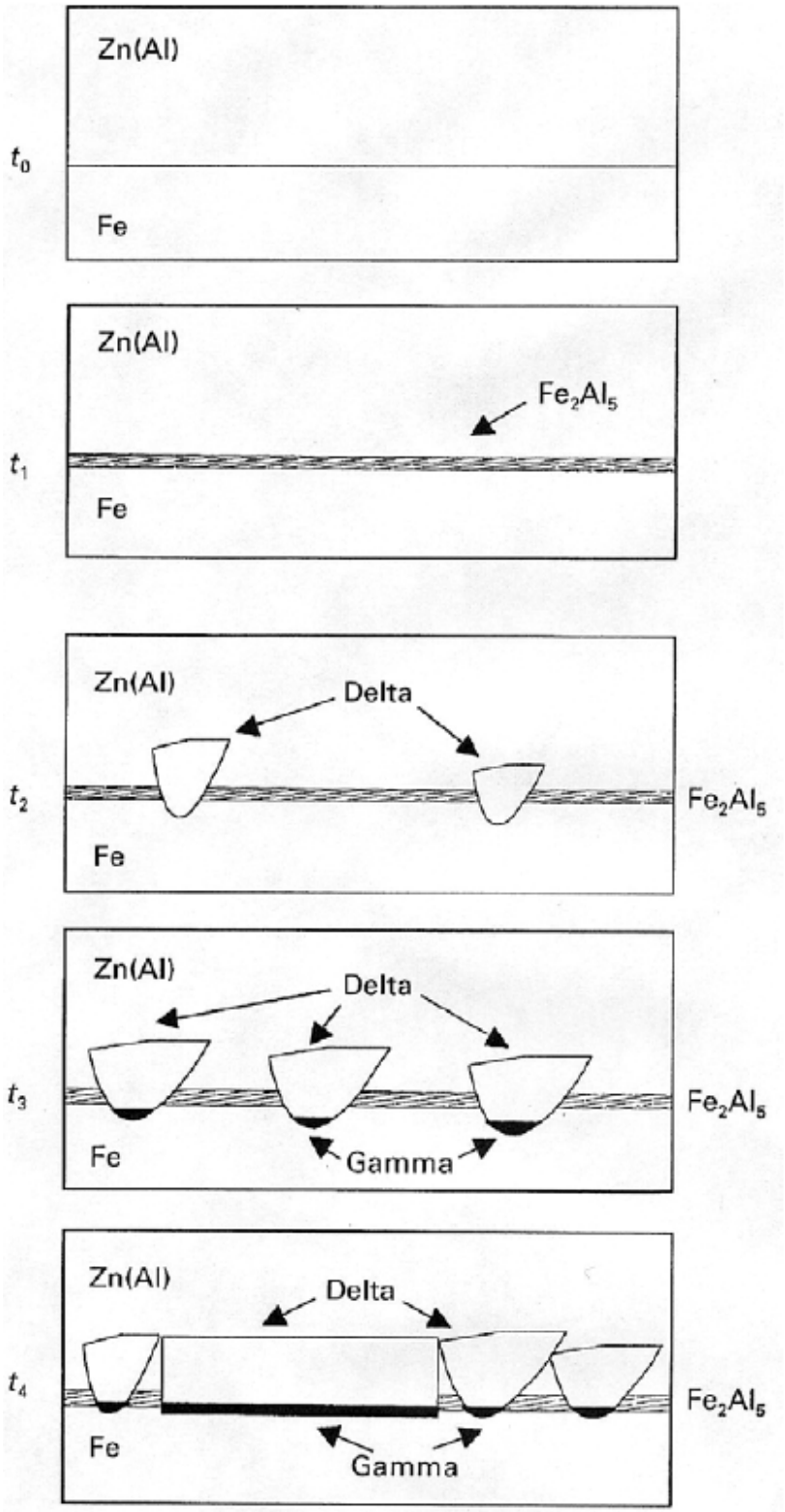

Figure 2-12: Schematic representation of the phases formed in 0.2wt % Al-Zn bath Time t0corresponds to zero and phases form at time t1, t2, t3, t4.

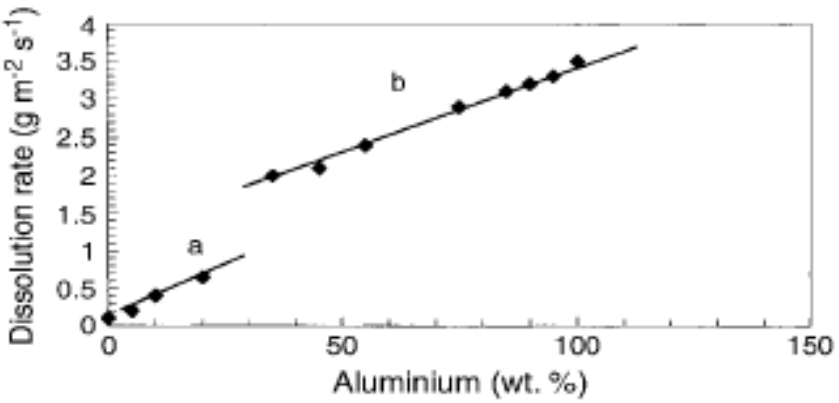

Figure 2-13: Effect of Aluminum content in the dissolution of Fe in the Al-Zn bath.

Zn bath containing Al 35-90 wt %

The reaction between iron and the Zn baths containing 35-90 wt % Al is controlled by the outward diffusion of iron and the inward diffusion of Al-Zn, which leads to the formation of an alloyed layer with the basic structure Fe_2Al_5 indicating that as the Al content increases in the bath, Al diffusion is more than the diffusion of Zn. Diffusion through the alloyed layer is again hindered because the structure of this layer is strong and the molten species cannot reach the base metal surface by dissolving it or by penetrating it by diffusion.

55%Al-Zn Alloy

Researchers from BIEC International Inc., developed much more corrosion resistant Steel coated with 55%aluminum-zinc alloy. The 55%Al-Zn is known by many different trade names throughout the world, viz., GALVALUME ®, Z-NAL ®, ZINCALUME ®, ZINTRO-ALUM™ and GALVAL™. Superior corrosion resistance of Zn-55Al coated steel structures have been estimated to have more than 40+ years of life without much of

corrosion. Compared to other galvanized coated steels, the Zn-55Al has 4 to 12 times more service life [1]. The Zn-55Al coating exhibits the following characteristics:

- Superior corrosion resistance
- Heat reflectivity
- Bare edge protection and
- Forming qualities.

Corrosion resistance of steel coated with Zn-55Al has been rep006Frted to be much better than other galvanized coatings based on a survey conducted by the engineers from BIEC International Inc., which shows that even in different environment conditions, such as rural, industrial and marine (both severe and moderate) conditions, the Zn-55Al out performs much better than other coatings as shown in Figure 2-14.

When the steel sheet enters the Zn-55Al bath maintained at 600^{o}C, the Fe reacts with the Al and results in an immediate formation of intermetallics due to the severe exothermic reaction between the bath and the steel sheet. In order to control the exothermic reaction and the growth of the intermetallic layer, silicon is added to suppress the intermetallic layer growth. In general the dross (intermetallic) layer formed was Fe-Al- Zn and due to the addition of silicon, the dross formed will consist of Fe-Al-Si-Zn. It has been reported that as the content of aluminum changes (increases or decreases), the activation energy of the dissolution rates of the steel substrate changes as shown in Table 2-5. The activation energy for the steel substrate is calculated by using the Arrhenius equation.

$$\mathbf{dw/dt = Ae^{-EaRT}}$$

Where,

A is the arrhenius constant **R** is the gas constant

T is the absolute temperature $\mathbf{E_a}$ is the activation energy and

dw/dt is the dissolution rate.

Table 2-5: Activation energy of the different Al-Zn melts.

Al wt% in the melt	Ea (Kcal/mol)
0	24.0
10	22.0
55	11.5
90	16.2
100	17.3

It is evident that the dissolution of the steel decreases in molten pure Zn, where Ea is found to be 24 kcal/mol. The dissolution rate of steel in molten pure Al increases and the Ea value is smaller at 17.3 kcal/mol. Furthermore, the activation energy of the dissolution rate of iron in the Al-Zn melt decreased with increasing content up to 55% wt and was found to be 11.5 kcal/mol. Based on these values, it suggests that the kinetics of the dissolution process are diffusion controlled and the reaction mechanism is independent of the Al content in the melt. Also it is evident that the increase in Al content and decrease in the Ea value indicates that the reaction between Fe and Al will be violent, thus the addition of silicon is necessary to inhibit the violent reaction between the steel substrate and the melt. Effect of addition of Si in various amounts was previously studied [2]. From these studies, it was observed that 96% of reaction was inhibited by the addition of 1% of Si as shown in Figure 2-15.

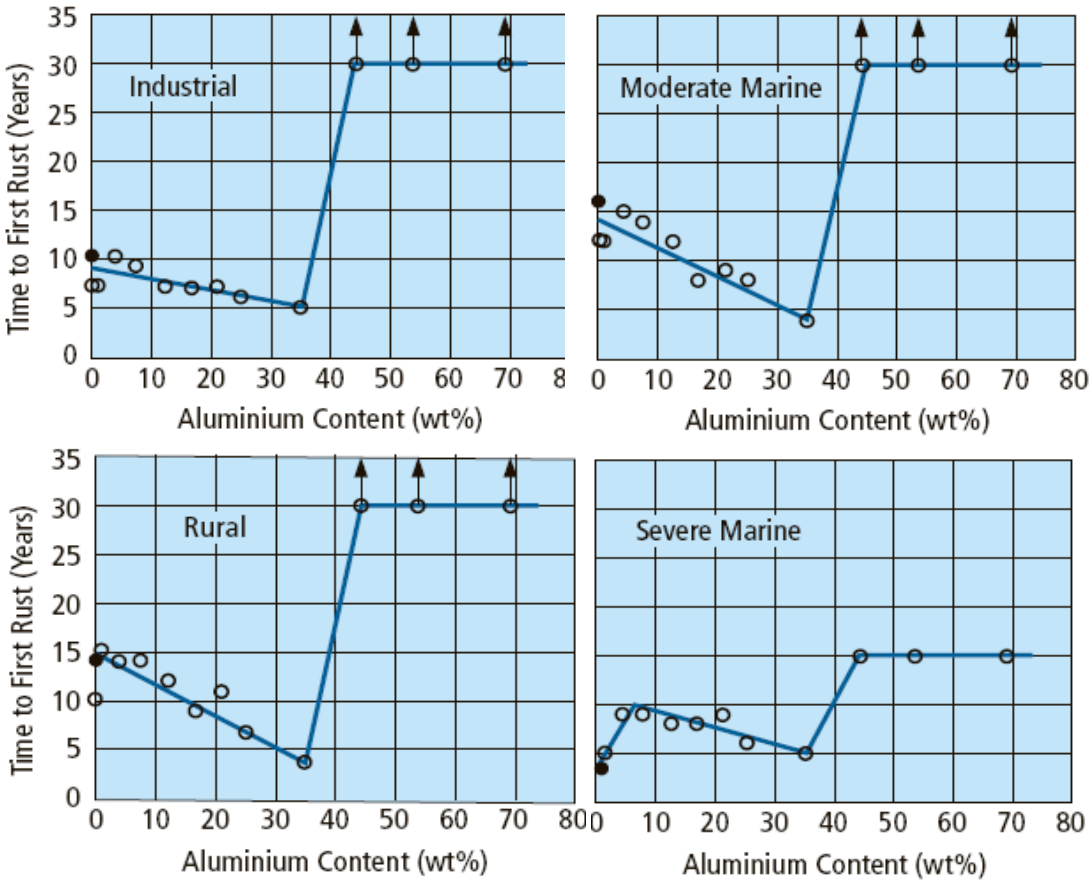

Figure 2-14: Corrosion resistance in various environmental conditions (Time to First Rust) for coatings with different wt % Al- Zn.

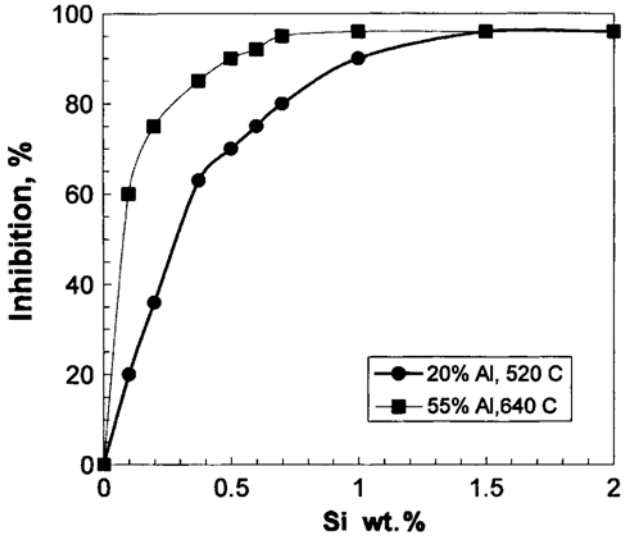

Figure 2-15: Effect of Si content on the inhibition of dissolution of Fe in Al-Zn baths.

The composition of the interfacial layer formed is reported to contain 55.8 wt% Al, 33.7 wt% Fe, 6.7 wt % Si and 3.6 wt % Zn [14].

Zinc-Aluminum-Silicon-Iron Phase Diagram

To understand the reactions between the pot hardware and the Zn-55Al melt, but as the Fe-Zn-Al-Si phase diagram is still not available so one has to extend the ternary phase diagrams of Fe-Si-Al and Zn-Al-Fe.

Aluminum-Silicon-Iron Phase Diagram

The ternary Fe-Al-Si system [15] shows the presence of several binary as well as ternary phases as shown in Figure 2-16. The highlights of the Fe-Al-Si system is that (i) the binary Fe-Si phases would form only at very high concentrations of Si, (ii) at the Al-end, the Fe-Al phases, especially $FeAl_3$ and Fe_2Al_5 have a solubility of about 6% and 4% (atomic) Si respectively and (iii) formation of ternary phases is promoted at Si levels at 12% atomic and above. Table 2- summarizes the intermetallic phases formed by the ternary system [16]

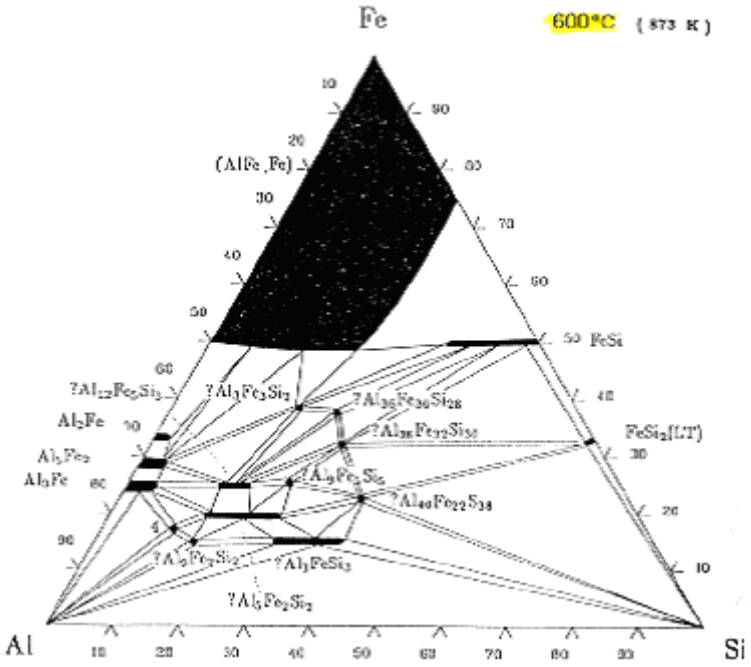

Figure 2-16: Ternary Fe-Al-Si Phase Diagram at 600°C

Table 2-6: Ternary solid phases in Fe-Al-Si system [17]

Phase	Formula	Composition (wt%)			Symmetry
		Al	Fe	Si	
t_1	$Al_3Fe_3Si_2$	26.6	55.0	18.4	
t_2	$Al_{12}Fe_6Si_5$	40.5	41.9	17.6	Monoclinic
t_3	$Al_9Fe_5Si_5$	36.6	42.1	21.2	
t_4	Al_3FeSi_2	41.9	28.9	29.1	Tetragonal
t_5	$Al_{15}Fe_6Si_5$	46.0	38.1	16.0	Cubic Hexagonal
t_6	Al_4FeSi	56.3	29.1	14.6	Tetragonal

Zinc-Aluminum-Iron Phase Diagram

The isothermal section of ternary Fe-Al-Zn system [9] at 575°C shows presence of Fe-Zn IMC with limited solubility for Al towards the Zn-end and presence of Fe-Al IMC with limited solubility of Zn towards the Al- end of the diagram. The $FeAl_3$ phase can

accommodate nearly 7% atomic Zn and the Fe_2Al_5 phase has maximum solubility close to 10% atomic. This means that excess of Zn in the coating produced during galvanizing would be rejected if a Fe-Al phase forms on the substrate. The Fe-Al-Zn ternary equilibrium diagram at 575^{o}C is shown in Figure 2-17.

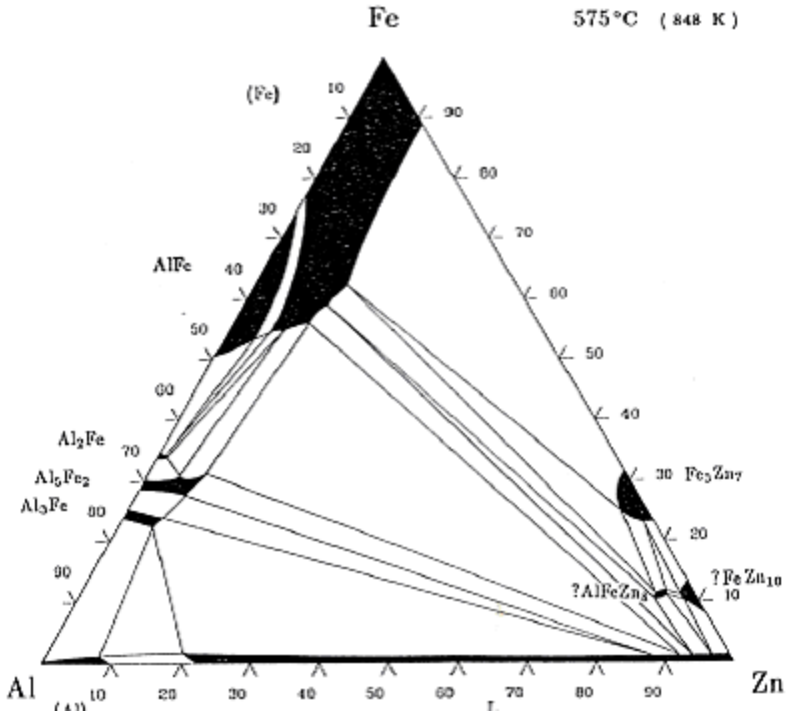

Figure 2-17: Ternary Fe-Al-Zn phase diagram at 575^{o}C

3. DROSS FORMATION MECHANISM

3.1 Introduction

One of the main problems faced by the galvanizing steel industries is the formation of intermetallic compounds (dross) on the pot hardware especially on the surface of the rolls (both sink and stabilizing) and causes frequent stoppage of the lines, resulting in huge energy and maintenance costs. In the past three decades, steel sheets coated with Zinc-55Al-1.6Si (wt pct.) have increasingly replaced the traditional galvanized construction products due to their high temperature corrosion resistance compared to other coated steel sheets with same thickness [1]. Dross particle formation is controlled by the bath, the steel sheet and also the pot hardware and the rate of dross formation is controlled by the bath composition and the bath temperature. However, in general, the bath temperature is maintained depending on the specified aluminum content in the bath [2]. The reaction mechanisms of the coatings formed during hot dipping of iron in zinc baths with 0-10% aluminum were originally studied by Ghuman and Goldstein [3]

The hot dipping process of coating steel with Zn-55Al-1.6Si is typically performed at 600^{o}C and silicon is added to the molten alloy bath to control the growth of the intermetallic layer on the steel sheet, which, according to Selverian, et al. [17], improves the adhesion between the alloy coating and the steel substrate. Silicon addition also inhibits the rapid exothermic reaction between the iron substrate and molten bath constituents [17]. Numerous researchers have developed several static and dynamic tests to determine the corrosion of pot hardware materials in the galvanizing bath [10, 17-25] but information relating to the mechanism of dross formation on the roll surface has not

been fully explained. Reaction between the sheet/pot hardware and the Zn bath containing Al (>45 Wt %) is very severe and in all cases, the bath consumes the pot hardware in a very short period of time. According to Selverian et al [1-3], the alloy layer formed consists of two regions; adjacent to the steel substrate is a layer consisting of Fe2Al5 +Zn and between this layer and the solidified bath, is the layer consisting of FeAl3+Zn. The Zn in these phases remains as liquid and contains approximately 1% Fe and 1 to 2% Al in solution. As a well known fact, liquid phase diffusion is faster than the solid state diffusion and thus, the rapid movement of the liquid Al attacks the steel substrate.

Zn- 55%Al (commercially known as Galvalume) contains 1.6% of Si. This Si added to the bath, prevents the rapid exothermic reaction between the Al-Zn bath and the sheet steel/Pot hardware by forming a diffusion inhibition layer, which retards the reactivity between the Al rich Zinc bath and the pot hardware. Due to the presence of Si and high Al content in the Galvalume bath, the dross formation on the submerged pot hardware can not be correlated to the well established mechanism in other Zn baths. Hence, the aim of this chapter was to investigate intermetallic particle and coating formation mechanisms on the surface of pot hardware materials. Advanced understanding of these coating reactions may eventually contribute to reduced downtime, decreased maintenance costs and enhanced productivity for continuous coating lines.

3.2 Dynamic Dross Build-up Simulator

Based on the actual hot dip galvanizing lines, the test parameters were established to simulate the actual dross build up on the pot hardware. A lab-scale test rig was developed which consists of ¾ HP motor and a bench top muffle furnace with a ceramic crucible. The bath temperature was maintained at 1112^{o}F (600^{o}C) using a temperature controller. ASTM A276 309 stainless steel rod (Ø 0.5") was used as the sink roll sample attached to the motor and rotated at 110 RPM controlled by a Variac. The test rig was designed such that the platform which houses the motor connected with the sink roll can be moved up and down to facilitate the sample immersion in the bath (Figure 3-1)

Figure 3-1: Lab-scale Dynamic Dross Build-up Test Rig

The experimental procedure for the dynamic dross build up over the ASTM A276 309 stainless steel sample was as follows:

1) The samples (0.5”dia.) were cleaned with acetone to remove any surface contaminants.
2) The actual 55Al-Zn ingot obtained from the actual industrial line was melted and maintained at 600^{o}Cin a silicon carbide crucible in the bench top muffle furnace. (Figure 3-1)
3) Roll samples were mounted on to the motor
4) The mounted samples were rotated at 110 RPM
5) Samples were preheated over the furnace to avoid any thermal shock at the time of immersion.
6) At given time intervals, the immersed sample was removed from the bath.
7) At the end of each test, the samples were removed from the bath and allowed to air cool as water quenching the sample will create a strong convection in the liquid and disturbs the segregation of the intermetallic particles in the sample.
8) After the entire cycle of test was completed, the samples were prepared for analysis with the solidified bath as-is.
9) The as-is samples were sectioned using the Electric Discharge Machining (EDM) and were mounted and polished for microstructural and elemental analysis by scanning electron microscope (SEM) with energy dispersive spectrometry (EDS).

3.3 Dynamic Dross Build-up Mechanism

Sample-Bath Interface After 20 Minutes

The sample immersed for 20 minutes, had a very thin layer of frozen bath on the surface. After carefully polishing the sample cross-section and viewing through the SEM, the sample cross-section showed a reaction layer of uniform thickness at 250X magnification (Figure 3-2). Two distinct layers of varying composition were observed on the reaction layer at 1000X magnification (Figure 3-3). Based on the EDS analysis, the inner most reaction layer's (closer to the steel substrate) composition was rich in silicon compared to the next layer. Presence of Si rich layer can be observed in Figure 3-4.

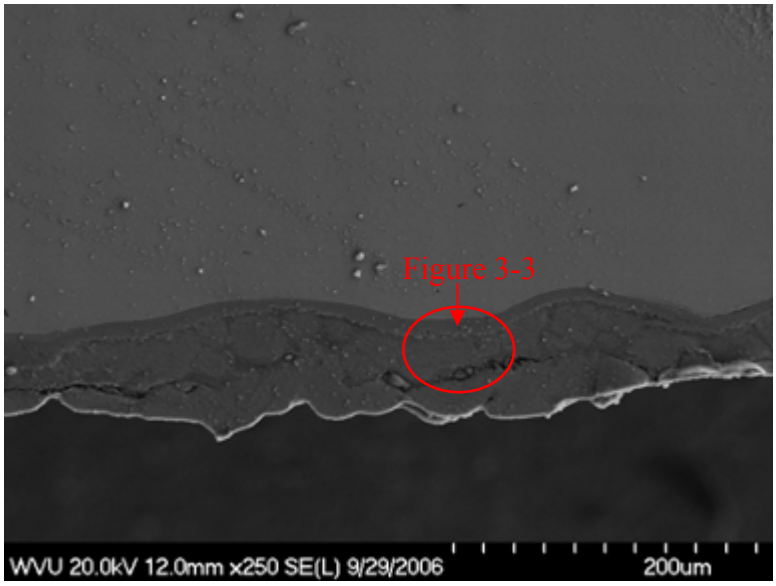

Figure 3-2: Sample Cross-section after 20 minutes of immersion (250X)

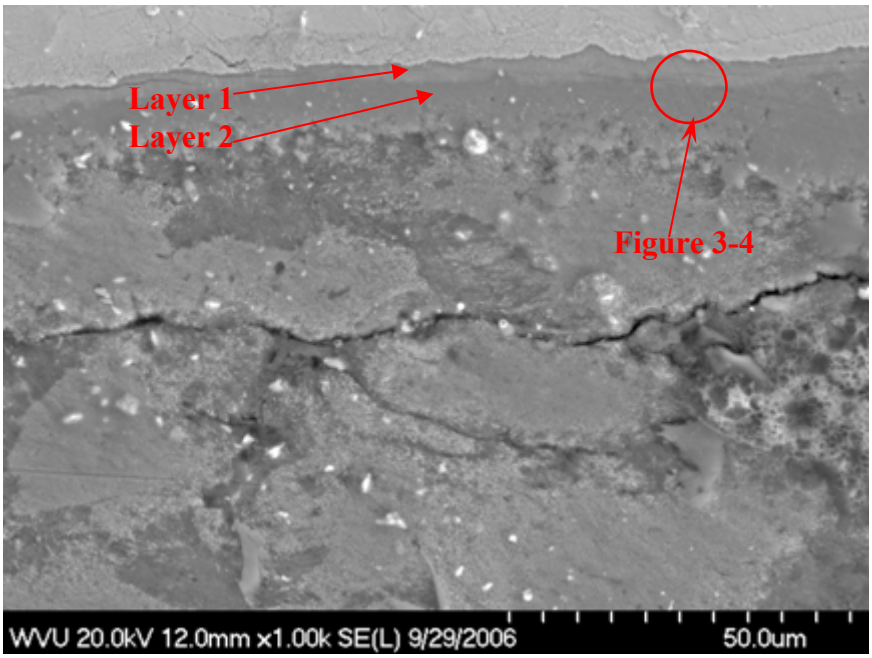

Figure 3-3: Substrate Bath Interface Layer Cross-section after 20 minutes (1000X)

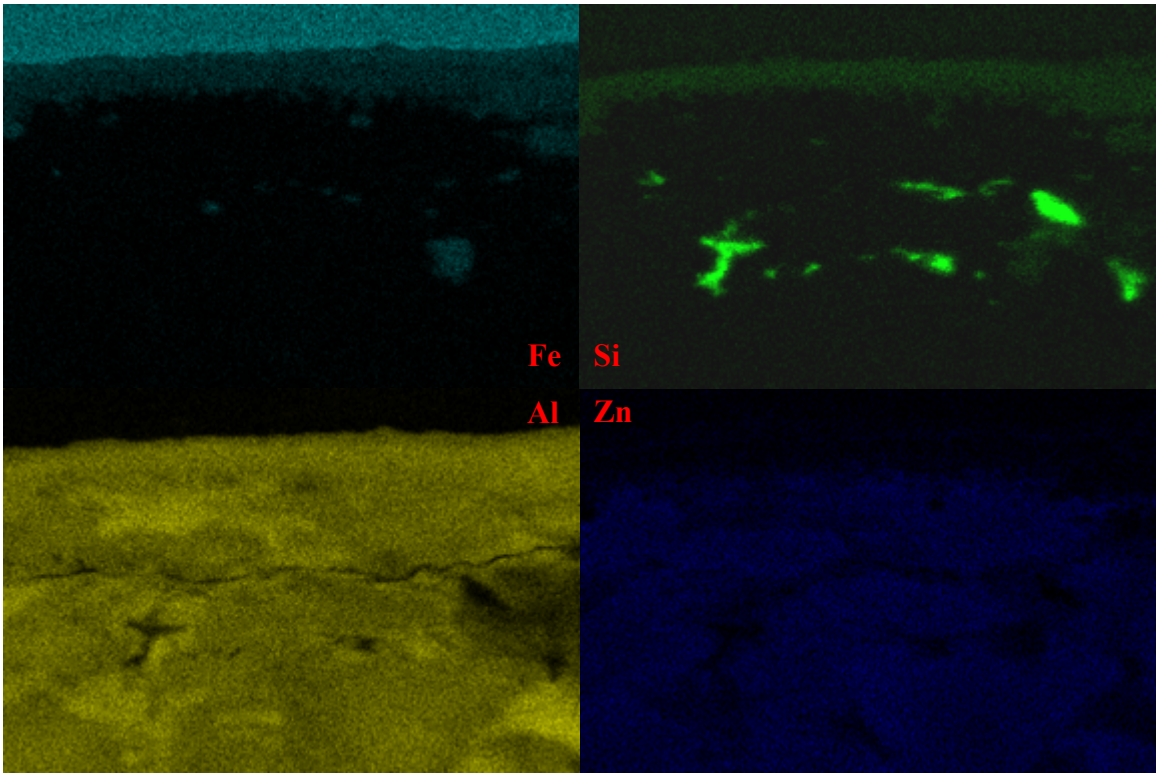

Figure 3-4: EDS Map showing the Elemental Composition of Substrate-Bath interface

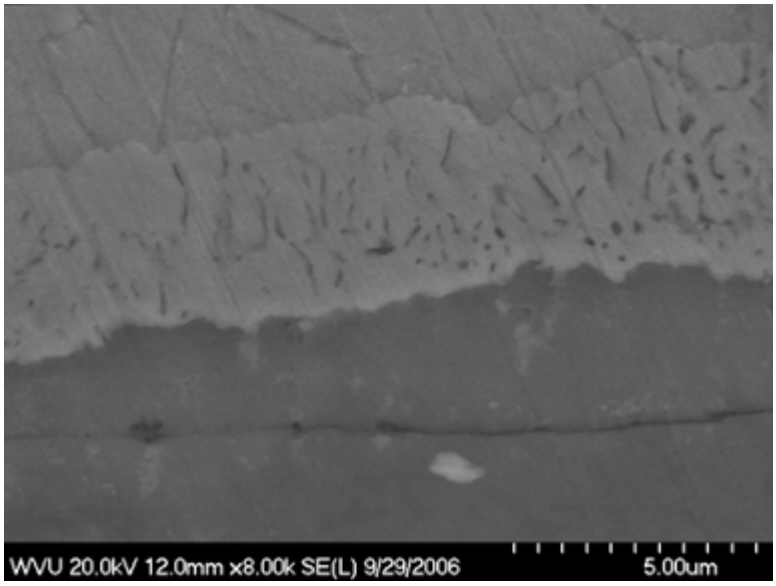

Figure 3-5: Reaction Layer rich in Silicon (8000X)

Sample-Bath Interface After 40 Minutes

The sample cross-section, immersed for 40 minutes, had two main characteristics features, all along the substrate-bath interface,

1. Micro-cracks in the reaction layer
2. Small discontinuous dross particles on the bath side of the reaction layer (average size = 12μm)

Although continuously covered with the bath over the entire surface for the naked eye, analyzing the cross section of the substrate- bath interface, the interface layer had numerous cracks all along the surface as seen in Figure 3-6. The cracks observed on the interface layer were not seen either propagating into the substrate or towards the frozen bath, thus providing a characteristic feature and not formed while cooling, due to the

mismatch of the thermal expansion coefficient. Figure 3-7 and 3-8 shows the micro-cracks on the inner-most reaction layer, which was not seen propagating either towards the substrate or the outer towards the frozen bath.

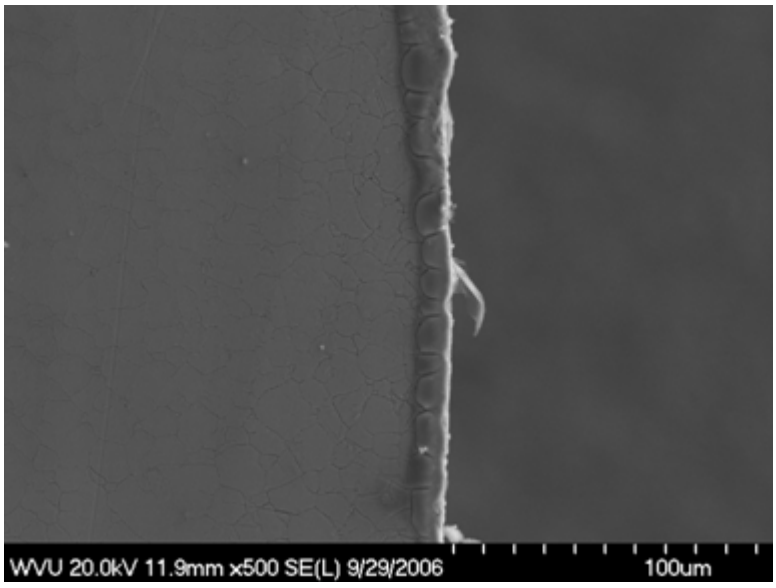

Figure 3-6: Micro-cracks along the Substrate – Bath Interface Layer After 40 minutes (500X).

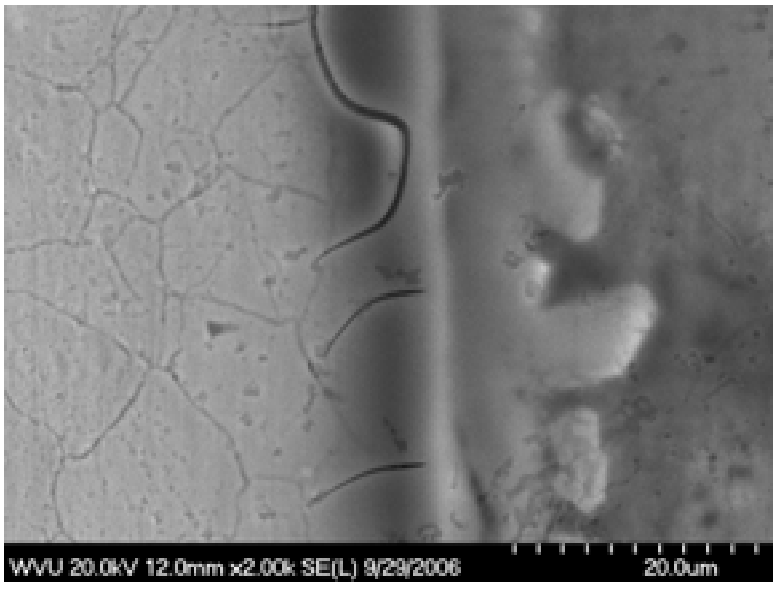

Figure 3-7: Micro-cracks on the on the Interface cross-section (2000X)

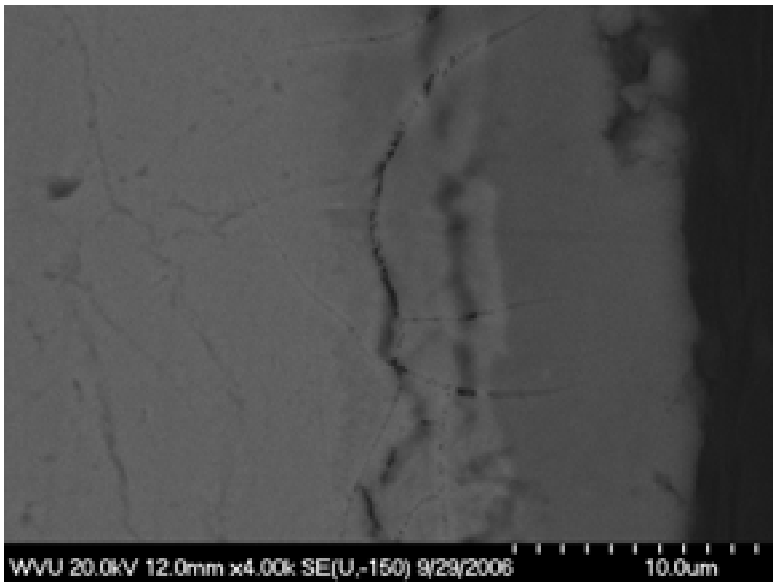

Figure 3-8: Micro-cracks on the on the Interface cross-section (4000X)

Dross particles (~ 8μm avg.) were observed at the end of the reaction layer towards the bath side. These dross particles were neither uniform in size nor distribution. The dross particles were formed due to the reaction between the Fe and Al diffused through the micro-cracks developed and thus the micro-cracks may have acted as the nucleation sites for these dross particles (Figure 3-9). Depending on the micro-crack density and diffusion of Fe and Al through these cracks, the size and distribution of the dross particles varied along the reaction layer.

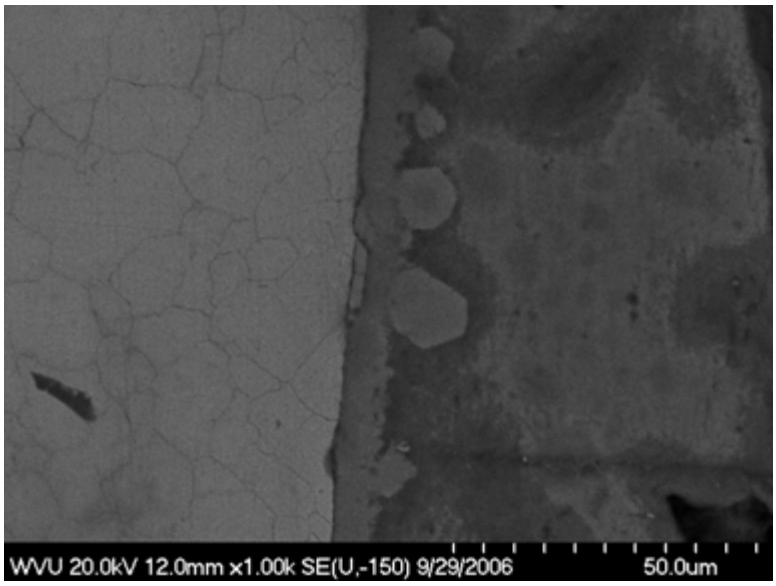

Figure 3-9: Dross Particles over the reaction layer on the bath side

After 40 minutes (1000X).

Sample-Bath Interface After 60 Minutes

The stainless steel sample immersed in the Zn-55%Al bath for 60 minutes, has a uniform agglomeration of dross particles formed as a continuous layer for dross over the steel substrate. At 250X (Figure 3-10) and 1000X (Figure 3-11) magnification, the cross-section of the sample bath interface shows the average thickness of the dross layer at the end of 60 minutes to be 40μm. At higher magnification (4000X & 8000X) (Figure 3-12 & 3-13), small particles agglomerating to the existing layer was observed. The EDS analysis shows the composition of the dross layer formed was rich in Fe-Al-Si intermetallic compound. The analysis showed that the intermetallic compound layer formed on the steel surface was a Fe-Si-Al ternary compound compared to that of the other coating lines which have binary intermetallic compounds.

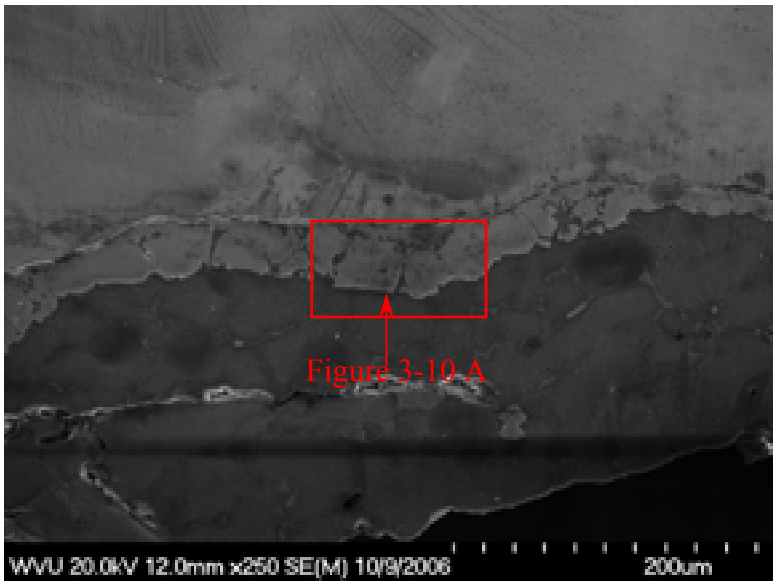

Figure 3-10: Stainless Steel - Bath Interface after 60 minutes (250X)

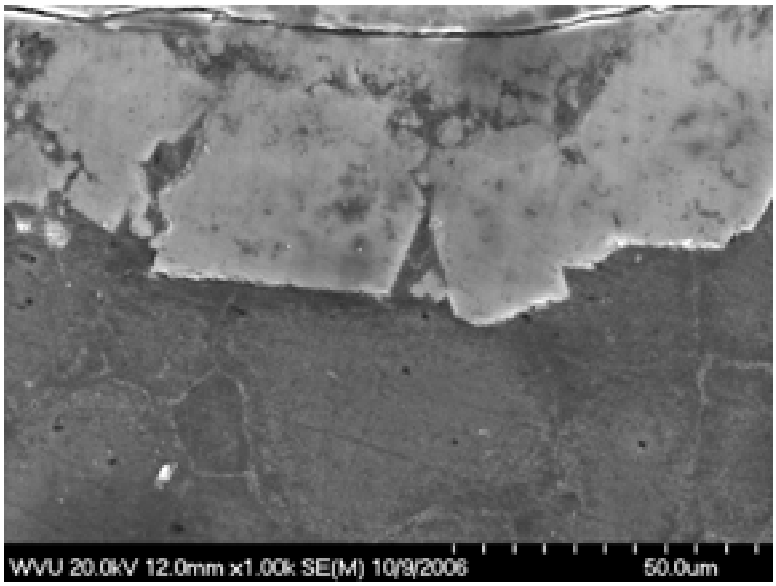

Figure 3-10A: Stainless Steel - Bath Interface after 60 minutes (1000X)

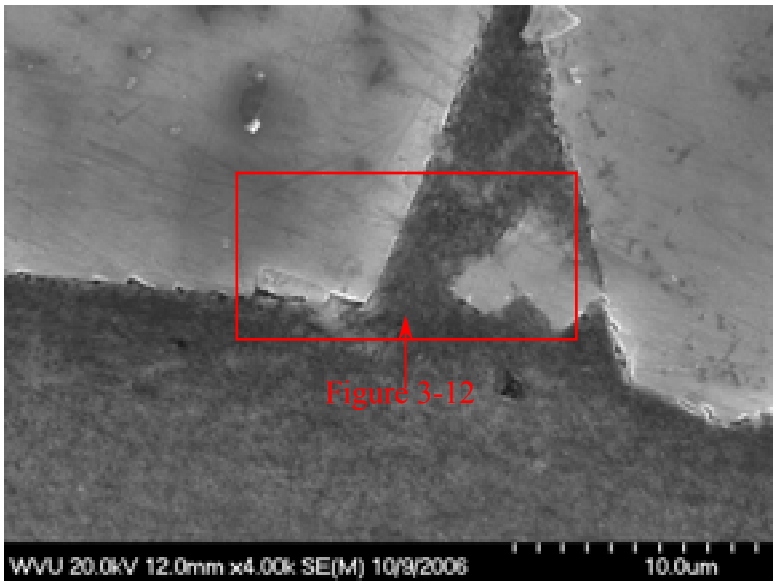

Figure 3-11: Agglomeration of Dross Particles on to the Dross layer formed over the Steel Substrate (4000X)

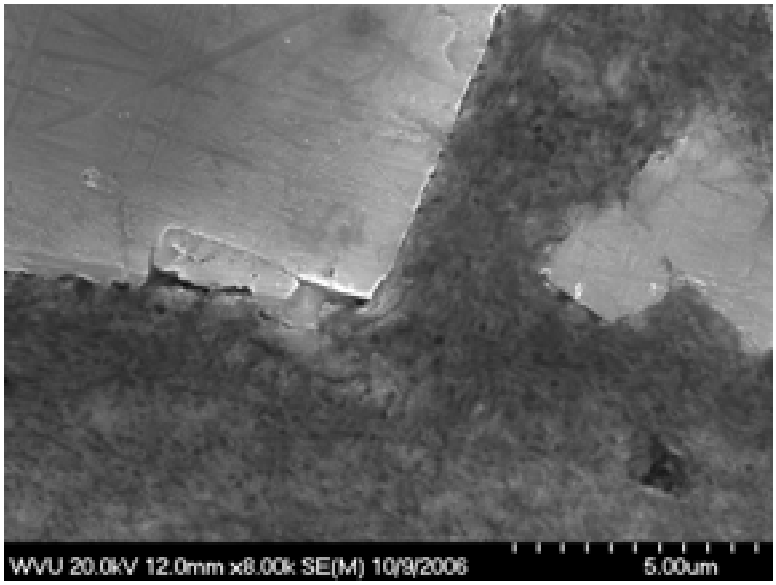

Figure 3-12: Agglomeration of Dross Particles on to the Dross layer formed over the Steel Substrate (8000X)

Sample-Bath Interface After 80 Minutes

The micrographs of the 80 minute sample (Figure 3-13) showed two distinct layers of dross with slight changes in the aluminum and iron content based on the EDS analysis. The inner layer (closest to the roll) was continuous and had uniform thickness, whereas the outer layer was irregular and similar to the 60 minute sample, contained small dross particles agglomerating towards the dross layer.

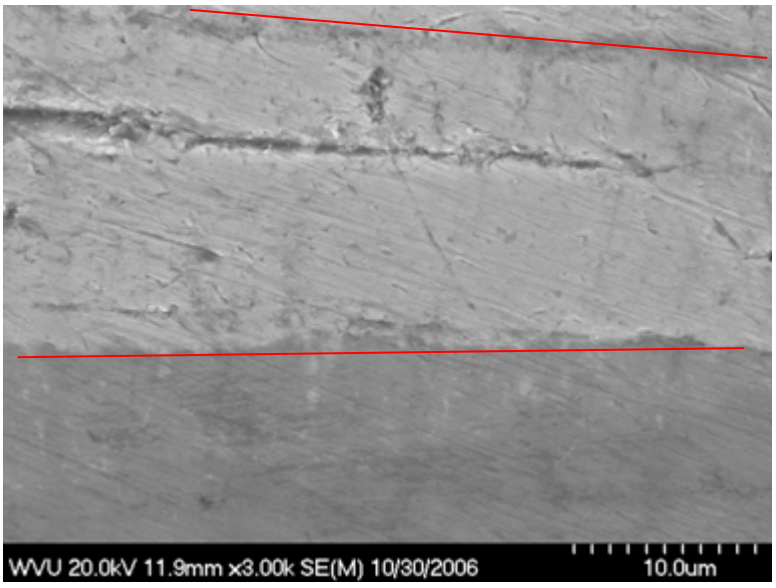

Figure 3-13: Cross-section of the Substrate-Bath Interface after 80 minutes (3000X)

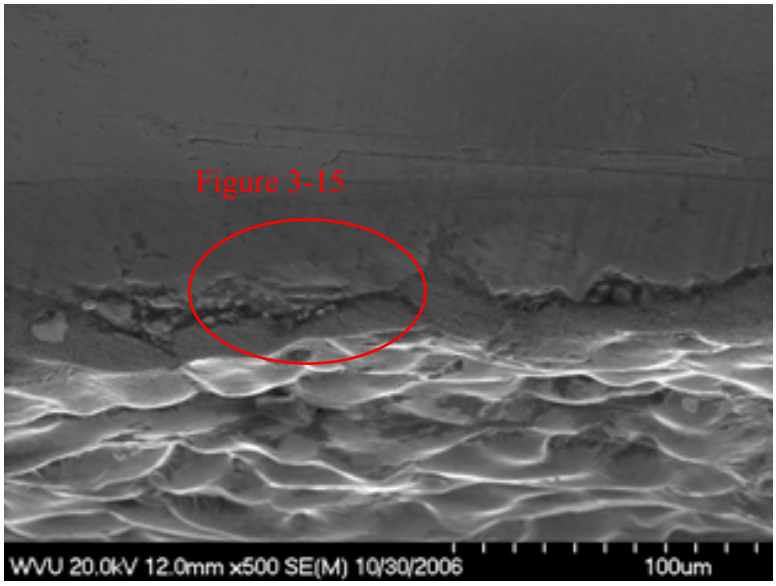

Figure 3-14: Micrograph of Cross-section of the Substrate - Bath Interface after 80 minutes (500X)

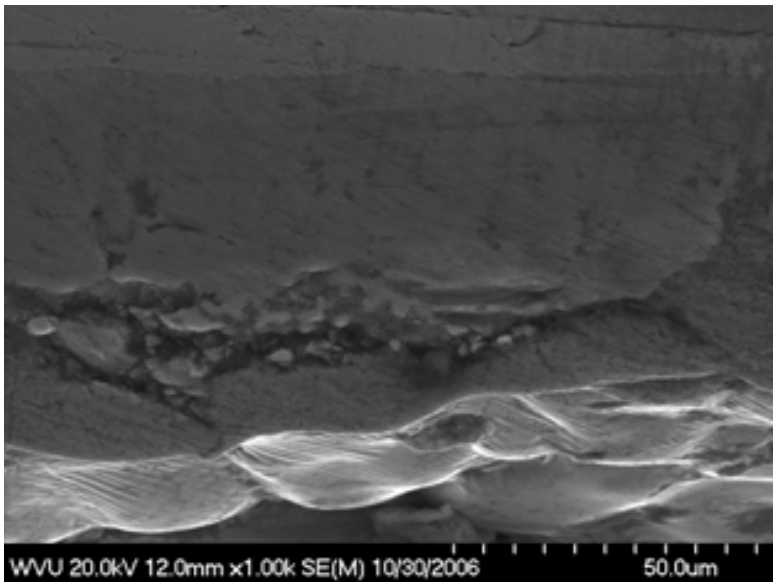

Figure 3-15: Micrograph of Cross-section of the Substrate - Bath Interface after 80 minutes (1000X)

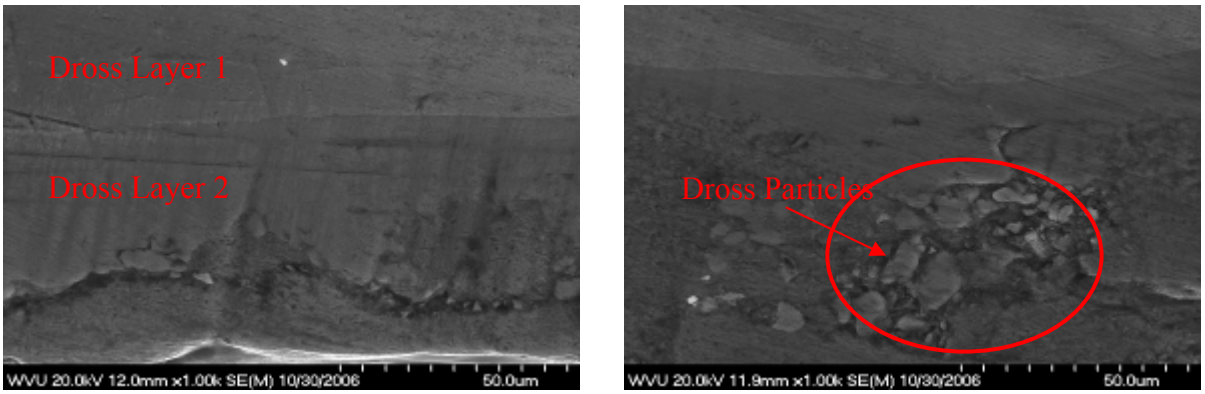

Figure 3-16: Micrograph of Cross-section of the Substrate - Bath Interface after 80 minutes (1000X)

Sample- Bath Interface After 100 Minutes

After 100 minutes, the cross-section of the substrate-bath interface revealed the two distinct dross layers, similar to the 80 minutes sample. Apart from these, the main differences observed were the increase in the thickness of the dross layers and the size of the dross particles as shown in Figure 3-17 and 3-18.

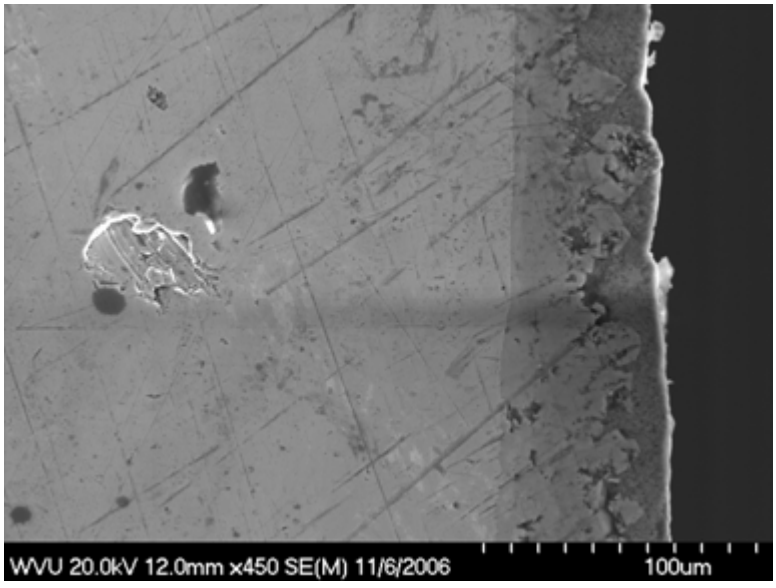

Figure 3-17: Cross-section of the Substrate-Bath Interface after 100 minutes (450X)

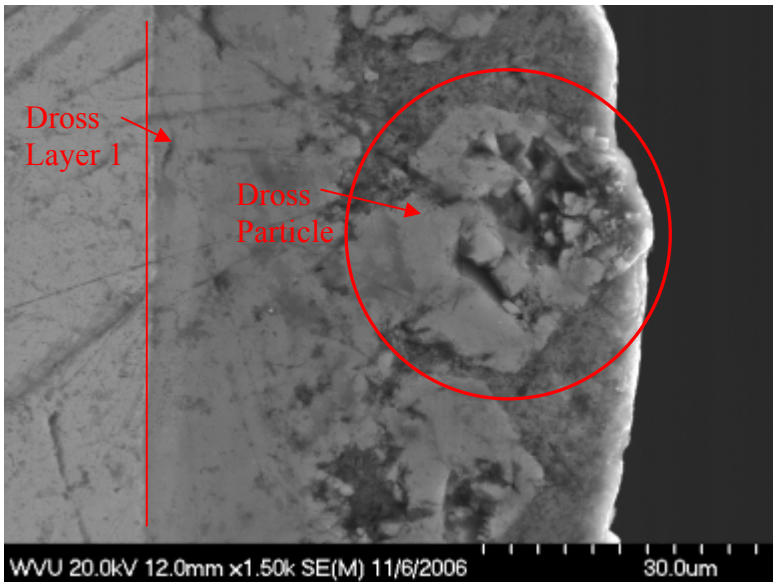

Figure 3-18: Cross-section of the Substrate-Bath Interface after 100 minutes (1500X)

Sample-Bath Interface After 120 Minutes

After 120 minutes of immersion, the darker inner dross layer and the lighter in contrast outer layer were observed (Figure 3-19 & 3-20) on the cross-section of the stainless steel substrate-bath interface. The outer dross layer (away from the substrate) was bigger compared to that of the 100 minutes sample, indicating the agglomeration of bigger dross particles and formation of the dross layer.

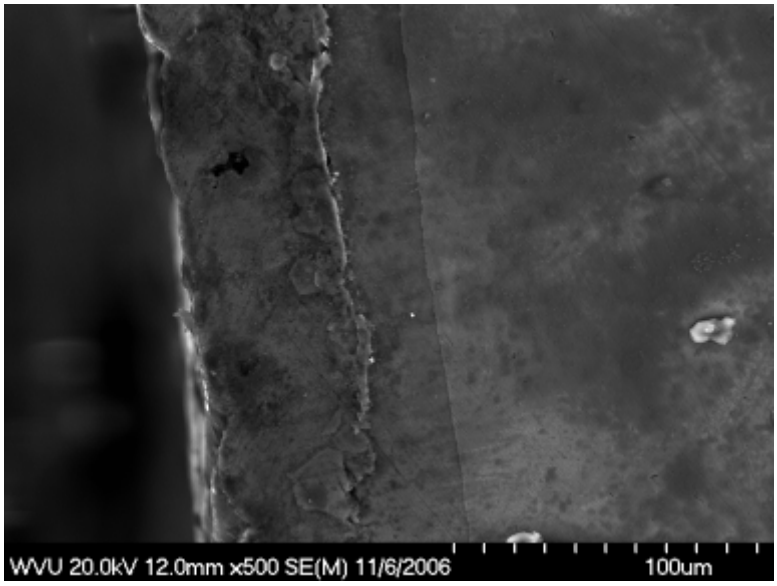

Figure 3-19: Cross-section of the Stainless Steel Substrate-Bath Interface After 120 minutes (500X)

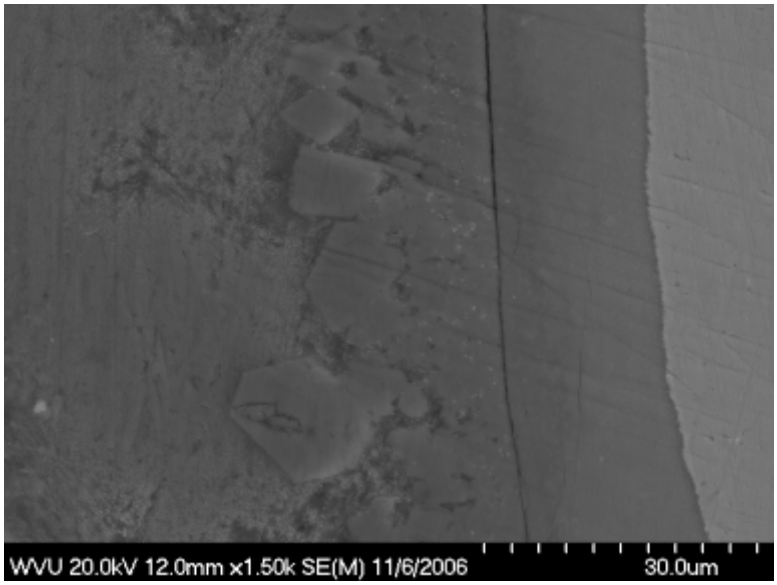

Figure 3-20: Cross-section of the Stainless Steel Substrate-Bath Interface After 120 minutes (1500X)

Sample-Bath Interface After 140 Minutes

After 140 minutes of immersion, the cross-section of the substrate-bath interface revealed a disintegrated inner dross layer and very thick outer dross layer as shown in the Figures 3-21 & 22.

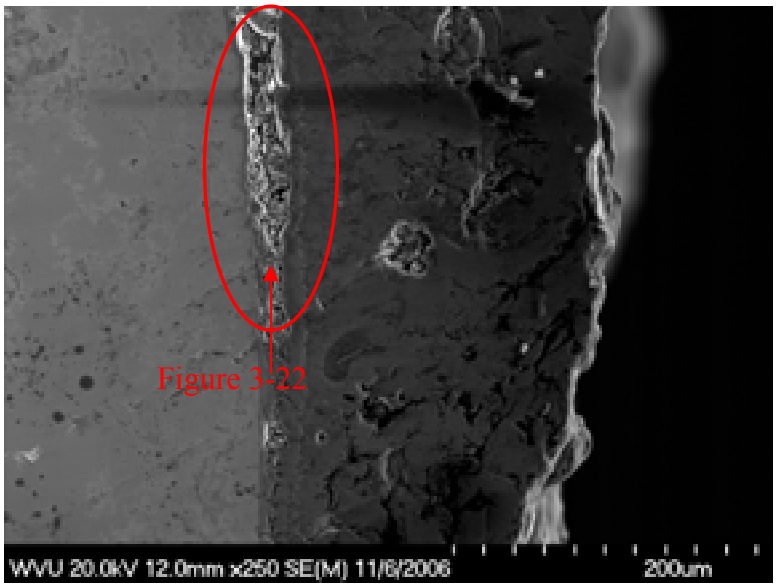

Figure 3-21: Micrograph showing the dross layers on the substrate after 140 minutes

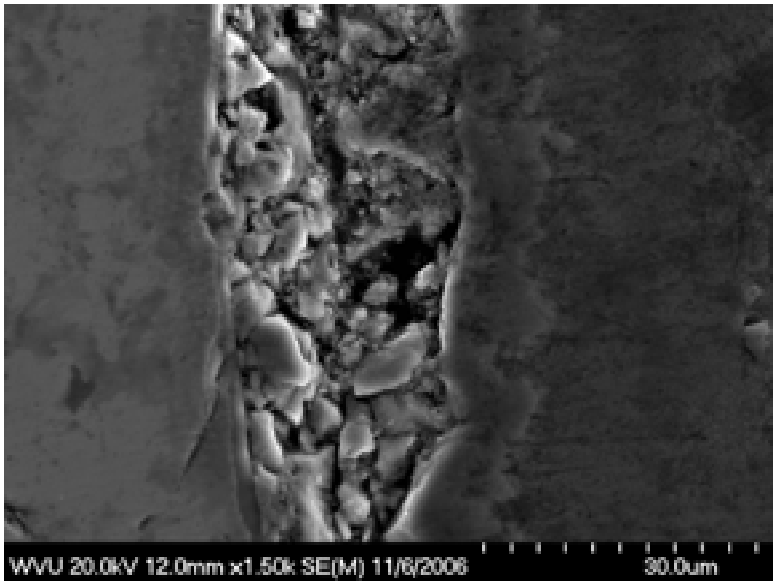

Figure 3-22: Dross particles on the substrate after 140 minutes

3.4 Dross Layer Analysis

To identify the composition of the dross layer formed over the roll surface after the dynamic tests, the samples prepared were analyzed with EDS using the technique of line mapping spectrum. The spectrum provided a semi-quantitative analysis to identify the composition of the dross. The analysis carried out was mainly with the four key constituents of the dross particles reported earlier by other research works (Fe, Al, Si and Zn). Hence the diffusion of Ni, Cr and other alloying elements present in the stainless steel substrate were not considered.

In the 20 minute test sample, the line spectrum showed the changes in the elemental composition along a pre-defined line over the cross section of the substrate bath interface. It can be observed from Figure 3-23, that the increase in the silicon count in the bath substrate interface shows that the inhibition layer formed initially was silicon rich layer and not Fe_2Al_5 as in the case of other galvanizing lines.

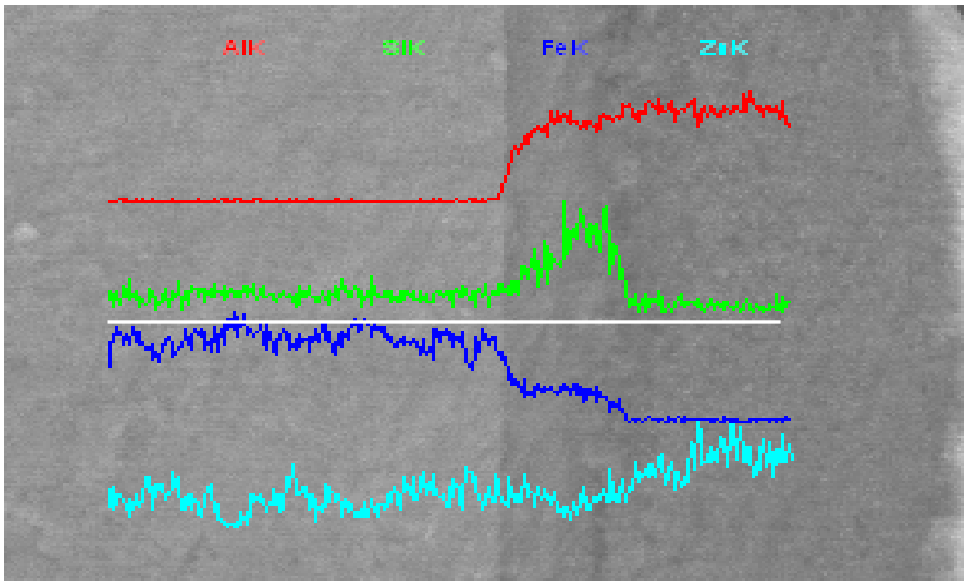

Figure 3-23: EDS Line spectrum of the Substrate- Bath interface after 20 minutes

The line spectrum analysis on the cross section of the 40 minutes sample revealed the drop in the silicon count near the bath substrate interface and increase in the count was observed (Figure 3-24) on the bath side, indicating the break down of the silicon rich inhibition layer.

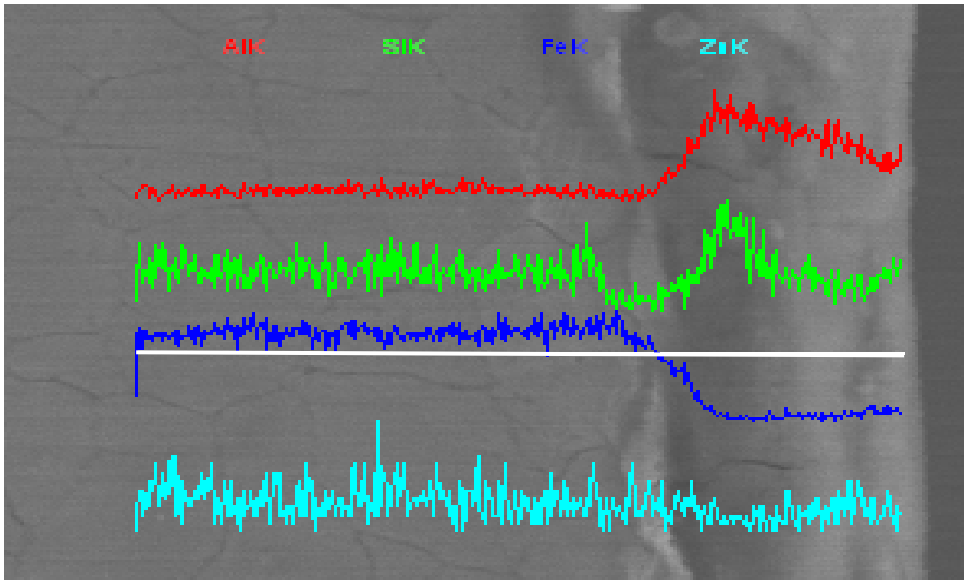

Figure 3-24: EDS Line spectrum of the Substrate- Bath interface after 40 minutes

The 60 minutes sample, the analysis showed that the dross layer formed over the roll surface constituents of Fe-Al-Si ternary intermetallic layer and not Fe-Al binary intermetallic as in other galvanizing baths, as significant presence of the 3 elements were observed over the dross layer (Figure 3-25).

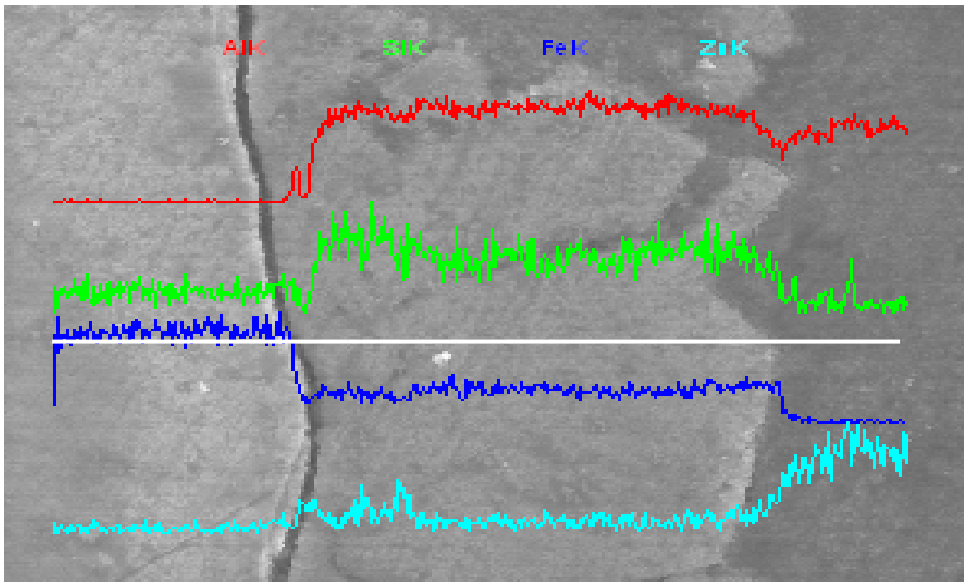

Figure 3-25: EDS Line spectrum of the Substrate- Bath interface after 60 minutes

In the 80, 100, 120 and 140 minute samples, presence of two different dross layers were observed and based on the analysis the inner dross layer formed is Fe_2Al_5 and the outer layer from the roll surface is the Fe-Al-Si intermetallic layer (Figures 3-26, 3-27, 3-28 &3-29)

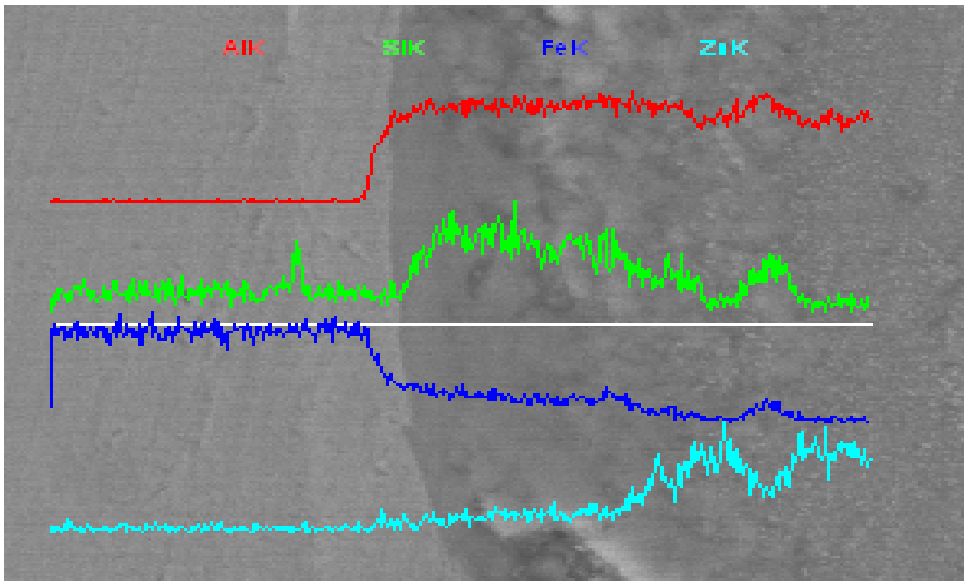

Figure 3-26: EDS Line spectrum of the Substrate- Bath interface after 80 minutes

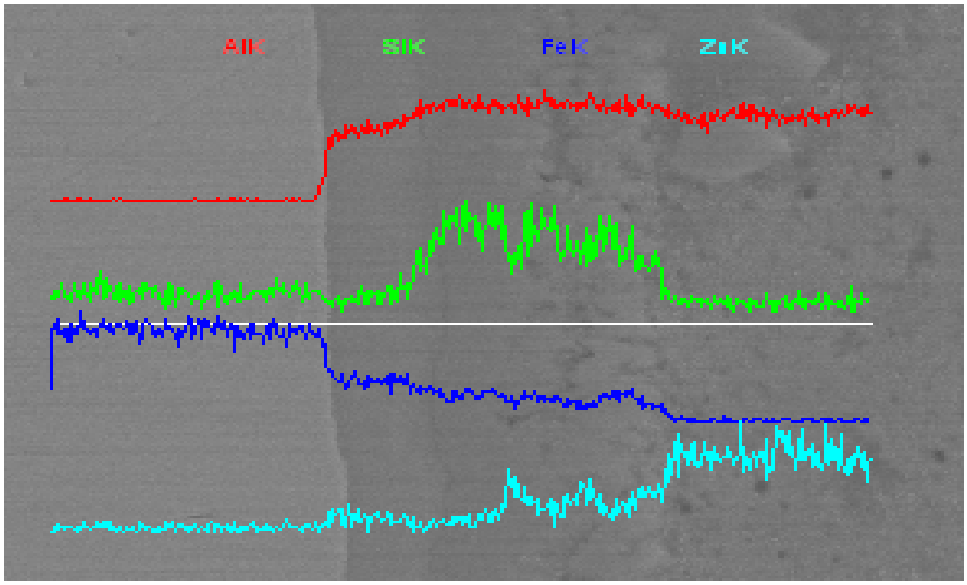

Figure 3-27: EDS Line spectrum of the Substrate- Bath interface after 100 minutes

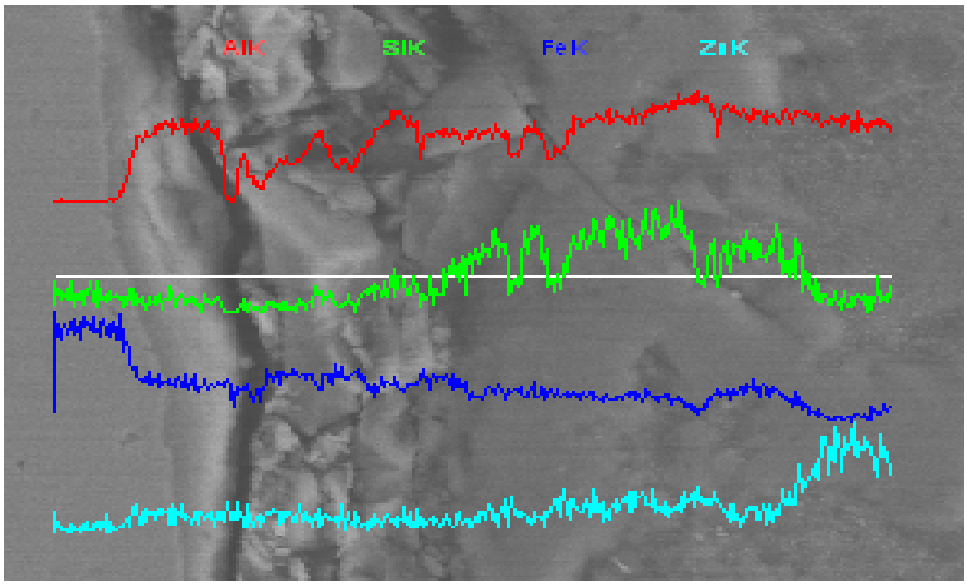

Figure 3-28: EDS Line spectrum of the Substrate- Bath interface after 120 minutes

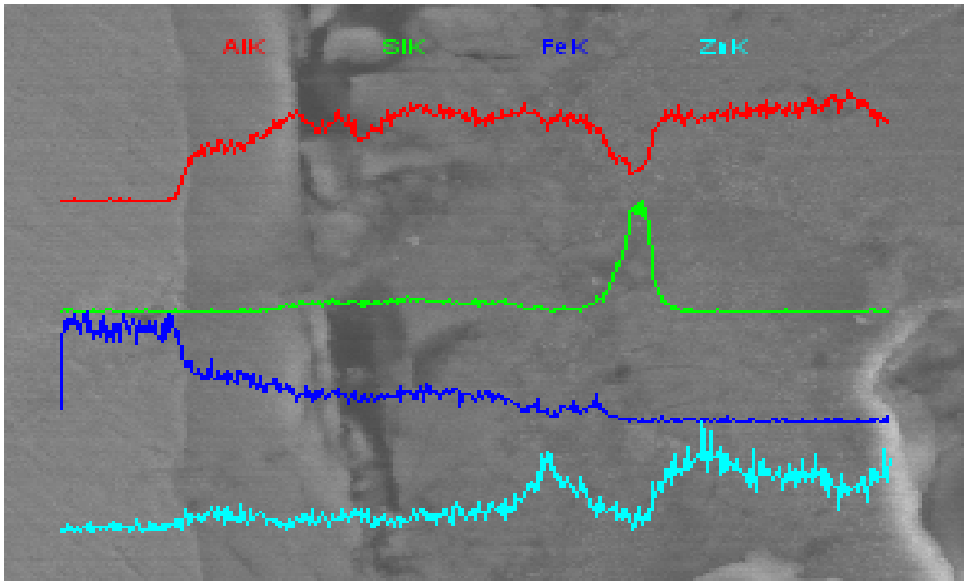

Figure 3-29: EDS Line spectrum of the Substrate- Bath interface after 140 minutes

3.5 Static Immersion Tests

In order to study the effect of the dynamic motion of the sink roll in the dross formation mechanism, static immersion test on roll samples were conducted. After the given time interval, the samples were removed from the bath and mounted and polished to analyze using SEM and EDS similar to the dynamic test samples. Presence of silicon inhibition layer was observed in both the 20 minute and 40 minute samples (Figure 3-30 & 3-31). This indicates that cracks formed on the silicon rich inhibition layer of the 40 minute dynamic sample may be due to the dynamic motion of the roll which must have caused the random motion of the dross particles in the bath towards the roll surface.

In the 60 minute static sample, formation of the dross layer was not evident as compared to the dynamic sample, whereas corrosion attack on the roll surface by the bath was observed. Similar to the 60 minute sample, the corrosion attack on the roll surface of the 120 and 140 minute samples were evident as the disintegration of the roll surface was observed (Figure 3-32)

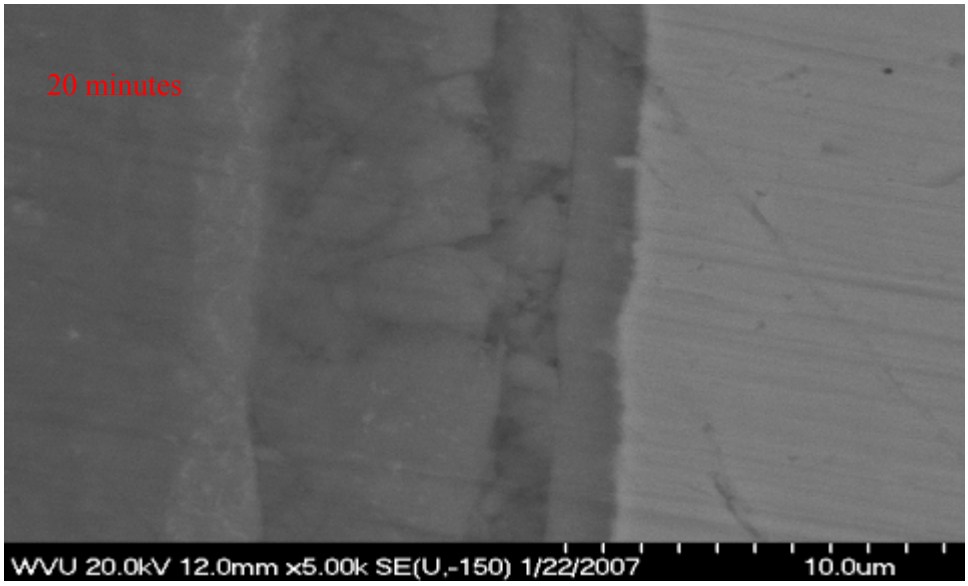

Figure 3-30: Cross section of the Bath- Substrate Interface after 20 minutes (Static)

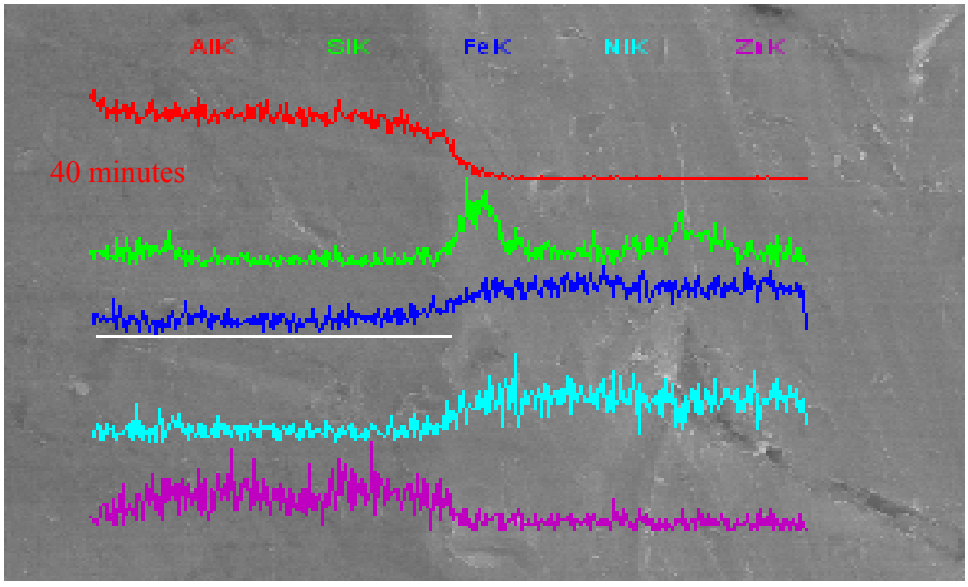

Figure 3-31: Cross section of the Bath- Substrate Interface after 40 minutes with the EDS Spectrum showing the presence of Si rich Interface Layer (Static)

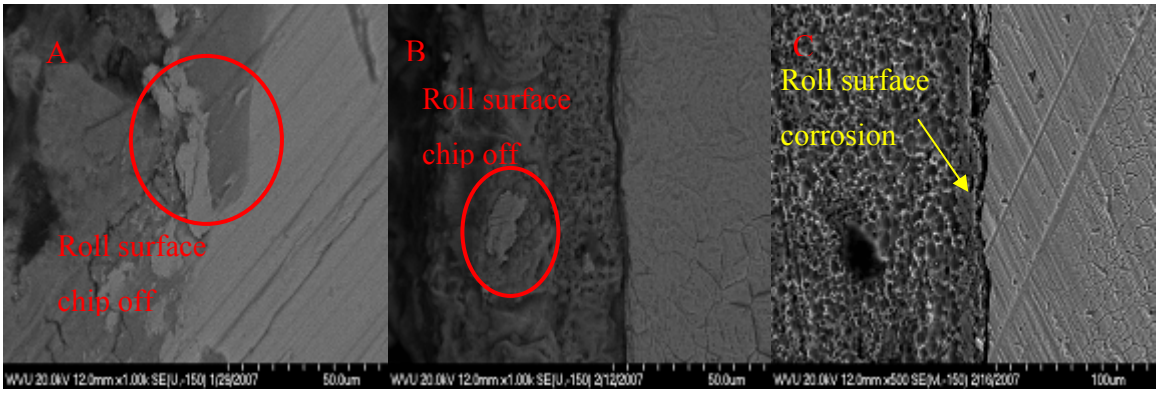

Figure 3-32: Cross section of the Bath- Substrate Interface after Static Immersion

(A) 60 minutes (B) 120 minutes (C) 140 minutes

3.6 Discussions

Based on the time series tests, the overall dross formation mechanism on the submerged pot hardware in the Zn-55%Al bath can be schematically represented as shown in Figure 3-30.

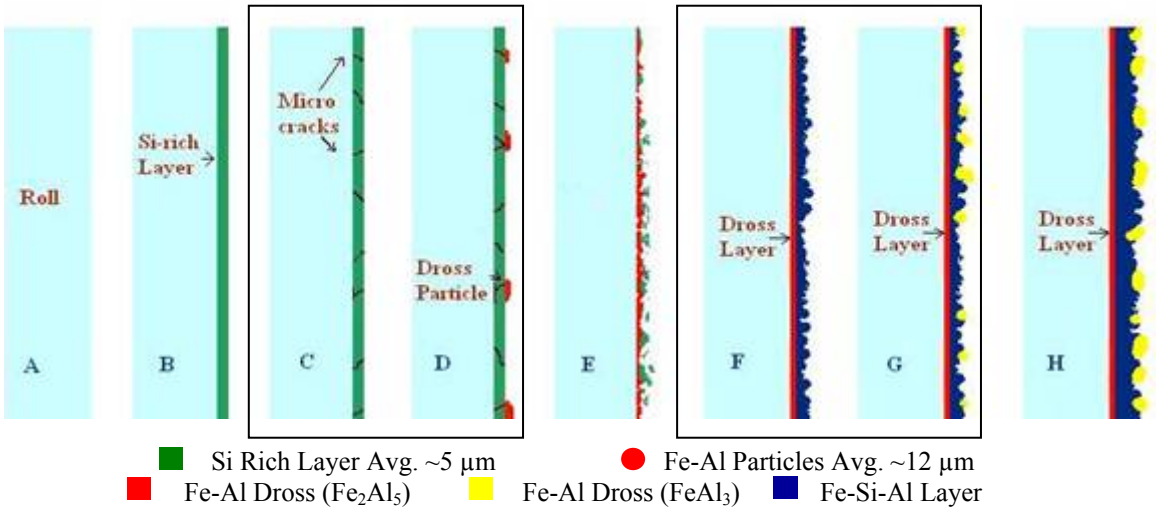

Figure 3-33: Schematic representation of Dross formation on Roll Surface in Zn-55%Al bath.

After 20 minutes, a uniform protective layer of silicon was observed between the sample and the bath interface (Figure 3-33-B). The source of Si-rich layer formed after 20 minutes may be due to the Si atoms liberated from the roll surface as a result of dissolution of the steel or due to solidification of the metallic phase silicon, which has a higher melting point (1414^{o}C) than that of the molten bath (600^{o}C) [26].

Subsequently after 40 minutes (Figures 3-33-C and 3-33-D), cracks were observed over the uniform layer of silicon and agglomeration of small dross particles were identified. These dross particles must have formed elsewhere in the bath due to the reaction between the iron and aluminum and the dynamic motion of the bath caused the particles to agglomerate on the sample surface. After 60 minutes (Figure 3-33-E), a uniform dross layer was observed on the sample surface and silicon-rich areas were observed in the outer regions of the build-up. After 80 minutes (Figures 3-33-F and 3-33-G), two layers of dross were observed, the inner most thin layer consisted mainly of Fe and Al and the outer non-uniform layer contained Fe-Si-Al. At indeterminate locations, larger dross particles (Fe-Al) were observed. After 100 minutes (Figure 3-33-H) the dross layer and the dross particles observed were larger in size as compared to the 80 minutes sample.

It has been reported [27] that the silicon phase present in the bath converts the Fe-Al particles to a more stable ternary Fe-Si-Al intermetallic layer. The increase in size of the layer and particles were observed on the remaining samples.

Based on these tests, the mechanism of the dross formation can be categorized under three dominant stages:

1) Formation of silicon rich inhibition layer
2) Break up of the inhibition layer and agglomeration of small dross particles on the roll surface due to the dynamic motion of the bath
3) Formation of continuous dross layer over the roll surface

Furthermore, EDS analysis of the sample-bath interface revealed the intermetallic compound formed was a ternary phase containing Fe, Al and Si in addition to the typical Fe_2Al_5 and $FeAl_3$ phases and from the ternary equilibrium diagram shown in Figure 3-34 the Fe-Al-Si compound possibly be $Fe_3Al_3Si_2$, $Fe_5Al_9Si_5$ $Fe_2Al_5Si_2$, $Fe_2Al_9Si_2$, $FeAl_3Si_3$.

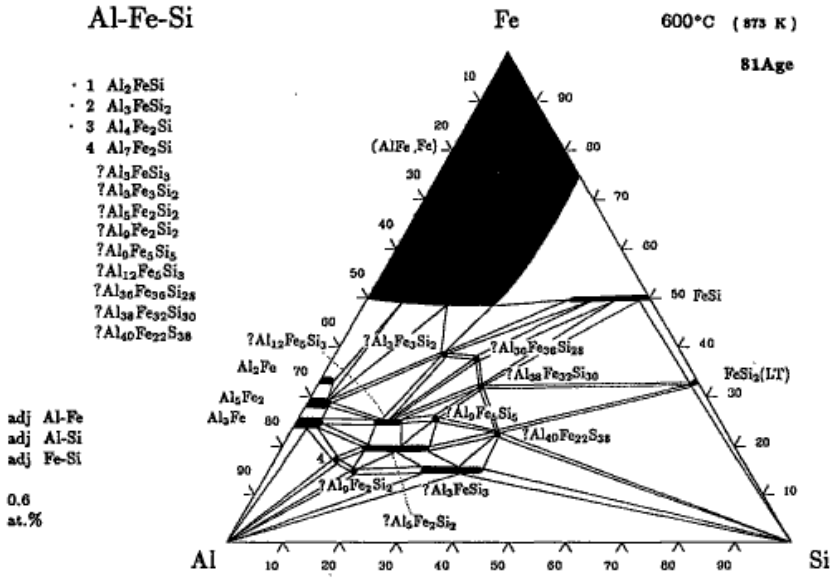

Figure 3-34: Fe-Al-Si Equilibrium Diagram at 600°C

(Reproduced from Handbook of Ternary Alloy Phase Diagrams)

The dross layer formation at each stage was measured and the layer thicknesses were plotted relative to time. As outlined in Figure 3-35, the initial growth was slower due to the formation of a silicon inhibition layer. However, after 60 minutes, the dross growth rate settled into a parabolic trend.

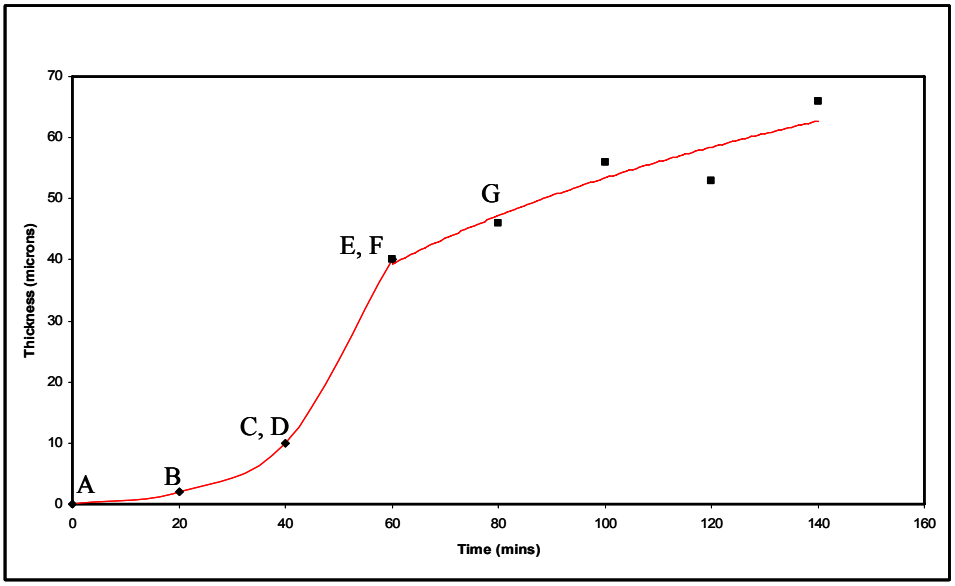

Figure 3-35: Dross layer growth pattern.

Based on the results from the dynamic tests, which showed the presence of Si in the bath formed an initial protective (inhibiting) layer on the roll surface, static tests were carried out to evaluate the effect of Si-rich inhibiting layer against corrosion in static mode.

3.7 Summary

The mechanism and the rate of dross formation are explained based on the dynamic tests and the effect of the silicon in the 55%Al-Zn bath to convert the Fe-Al intermetallic compounds to a stable ternary Fe-Si-Al intermetallic compound has been established.

- Initial formation of Si rich inhibition layer preventing the exothermic reaction between Fe and Al.
- Outward diffusion of Fe from the steel substrate.
- Breakdown of the Si rich layer and inward diffusion of Al towards the substrate.
- Formation of Fe_2Al_5 intermetallic layer. Further diffusion of Al and Zn from the bath is hindered because of the strong structure of the Fe_2Al_5 layer formed.
- Agglomeration of smaller $FeAl_3$ dross particles formed in the bath on the roll surface.

4. DROSS REMOVAL SYSTEM

Introduction

Continuous hot dip coated steel sheets are developed in to a variety of finished products ranging from automotive components to building and construction components. Overall the products coated can be broadly classified in to the following groups.

A. Automotive exposed/painted
B. Automotive unexposed
C. Construction painted
D. Construction exposed
E. Construction unexposed

Among the five classifications, the first three have strict quality standards towards the surface finish of the coating. Hence, all coating lines work towards enhancing the quality of the surface appearance by paying attention to technologies capable of minimizing the major issues in the zinc pot and thus improving the campaign life.

Operational Issues

Based on the survey conducted by Becherer on the coating lines in North America and some European companies, the major operational issues are discussed below:

Flaking: Building up of Iron oxide in the furnace due to shut down and resulting in the formation of large particles “flakes” and dropping of refractory into the bath during startup.

Zinc Dust: Vaporizing of molten zinc bath during a shutdown and condensing of the same over the pot hardware.

Top dross: The tendency of the floating top dross to adhere over the sheet surface affecting the coating quality.

Transition Issue: conversion of bottom dross to top dross in the lines which produce both galvanize and galvanneal coating.

Roll Buildup: Adhesion of the top dross to the surface of the sink roll and forming thick non-uniform layer affecting the surface finish of the coating.

Skidding: Caused due to roll "lock up"

Vibration: Due to the wear on the bearings. Also affects the ability to control the thickness of the coating.

Table 4-1: Summary of the survey result

Areas of Concern	Number of Sites	% of Sites
Flaking	8	23%
Zinc dust	5	15%
Top Dross-General	11	32%
Transition	5	15%
Roll Build-up	13	38%
Roll Lock-up/Skidding	10	29%
Vibration/Flutter	4	12%
Sink Roll Bearing Life	30	88%

Based on the survey, dross build-up over the sink roll has been reported in 38% of the lines, ranking it the second major issue which needs to be addressed to maintain the surface quality and to increase the productivity.

Dross Buildup in Galvalume lines

Previous studies showed that the reaction between the iron substrate and the molten Al-Zn alloy were very violent for the baths containing >10% of Al when compared to baths containing <10%Al. Due to the presence of high aluminum content in the Galvalume bath, the dross formation is very rapid compared to other baths and thus dross build-up on the roll surface is inevitable (Figure 4-1 & 4-2). Hence the only way to maintain the quality of the coating on the sheets is by removing the dross formed on the roll.

Figure 4-1: Dross build-up on the Sink Roll surface used in the Zn-55%Al CGL.

Figure 4-2: Dross build-up on the Sink Roll Pinion arm used in the Zn-55%Al CGL.

Dross Removal System

Continuous Galvanizing lines consist of two main rolls, the sink roll and the stabilizing roll of the submerged pot hardware. The strong corrosive nature of the Zn-55%Al bath damages the pot hardware components and thus reducing the efficiency of the lines.

Due to the dross build-up on the roll surface, the productivity and the quality depends on the submerged pot hardware (rolls) which makes contact with the steel sheet during the coating process. The failure rate curve of the submerged pot hardware takes the form of a "bath tub" and the current failure rate is shown in Figure 4-3. In order to have energy efficient, high productive, low maintenance CGL, the section 2a indicated in the curve has to be extended till 2b as shown in dotted lines.

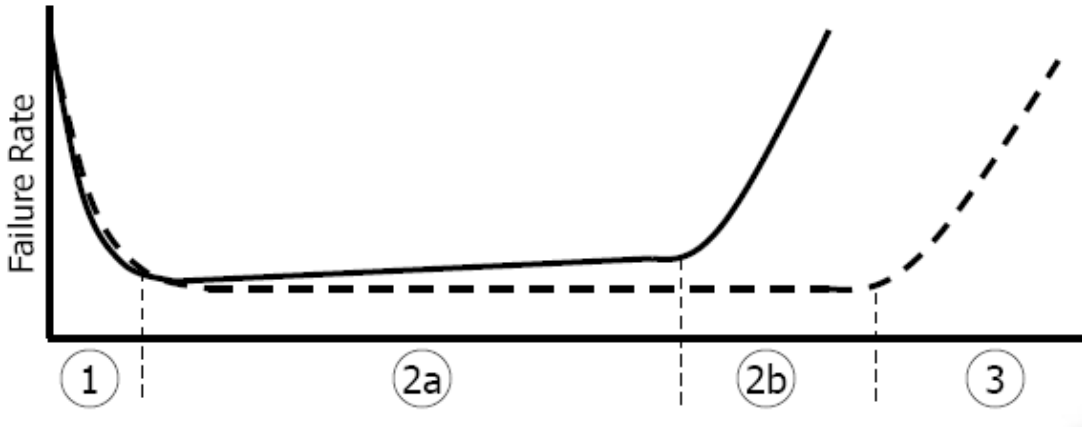

Figure 4-3: Failure Rate of the Sink Roll used in the CGL lines.

Extending Life of Pot-Hardware by dross management

Based on research work done by various researchers, dross buildup on the pot hardware can be reduced or eliminated (to a certain level) by controlling various parameters, such as:

- Controlling uniformity of the temperature over the bath
- Minimizing fluctuations in the temperature
- Maintaining uniformity of the bath composition etc.

Even utilizing new and improved technologies in controlling the above parameters, the dross buildup may be controlled in baths with less Al content, whereas Zn-55Al pots differ from other galvanizing pots, which often have greater volume and contain a much greater mass of molten metal due to higher density of zinc. The operating temperature is also much higher for 55%Al-Zn (600^{o}C) and others operate at 460^{o}C. Even the strip temperature entering the melt is typically between 450- 460^{o}C whereas for 55Al-Zn the

strip entry temperature is typically between 520 – 580°C where as the pot is at 590 – 610°C. Therefore the temperature difference between the melt and the strip is more significant than for other galvanizing pots.

55%Al-Zn material properties also differ from other galvanizing baths for example comparison between 0.14%Al-Zn bath is given below in Table 4-2.

Table 4-2: Material Properties of 55Al-Zn and 0.14Al-Zn

Property	*55% Al-Zn at 600°C*	*Zn-0.14% Al at 460°C*
Density (kg/m^3)	3327	6600
Viscosity (Pa·s)	0.001648	0.004
Specific heat (J/kg·K)	860	512
Thermal conductivity (W/m·K)	50	60
Thermal expansion coefficient (K^{-1})	1.153×10^{-4}	1.666×10^{-4}

Considering these facts and the differences between 55Al-Zn and other galvanizing lines, maintaining temperature at one fixed value is more difficult due to the entry of the strip at much reduced temperature, which causes fluctuations in the bath temperature.

As dross management is critical for the line productivity, various materials (alloys) have been developed and researchers have studied the effect of dross growth rate on these materials. Liu, et.al., reported that due to the presence of high Al content in the 55Al-Zn bath, once the initial build up took place, the process was dependent on the availability of

dross particles and was independent of the type of the substrate (Figure 4-4 & 4-5) and also concluded that no correlation can be determined between the thickness of the build-up layer and the reaction layer.

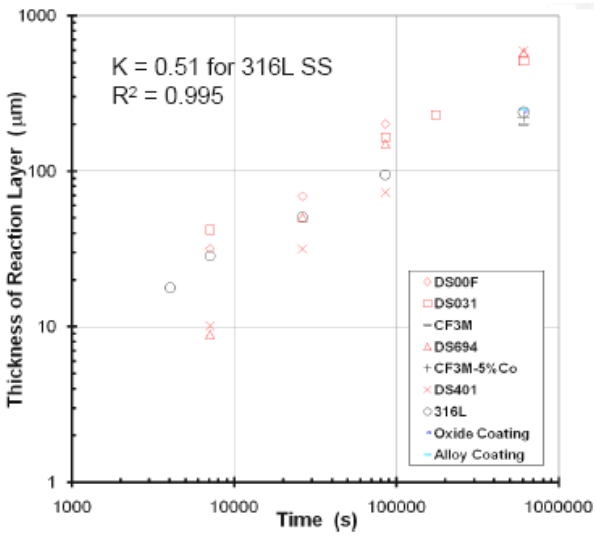

Figure 4-4: Thickness of Reaction Layer

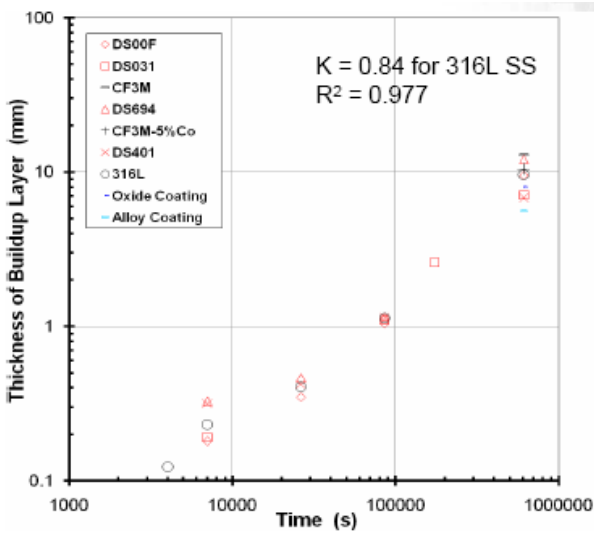

Figure 4-5: Thickness of Build-up Layer

Steel mills with 55%Al-Zn coating lines, in order to extend the productivity of the line have developed and incorporated various modifications (either manual or semi-automatic or automatic) to the actual lines in order to improve the productivity, energy savings, improvement of the overall sheet quality, reduce cost of repair or replacement parts and to reduce the overall downtime. One of the major developments (change) required was to maintain the sink roll surface clean by the removal of dross accumulated over the roll by means of mechanical scraping devices.

The process of dross removal from the sink roll surface involves a series of blades breaking down the dross layer by scraping action. The schematic representation of the process is shown in Figure 4-6. The dross removal mechanism is based on the "*contact stresses*" caused by the pressure of one solid on another over limited areas of contact.

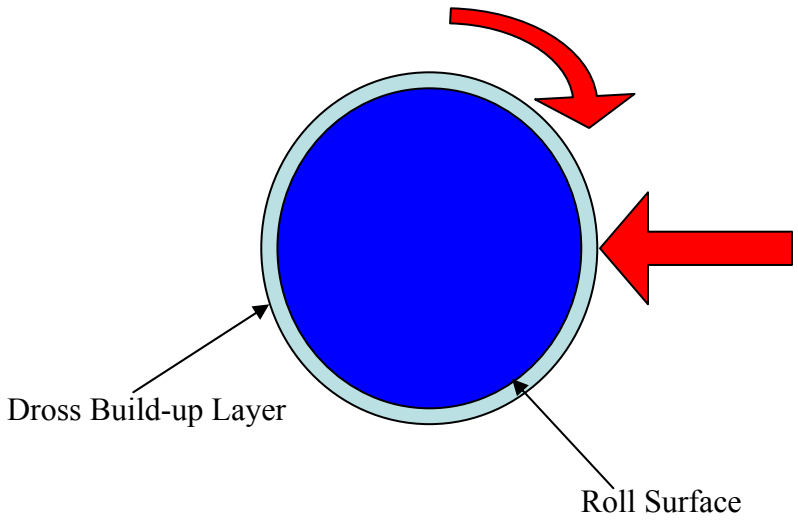

Figure 4-6: Schematic Representation of the Scraper Working Principle.

In general, the sheet strip which comes in to the bath makes contact with the sink roll and exits the bath, through the stabilizing rolls. The overall contact made by the strip over the sink roll is roughly about ~42% of the surface at any given time as shown in Figure 4-7.

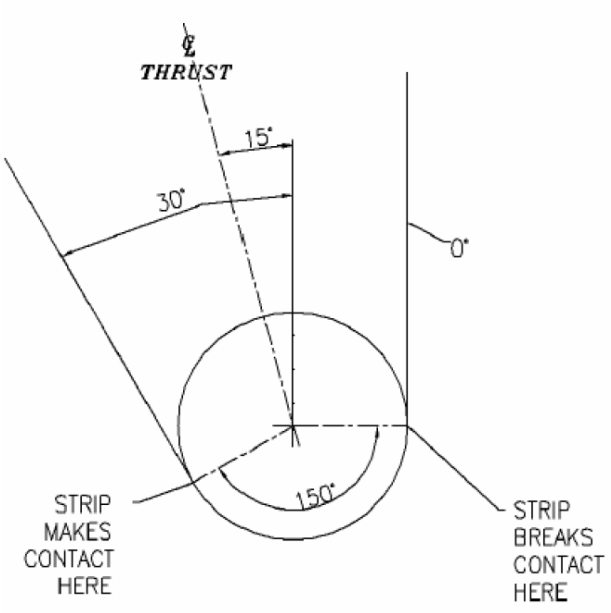

Figure 4-7: Steel Strip- Sink Roll Interface [28]

Hence cleaning of the entire surface of the sink roll depends on the speed at which it rotates. The scraper blades have to make contact on the roll surface along the thrust line (Figure 4-7) to maintain equal distances from the sheet on both entry and exit sides thus avoiding any debris settling over the sheet surface.

The inward movement of the scraper set up towards the roll surface along the thrust line, upon contact induces a compressive force over the dross layer. This force applied by the scraper blades over a limited area of contact on the sink roll surface breaks down the hard and brittle dross layer and as the roll is rotating at a constant speed, imparts a tangential (shear) force which helps in continuous removal of the dross layer from the roll surface

as shown in Figure 4-8. Figure 4-9 shows the schematic representation of the forces acting over the roll surface.

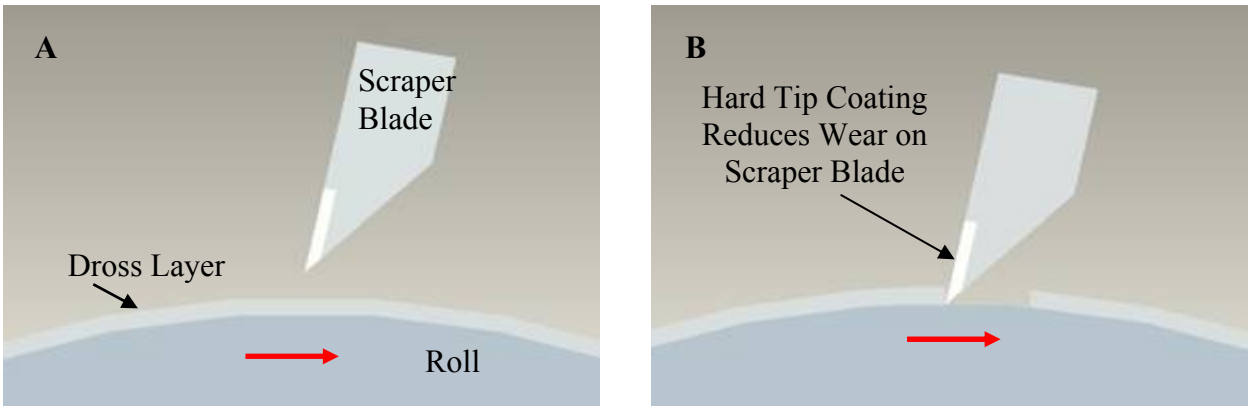

Figure 4-8: Schematic Representation of the Scraper Mechanism.

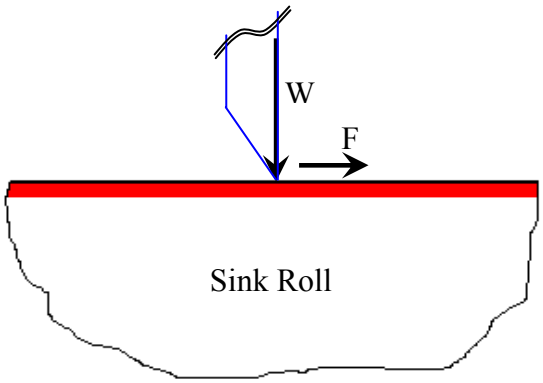

Figure 4-9: Forces Acting on the Roll Surface when in contact with the Scraper.

Various combinations of scraper blades in different arrangements can be utilized to remove the dross layer. The process control depends on the line parameters such as line speed, thickness of the coating, quality of the bath composition, quality of the sheet to be coated and temperature fluctuation. In addition to these parameters, the actual time period

of the roll submerged in the bath (stationery and rotating) determines the rate of dross accumulation. Based on these parameters, the scraping process can be from 2 to 5 minutes for every 30 to 45 minute time period.

Use of the scraper system, in the actual industrial CGL lines, have reported [29] in 50% decrease in line stoppages due to the dross build-up on the roll surface and thus increase in the overall production of the coated steel sheets.

Scraper Blade Material

In general the scraper is made of 309 Stainless steel body which has a hard material brazed on it as shown in Figure 4-10. The use of stainless steel body provides the toughness for the blade and reduces the cost compared to using the entire hard tip material as the blade.

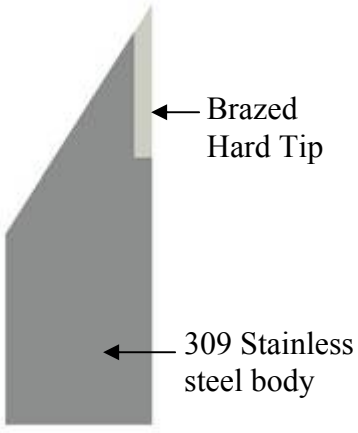

Figure 4-10: Cross Section of the Scraper Blade.

Due to the severe corrosive nature of the 55%Al-Zn bath, the material to be used as the scraper blade must possess the following important characteristics:

- Corrosive Resistant
- High Hardness at elevated temperatures
- Wear Resistant
- Ductile

Corrosion Resistant: Metallic materials are known to react with the galvanizing bath to form intermetallic phases and therefore the material to be used as a scraper (pot hardware) must be corrosion resistant to withstand the galvanizing bath corrosion.

High Hardness at elevated temperatures: As the galvanizing bath temperature varies from 470 to 700^{o}C depending on the Al content (55%Al-Zn = 600^{o}C), the scraper material must have higher hardness compared to the dross particles at high temperatures.

Ductile and Wear Resistant: Thermal shock, thermal cycling and mechanical impact and vibration can cause premature failure of the scraper, thus the material must be ductile to perform the scraping process for long periods. Also, the material must be abrasive wear resistant to effectively remove the dross formed over the roll surface.

The implementation of the scraper system reduced the line stoppages almost by 50% and increased the productivity and reduced the cost per tonnage of coated steel. However, to reduce the energy cost and the cost on repair and replacement parts further, in the spring of 2001, the U.S. Department of Energy – Office of Industrial Technologies (OIT)

awarded a contract with an expansive collaboration with the industrial participants to understand, develop and extend the life of pot hardware in steel mills continuous galvanizing lines. [30-53].

One of the industrial participants (Wheeling Nisshin Inc.) uses a scraper system to remove the dross layer build-up over the sink roll. The effective average life of the scraper blades with the brazed hard tip in removing the dross layer and maintaining the roll surface clean was around 7 days and after which the wearing of the scraper blades reduces the efficiency in cleaning the roll surface. As the scraper wears out (Figure 4-11), the quality of the coated steel reduces drastically and increases the scrap rate.

Figure 4-11: Worn out Scraper Blade after ~7 days in GL line.

Research Objective

The main objective of this work is to increase the effectiveness of the scraper system used in the 55% Al-Zn coating lines to remove the heavy dross build-up over the sink roll. The basis of this study is to achieve the same results in a prototype lab scale arrangement similar to that of the industrial coating lines.

Different methodologies can be followed in order to achieve an efficient scraping system.

i. Hard material with better corrosion and wear resistance.

ii. Scraping process parameters such as time interval between each scraping.

New Overlay Material for Scraper Blade

Material properties such as ductility, hardness, corrosion resistant and wear resistant are the important parameters to be considered in selecting a suitable material for the scraper overlay. Alloys which posses these qualities and able to perform in normal galvanizing coating lines for longer periods have been reported earlier by various researchers. The hardness values for some of the materials identified are given below in Table 4-3.

Table 4-3: Hardness value of Intermetallic compounds and Pot Hardware Materials

Material	Hardness (HV)
Eta (Zn)	45
Zeta ($FeZn_{13}$)	181
Delta ($FeZn_7$)	265
Gamma (Fe_3Zn_{21})	421
Al-Fe-Zn-Co-W	763
Stellite 4	528
Stellite 6	515
MSA 2001	465
MSA 2020	611
Tribaloy 800	580

Duplication of Actual Continuous Coating line Conditions

A test rig was designed and constructed at West Virginia University (WVU-Hangar) with the aim of providing reliable wearing rate and life expectancy of each scraper material when used in the 55Al-Zn bath to remove the dross build-up on the sink roll. In order to carry out the tests in the exact industrial scenario, the test rig was designed to simulate the actual line operating conditions as shown in Figure 4-12.

The test rig was also designed to provide

- Repeatable data for variety of scraper materials.
- Cost effective to install and analyze new test samples
- Reduced scraper and roll dimensions to avoid high material cost.

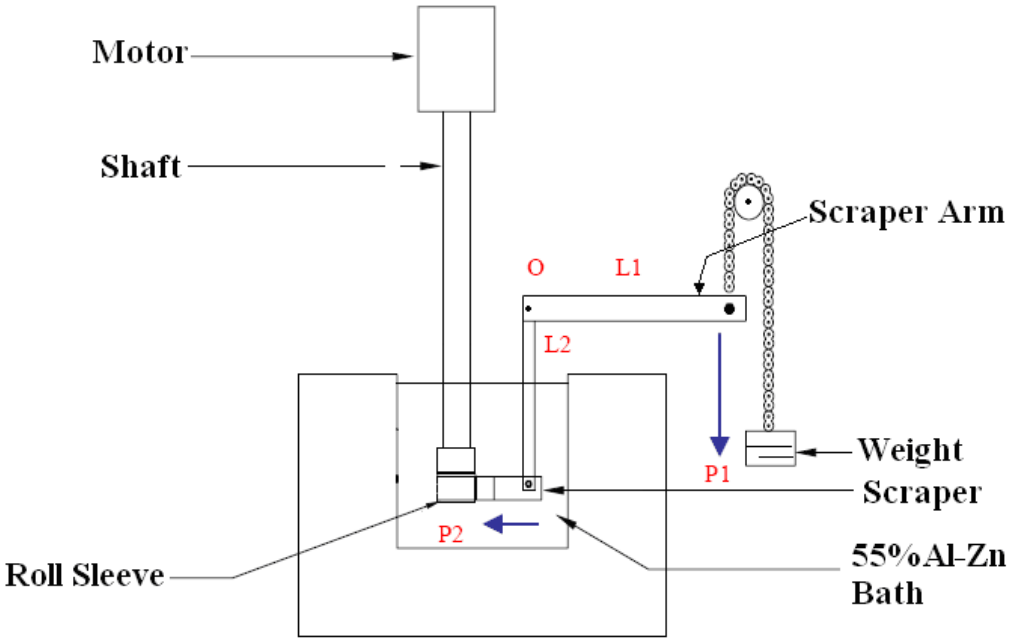

Figure 4-12: Schematic Representation of the Test Rig- WVU Hangar

The WVU-Hangar test rig consists of the following:

Furnace

A rectangular steel shell comprises of 12 induction coil panels arranged in circular fashion which encompasses an Ø30" silicon carbide crucible with a capacity of 500 lbs of the liquid bath (Figure 4-13). The floor of the furnace shell was made of refractory liners to avoid any heat loss. The furnace is placed on rails for the easy handling of the same with fully laden with the molten metal.

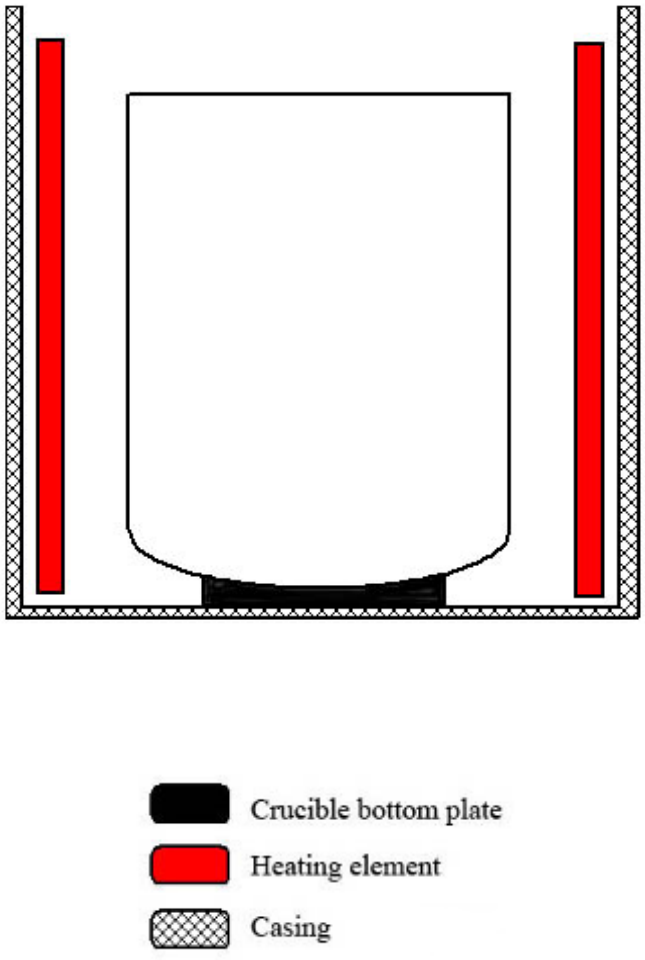

Figure 4-13: WVU-Hangar 500 lbs Capacity Furnace

A motor housed at the top of the setup drives a low carbon steel shaft (Ø 2.85", 29" long) and the other end of the shaft is connected to the sink roll (Ø 4" OD, Ø 2.85" ID and 4" long). The sink roll was sleeve was made of 316L stainless steel, similar to most of the sink rolls used in the 55Al-Zn.

Scraper Arm Setup

In order to apply a compressive force on the roll, the scraper was attached to a scraper arm as shown in Figure 4-12. The load was applied to the scraper arm, which in turn pushed the scraper towards the roll. The load ratio between the load applied and the load acting over the roll surface through the scraper was obtained by taking moment along the point O as shown in Figure 4-12.

Moment at point O:

$$\mathbf{P_1 * L_1 = P_2 * L_2}$$

As L_1= 33" and L_2 = 11"

$$\mathbf{P_2 = 3 * P_1}$$

The overall setup of the WVU- scraper wear test rig is shown in Figure 4-14.

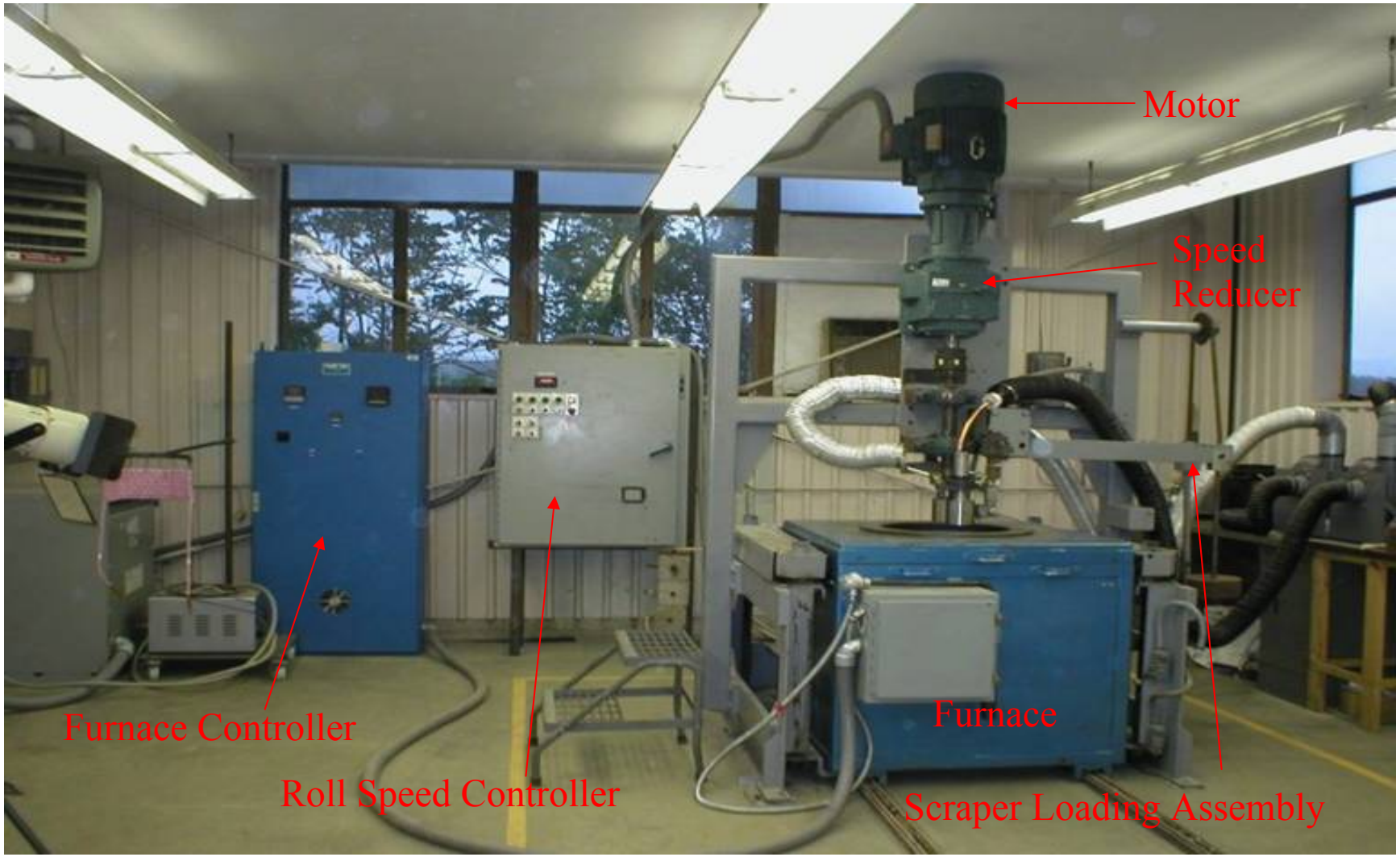

Figure 4-14: WVU Scraper Wear Test Rig

Scraper Set-up

Corresponding to the sink roll dimensions and the space available for the free movement of the scraper considering the scraping action and the crucible size, the actual scraper (12.6”x5.3”x1.6”) (Figure 4-15) was scaled down to 4”x 2.5”X 1”. Instead of welding the scraper blade to the scraper arm as in the actual lines, Ø 0.5” hole was drilled on the center of the scraper body as shown in Figure 4-16 and the scraper was bolted to the scraper arm, for the easy removal of the scraper blade after the test for cleaning and measuring the wear rate.

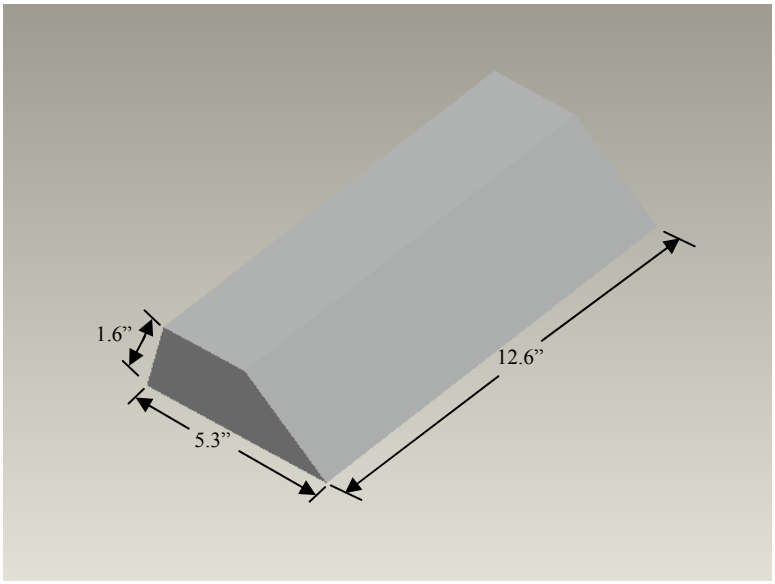

Figure 4-15: Actual Scraper welded to the Scraper Arm in the CGL lines

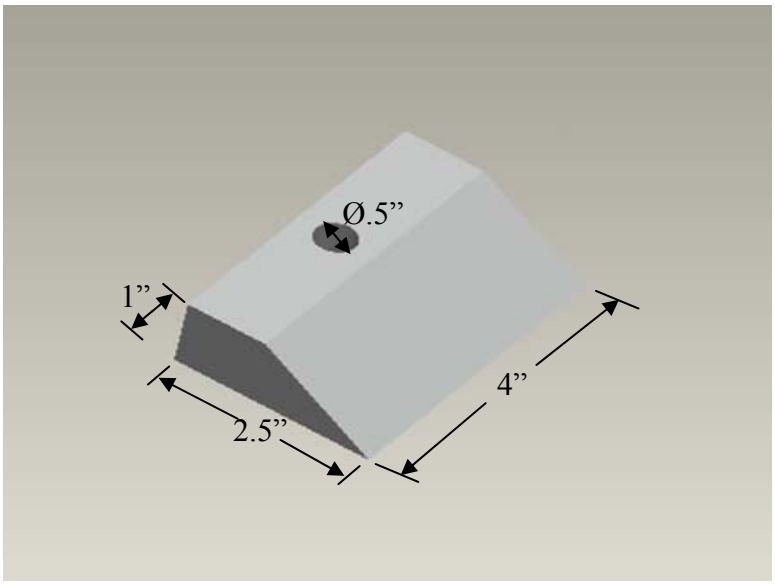

Figure 4-16: Scraper Dimensions used in the WVU Test Rig

Scraper Tip Overlay

Various materials which have higher hardness and wearing resistance can be considered for scraper tip overlay, but the important factor to be considered is that it must have higher corrosion resistance in the Zn-Al environment at higher temperature and the corrosion products, if formed must not alter the bath composition. Different alloys have been developed to use for pot hardware, which have minimal effect due to the Zn-Al environment in the galvanizing baths. For example, Co- based alloys, such as Tribaloy T-400, Tribaloy T-800, Tribaloy, T-401, Stellite 21, Stellite 6 are widely used as bearing materials in the galvanizing industries. The tribaloy alloys are strengthened by laves phases formed while the stellite alloys are strengthened by the carbide dispersion. As in any material, the chemical composition influences the mechanical properties, so the chemical composition of T-401, Stellite 6B and Stellite 21 are given in Table 4-4.

Table 4-4: Chemical Compositions (Wt %) of the alloys considered for Scraper Tip

%	Stellite 21	Stellite 6B	T-401
Cobalt	59.25	53.90	60.50
Nickel	2.50 max	3.00 max	1.50
Iron	3.00 max	3.00 max	1.50
Carbon	0.25	1.10	0.3
Chromium	27.00	30.00	16.00
Manganese	1.00	1.00	
Molybdenum	5.50	1.50	16.00
Silicon	1.50	2.00	1.20
Tungsten		4.5	

Yao et.al. [54], after conducting immersion test in Zn-0.22Al bath and other mechanical tests on T-400, T-800, T-401 and Stellite 6 alloys, reported that the Tribaloy alloys outperform the Stellite alloys in the immersion test.

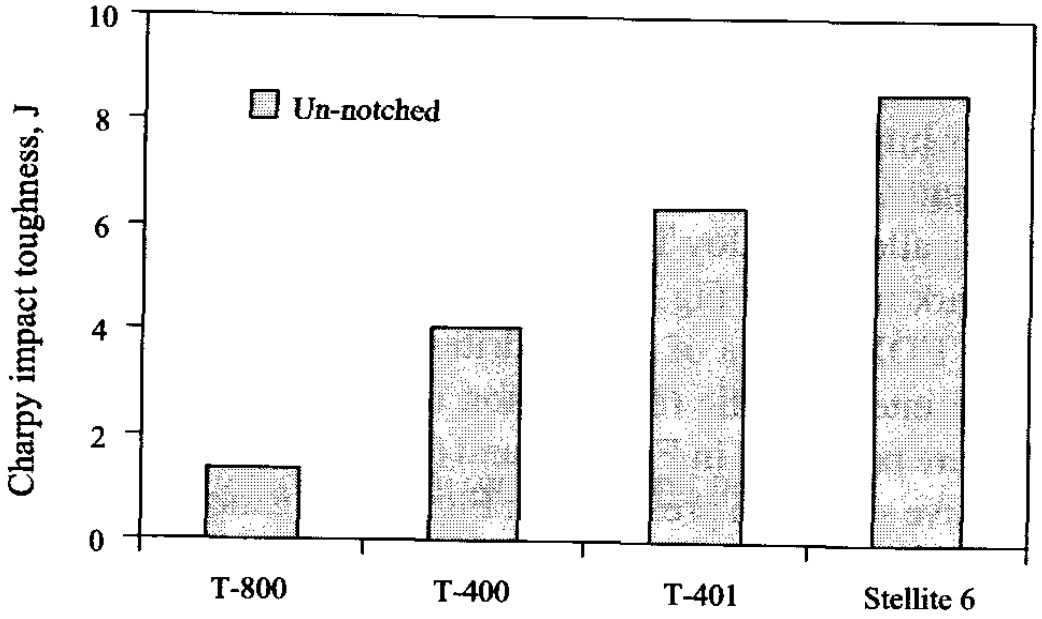

Figure 4-17: Bulk Ductility measured from Charpy test on Un-notched Samples

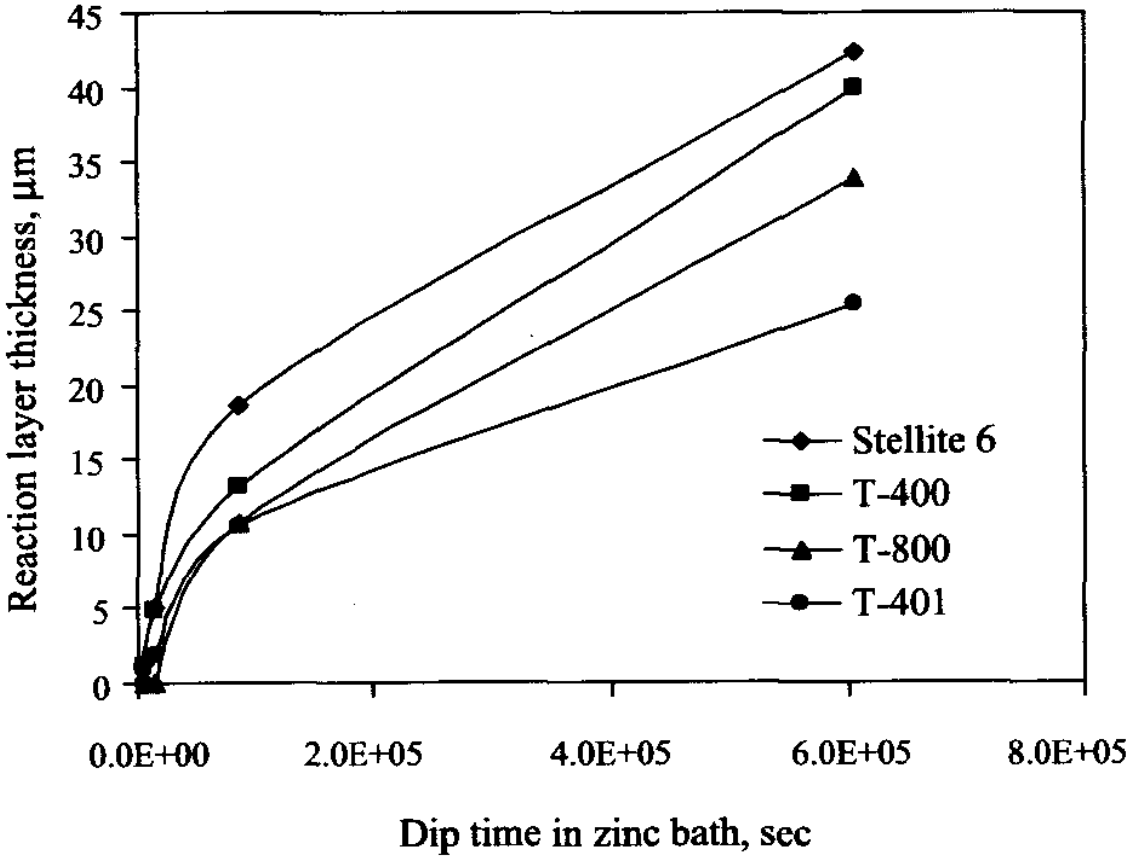

Figure 4-18: Reaction Layers Thickness as a Function of Dipping Time

Based on these results and the technical insights from the Industrial participants, the alloys Tribaloy T-401 and Stellite 6B were selected for the scraper overlay tip, as they exhibit better ductility as shown in Figure 4-17 and higher hardness value for Stellite 6B and the resistance of T-401 to the reaction layer formation in the Zn-Al bath prompted to test them as scraper overlay material. The wear results were compared with the wear rate of Stellite 21 scraper, which is currently used as the scraper tip in one of the Industrial participants 55Al-Zn coating line.

Test Procedure

Once the test rig was completed, the crucible was baked to get rid of any moisture present in the crucible. 55%Al- Zn ingots received from Wheeling Nisshin Inc., were added to the crucible and maintained at 600^{o}C. Since the ingots were obtained from the actual coating lines, the melt was saturated with Fe. The entire scraper assembly was coated with boron nitride to avoid wetting and corrosion of the scraper arms, so that the removal of scraper blade from the assembly was east after the tests.

The sink roll was rotated using the drive motor and the required line speed was set. After the RPM was set, the roll and the scraper assembly were preheated to 535^{o}C using a flexible heating element covered with insulation (Figure 4-19), to avoid thermal shock on the roll and scraper material during the immersion time in to the bath. Also, the preheating avoids any temperature fluctuations in the bath which would have caused an increase in the dross formation on the roll surface and the scraper blade.

After preheating, once the melt reaches the steady set temperature (600^{o}C) (Figure 4-20), the furnace was moved under the roll and scraper assembly, which were later immersed (Figure 4-21, 4-22) into the melt. After an hour of immersion, the roll was rotated at the rated speed. (Figure 4-23). For each test, the scraper and the roll were aligned in such a way that they make a line contact. An offset of the roll and the scraper was maintained, so that the scraping action over the roll does not cover the entire surface, which acts as a reference point for measuring the wear rate of the scraper and the dross formation over the roll surface during the test period.

Figure 4-19: Preheating of the Roll and the Scraper Assembly.

At the end of the first hour of rotation of the sink roll, the load was applied on the scraper arm, which in turn applied a compressive force over the sink roll surface through the scraper. The scraping action was continued for 2 minutes similar to the actual industrial line and then the load acting over the scrapper was removed.

The scraping of the sink roll surface was carried out for 2 minutes with a 30 minute time interval. Figures 4-24 shows the entire test rig during the Stellite 21 10 hour test campaign. The test duration was 18 hours in total with 3 hours of idle immersion of the sink roll at the beginning and 15 hours of rotation with scraping process for 2 minute time periods. The test conditions are given in Table 4-5

Figure 4-20: Preheating and Premelt Stage.

Figure 4-21: Immersion of the Roll and the Scraper Assembly (Start)

Figure 4-22: Immersion of the Roll and Scraper Assembly (End)

Figure 4-23: Checking the Sink Roll Speed.

Figure 4-24: Test Rig during 10 hour Stellite 21 Test

Table 4-5: Test Conditions for the Scraper Wear Rate Evaluation

(A) Test 1.

Bath Chemistry	55% Al, 1.5% Si, 43.5%Zn
Bath Temperature	600^{o}C
Roll RPM	108
Time for Initial Dross Build-up	1 hour
Scraping Duration	2 minutes every 30 minutes
Testing period	10 hours
Roll Material	309 Stainless steel
Scraper	Stellite 21 Overlay tip on 309 SS

(B) Test 2.

Bath Chemistry	55% Al, 1.5% Si, 43.5%Zn
Bath Temperature	600^{o}C
Roll RPM	108
Time for Initial Dross Build-up	1 hour
Scraping Duration	2 minutes every 30 minutes
Testing period	24 hours
Roll Material	309 Stainless steel
Scraper	Tribaloy T-401 Overlay on 309 SS

After the completion of the first test, the scraper was removed from the assembly and cleaned for measuring the wear rate. Before the start of the second test with T-401 scraper, loss of power due to severe weather conditions resulted in bath solidification. When power was restored, the sudden expansion of the solidified bath cracked the crucible and damaged the inductors (Figure 4-25). This led to change in the design of the furnace with a smaller crucible (200 lbs capacity) housed in a stainless steel shell, to prevent any future leakages from reaching the heating panels. The modified furnace setup is shown in Figure 4-26.

Figure 4-25: Damaged Inductors and Broken Crucible

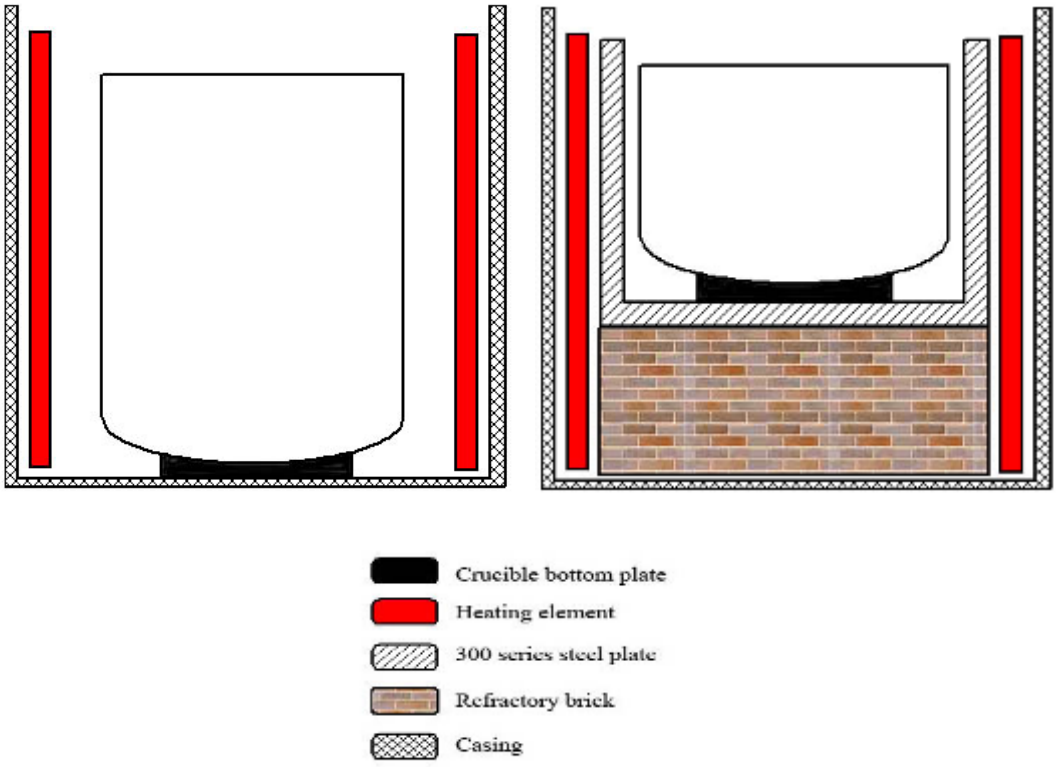

Figure 4-26: Modified Furnace Set-up.

With the newly designed furnace, the second test was conducted with Tribaloy T-401 as the scraper blade overlay. Based on the conclusions made by Yao et.al, "Tribaloy alloys outperform the Stellite alloys in the immersion tests", the test duration was increased to 24 hours instead of 10 hours (Test 1) as the scraper may not have any significant wearing in the 10 hour test period.

After the completion of both tests, the scraper blades were removed from the scraper assembly and they were cleaned to remove any residual bath on the surface using Muriatic acid. After cleaning, the thickness of the scrapers was measured using a dial gauge and the results are reported in Table 4-6.

Table 4-6: Measurement of Wearing Rate of the Scrapers.

Material	Initial Length (Lo) (Inches)	Wearing (ΔL) (Inches)	% Wearing (ΔL/ Lo)*100	100% Wearing (ΔL= Lo) (Days)
Stellite 21 (*After 10 hr test*)	1.635	0.087	5.324	~7
Tribaloy T-401 (*After 24 hr test*)	1.696	0.069	4.127	~24

The wearing rate of scraper with Stellite 21 overlay was found to be 5.324% for 10 hours of testing and extrapolating linearly to 100% wear (Figure 4-27) at which the scraper loses its efficiency, assuming the wearing rate is linear in the actual lines, the life of the scraper blade was calculated as ~7 days. Comparing the test result for the Stellite 21 overlay to the actual scraper blades used in the coating lines, the life time of the blades calculated matches well with that of the existing coating lines. Hence the results obtained

from these tests conducted in the lab scale correlates directly to the actual industrial coating lines.

In case of the Tribaloy T-401 overlay scraper, the wearing rate observed was 4.127% for 24 hours of testing and the 100% wear of the scraper requires ~24 days of production. Hence comparing the wearing rate of Stellite 21 and Tribaloy T-401, the T-401 scraper overlay performs 3.5 X better and can reduce the line stoppages by 75%.

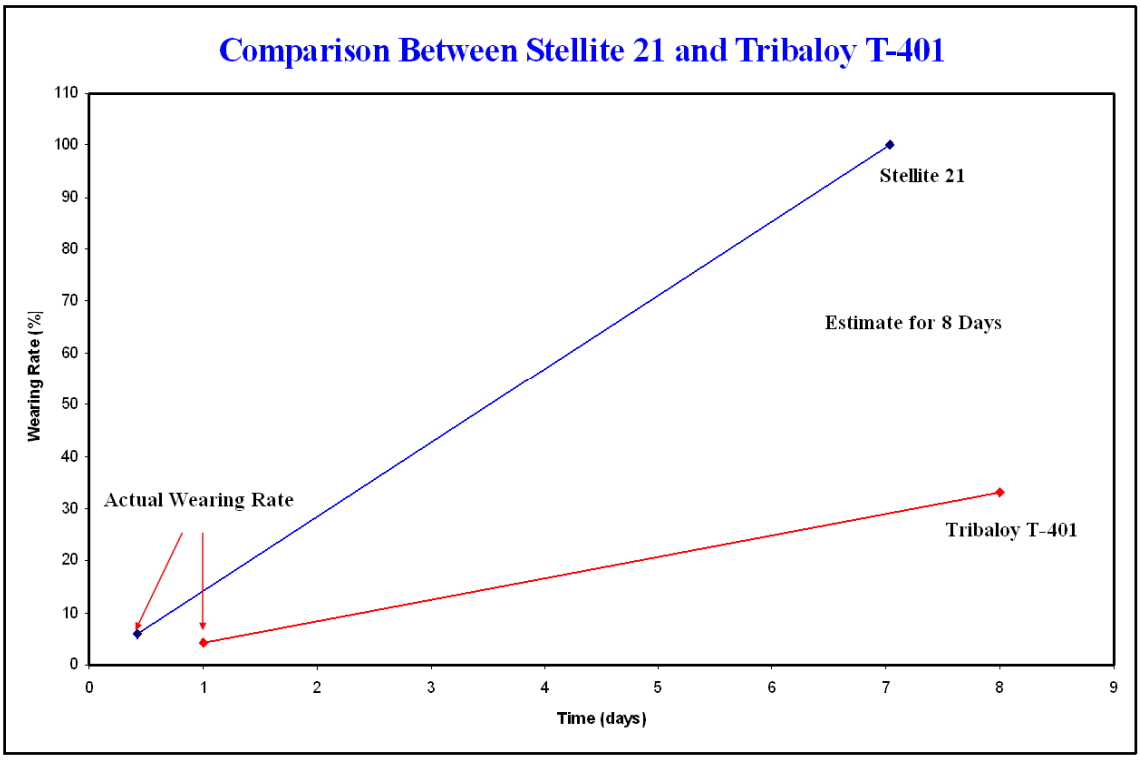

Figure 4-27: Comparison of Wearing Rate For 8 Days.

Modification of the Scraping Process

The first phase of the test as reported in the previous section was to select a new material for the overlay coating of the scraper blades by which the line stoppages can be reduced

due to the accumulation of the dross over the sink roll. The second phase of the tests was to develop a new scraping process to enhance the life of the scraper blades thus reducing the line stoppages.

Based on the dross formation mechanism over the sink roll as described in Chapter 3, the new method was based on the fact that the dross formation over the sink roll starts after 20 minutes and continues to grow by agglomeration of the dross particles over the course of time. Hence, instead of waiting for 30 minutes between each scraping process, the scraping process was changed to a continuous scraping mode with less force applied to the scraper. The load- time chart (Figure 4-28) indicates the existing and the proposed scraping process.

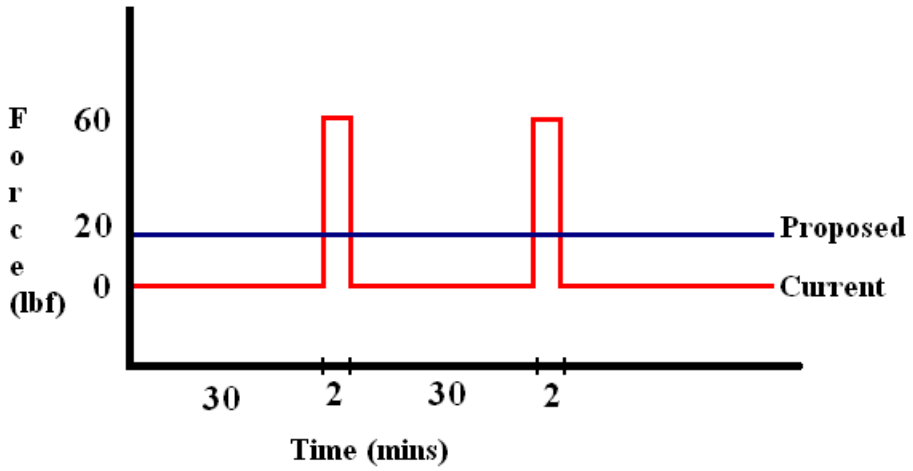

Figure 4-28: Load- Time Curve in Scraping Process

In the second phase, two scraper overlay materials were tested with the proposed scraping process. Stellite 21 overlay scraper which was the baseline test in the first phase was

studied again to evaluate the efficiency of the new process. The second overlay was Stellite 6B as it has a good ductility compared to the Tribaloy T-401 as shown in Figure 4-17. The operational parameters used in these tests are given in Table 4-7.

Table 4-7: Test Conditions for the Scraper Wear Rate Evaluation

(A) Test 3.

Bath Chemistry	55% Al, 1.5% Si, 43.5%Zn
Bath Temperature	600^{o}C
Roll RPM	108
Time for Initial Dross Build-up	3 hours
Scraping Duration	Continuous mode
Testing period	12 hours
Roll Material	309 Stainless steel
Scraper	Stellite 21 Overlay tip on 309 SS

(B) Test 4.

Bath Chemistry	55% Al, 1.5% Si, 43.5%Zn
Bath Temperature	600^{o}C
Roll RPM	108
Time for Initial Dross Build-up	3 hours
Scraping Duration	Continuous mode
Testing period	12 hours
Roll Material	309 Stainless steel
Scraper	Stellite 6B

After the completion of both tests, the scraper blades were removed from the scraper assembly and they were cleaned to remove any residual bath on the surface using Muriatic acid. After cleaning, the thickness of the scrapers was measured using a dial gauge and the results are reported in Table 4-8.

Table 4-8: Measurement of Wearing Rate of the Scrapers.

Material	Initial Length (Lo) (Inches)	Wearing (ΔL) (Inches)	% Wearing (ΔL/ Lo)*100	% Wearing (ΔL= Lo) (Days)
Stellite 21 (*After 12 hr test*)	1.635	0.074	4.525	~11
Stellite 6B (*After 12 hr test*)	1.635	0.017	1.039	~48

After the proposed method of scraping tests, the wearing rate of scraper with Stellite 21 overlay was found to be 4.544% for 12 hours of testing and linear extrapolation for 100% wear (Figure 4-29), the life of the scraper blade was calculated as ~11 days. Using the new scraping mode, the same overlay material (Stellite 21) was found to have an extended life time of 11 days when compared to 7 days from the previous test.

In the other test with Stellite 6B as the scraper blade, the wearing rate was calculated as 1.034% for 12 hours of test period. Based on this value, the 100% wear of scraper accounts for ~48 days. Thus using the new continuous scraping mode reduces the line stoppages. The life time of the entire process without any sink roll dross accumulation can be ~48 days with Stellite 6B as the scraper overlay material.

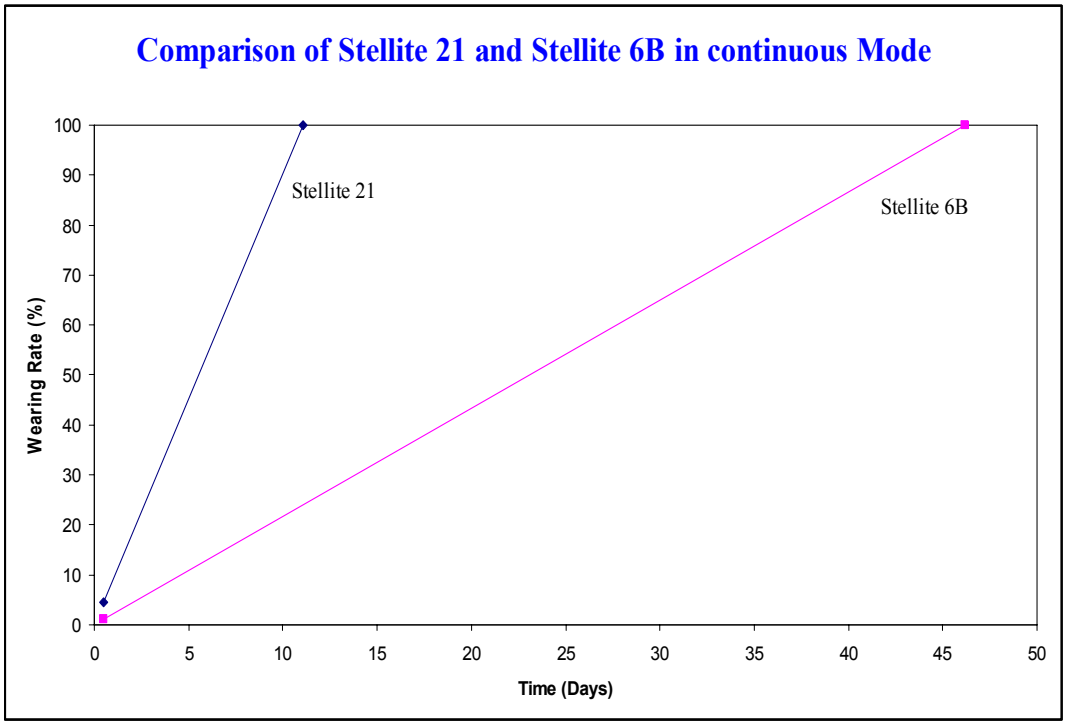

Figure 4-29: Comparison of Wearing Rate.

Comparison of the two scraping process with Stellite 21 overlay scraper is shown Figure 4-30.

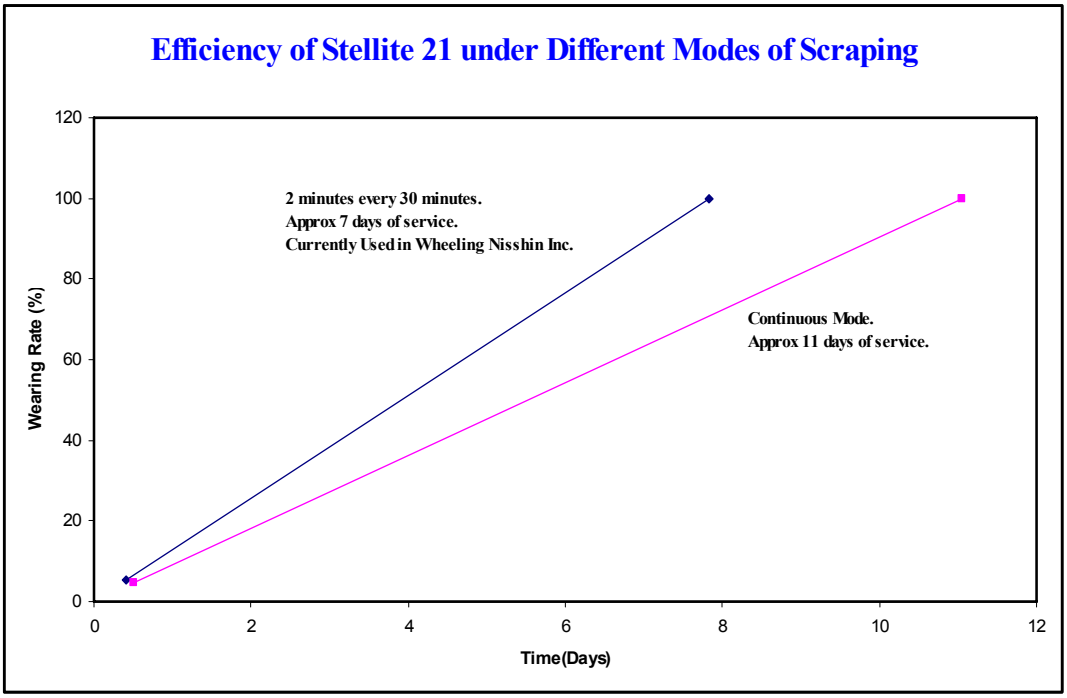

Figure 4-30: Comparison of Different Modes of Scraping

Summary

The first phase procedure (Test 1 & Test 2) of scraping action starts around 60 minutes from the time the roll enters the bath with 30 minutes interval between scrapping action. Based on this procedure, Stellite 21 overlay scraper can be effective for 7 days on the basis of linear projection and approximately 24 days for Tribaloy T-401.

The second phase procedure (Test 3 & Test 4) formulated with the understanding of the dross formation mechanism, shows that Stellite 21 overlay scraper can be effective for approximately 11 days and for Stellite 6B it showed a life of 48 days with the same linear projection.

Stellite 6B and Tribaloy T-401 can be used effectively to maintain the roll surface smooth, thus increasing the interval of down time and minimizing the energy losses. Avoiding the formation of hard dross layer by eliminating the smaller and discontinuous dross particles at the initial stages using the continuous mode proves more effective.

The optimized process should be able to reduce the scraper wearing rate significantly due to the following reasons

- Lower contact pressure for scraping action to reduce wearing rate.
- Scraper blade contact with smoother hard dross layer.

According to the empirical wear model **WR = C*P*V**, where WR is the wearing rate, C is the coefficient of wear, P is the Contact pressure and V is the velocity.

5. CONCLUSIONS AND CONTRIBUTIONS

A series of tests were conducted to establish the actual dross formation mechanism over the submerged pot hardware by immersing and rotating 316L stainless steel samples in 55%Al-Zn bath. From the SEM/EDAX analysis on the cross section of the immersed samples, the dross formation mechanism was developed. As numerous researchers have accepted that the fundamental principle of adding silicon to the 55%Al-Zn bath was to control the sudden exothermic reaction between the aluminum in the bath and the iron.

The dross formation mechanism study revealed the effect of the Si presence in inhibiting the attack of Al over the steel substrate by forming a Si rich inhibition layer. Due to hard nature of the dross particles formed, the breakdown of the inhibition layer occurs. Upon which these locations act as entry points for the Al to diffuse onto the surface and nucleation of dross particles takes place. Over the period of time, the dross particles agglomerate and grow in size and eventually cover the entire surface of the roll. The Fe_2Al_5 layer formed stops the further diffusion of the bath into the substrate, whereas the dross particles formed by the reaction between the bath and the steel strip travels towards the rotating sink roll due to the hydrodynamic motion in the bath. The presence of Si leads to the formation of ternary Fe-Si-Al intermetallic compounds. It was evident that the dross formation mechanism involves a dynamic condition. Comparing to static corrosion, hydrodynamic conditions play an important role on dross build-up layer uniformity and thickness (higher rpm, higher dross layer thickness).

From the scraper wear rate evaluation test, a better scraper overlay material was identified for the removal of dross build-up over the sink roll surface. A new scraping procedure was developed based on the dross formation mechanism, which enhanced the life of the scrapers and can considerably reduce the frequency of the line stoppages and thus increasing the productivity with better quality of coatings with more energy savings and reduced repair and replacement costs.

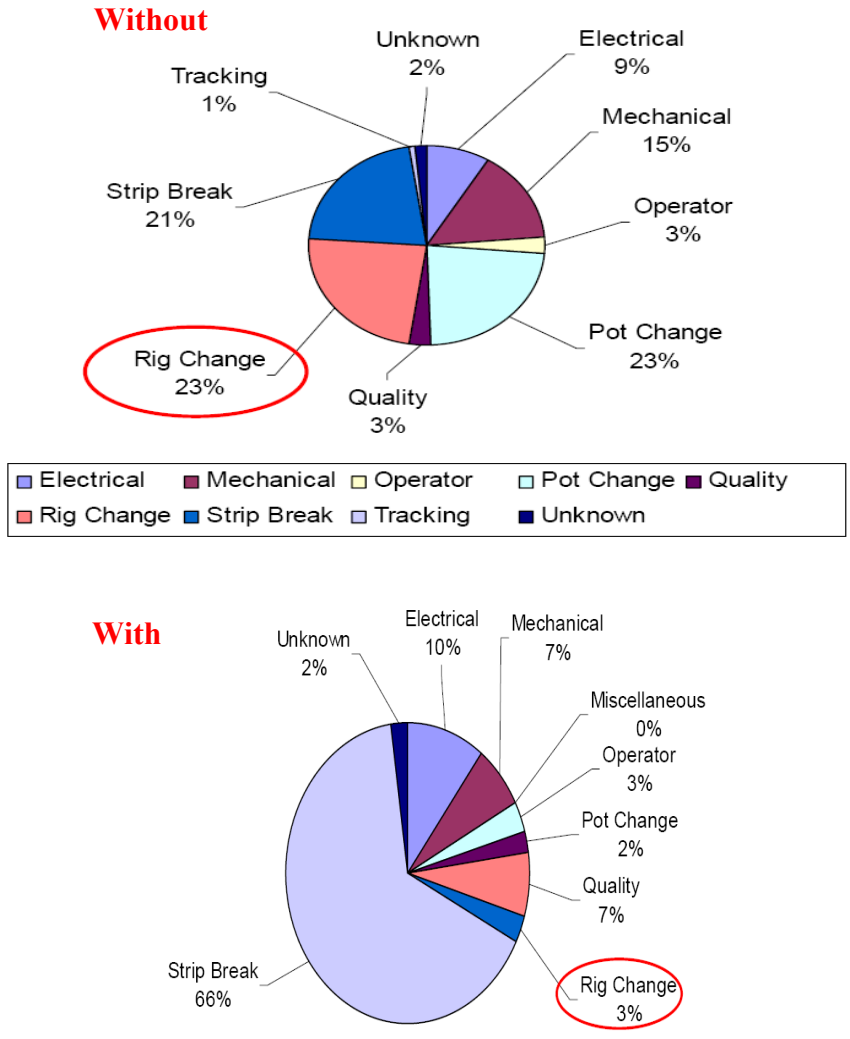

Figure 5-1: Production Performance – Without and With Scraper Process

Estimated Cost Savings

Rough Estimate of Annual Savings using Better scraper material with efficient scraping process is as follows:

The estimated overall cost for a sink roll change	~$15000
The average downtime for sink roll change	~3 hours
Overall cost to run the GL line for 1 hour	~$1000

Calculation of total cost involved for **28 days** in the industrial coating lines, considering one in line setup of 3 scrapers

Stellite 21 as the scraper material,

Campaign life	7 days
Cost of the scraper assembly [4 changes X ($700 X3pcs.)]	$8,400
Cost for sink roll changes (4 times) (4 X 15000)	$60,000
Loss incurred due to line stoppage (4 X 3hours) (12 X1000)	$12,000
Production loss (assuming $1500/hour) (12 x 1500)	$18,000
Total $$$$$	$98,400

Tribaloy T-401 as the scraper material,

Campaign life	24 days
Cost of the scraper assembly [1 change X ($3000 X3pcs.)]	$9,000
Cost for sink roll changes (Once) (1 X 15000)	$15,000
Loss incurred due to line stoppage (1 X 3hours) (3 X1000)	$3,000
Production loss (assuming $1500/hour) (3 x 1500)	$4,500
Total $$$$$	$31,500
Net savings using Tribaloy T-401 as scraper	**$66,900**

Adopting the newly proposed scraping process (**continuous mode**), the annual cost savings corresponds to ~***$40,700*** for the **Stellite 21** scraper blade assembly which has a campaign life of 11 days. Similarly with the **Stellite 6B** scraper blade assembly, (48 days campaign life) the cost savings per year estimates to ~***$90,950.***

Based on the results from this research, it can be concluded that more in-depth understanding about the dross formation in Zn-55Al bath and the effect of silicon in inhibiting the attack of Al over the steel substrate was established. Formation of Fe_2Al_5 hard layer over the substrate prevents the further inward diffusion of Al towards the roll surface. Finally, from the dynamic dross formation study, it was understood that the increase in the dross layer thickness was due to agglomeration of dross particles over the surface and not due to dissolution of the substrate. This mechanism can be further extended to understand the dross formation over other alloys utilized in the pot hardware. A new scraping process was developed considering the dross formation mechanism which proved to be more effective in maintaining the roll surface for a longer time period. New alloys with good ductility, wear and corrosion resistance can be used effectively as the scraper overlay to enhance the life of the sink roll without impacting the bottom line.

REFERENCES

1. GalvInfo Notes, “http://www.galvinfo.com/ginotes/GalvInfoNote_1_4.pdf”
2. S. Shawki and Z. Abdel Hamid. Surface and Interface Analysis, 35(2003).
3. A.R.P Ghuman and J.I. Goldstein. Metallurgical Transactions, 2(1971), 2903.
4. K. Chang, G. Psaros, J.J. Brinsky, R.L. Nester, R. Carter, V. Sikka, "New material research and life improvement for pot hardware in continuous hot-dipping processes," Steel Industry of the Future, Project Proposal to U.S. Department of Energy.
5. Jerc H, Brohply R, Rose M, Jhone W. “The Structure and properties of Materials”, vol. II. Willey Eastern Private Lime: Leone;(1964)
6. Massalski T.B; Ed: “Binary alloy phase diagram”; Vol.2, 1987, p.112-1128
7. Marder A.R, “The metallurgy of zinc-coated steel”, Progress in Materials Science, 45,2000, p.191-271
8. Jordan C.E, Marder A.R, “Fe-Zn phase formation in interstitial-free steels hot-dip galvanized at 450oC, Part 1 0.00 wt % Al-Zn baths”, J Materials Science, Vol.32,1997, p.5593
9. Villars P, Prince A, and Okamoto H: “Handbook of ternary alloy phase diagram”,ASM International, 1997, vol.3, p.3664
10. Tang N.Y, “450oC isotherm of Zn-Fe-Al phase diagram update”, Journal of phase equilibria, Vol.17, No.5, 1996, p.396-398
11. Horstmann D, “The course of reactions between iron and molten zinc containing aluminum”, Zinc Development Association, London, 1976, p.20-32

12. “The Role of Aliminum In Continuous Hot-Dip Galvanizing”. GalvInfoNote 10. “http://www.galvinfo.com/ginotes/G_Note10.pdf”
13. J.R.McBermid, E.Baril, W.T.Thompson, “Fe Solubility in the Zn-Al-Fe System for Use in Continuous Galvanizing and Galvannealing”, In Conference Proceedings Galvtech’ 04.
14. Selverian J.H, Marder A.R, Notis M.R, “The microstructure of 55 w/o Al-Zn-Si (galvalume) hot dip coatings”, J Materials Engineering. Vol.9, No.2, 1987, p.133-140
15. Raynor G.V, Rivlin V.G, “Phase equilibria in iron ternary alloys”, The Institute of Metals, 1998, p.122
16. Takeda S, Mutuzaki K, Tetsu-to-Hagane, 1940, 26, p.335-361
17. J.H. Selverian, A.R. Marder and M.R. Motis, Metallurgical Transactions, 20A (1989), 543.
18. K. Tani, T. Tomita, Y. Kobayashi, Y. Takatani, Y. Harada, ISIJ International, 34(1994) 822.
19. M.S. Brunnock, R.D. Jones, G.A. Jenkins, D.T. Llewellyn, Ironmaking and Steelmaking, 23(1996) 171.
20. F.E. Goodwin, K.-M. Chang, V. Sikka, “Galvanizer’s Association Proceedings”, Dearborn, MI (2002).
21. K. Zhang, N.-Y. Tang, M. X. Yao, Galvatech Conference Proceedings, Chicago, IL (2004) 617.
22. X. Liu, E. Barbero, V. Sikka, Galvatech Conference Proceedings, Chicago, IL (2004) 629.

23. X. Liu, E. Barbero, J. Xu, M. Burris, K.-M. Chang, V. Sikka, Metallurgical Transactions A, 36A(2005) 2050.
24. M.X. Yao, J.B.C. Wu, R. Liu, Materials Science and Engineering, 47(2005) 299.
25. K. Zhang, N.-Y. Tang, F. Goodwin, S. Sexton, Galvanizer's Association Proceedings, Columbus, Ohio (2006).
26. M. Bright, Doctoral Dissertation, West Virginia University, Morgantown (2007).
27. R.Y. Chen and D.J.Willis. Metallurgical and Materials Transactions A, 36A(2005),
28. N.-Y. Tang, Galvatech Conference Proceedings, Chicago, IL (2004) 683.
29. Edward J.Dean, Jr and Michael S. Brennan, "Reduced Downtime and Improved Strip Quality through the Use of ACD Wearguard Bearings & Praxair Laser Weld Overlaid End Caps/Sleeves", 2002 Galvanizers Association, Annual Meeting, Dearborn, MI.
30. Personal communication with Mr. Frank Mollica, Line Manager, Wheeling Nisshing Inc.
31. Chang, K.-M., "Project Overview", DOE-OIT Project: Development of Improved Materials for Pot Hardware, Kickoff Meeting, Pittsburgh, PA, May, 2001
32. Long, H., "Industry View", DOE-OIT Project: Development of Improved Materials for Pot Hardware, Kickoff Meeting, Pittsburgh, PA, May, 2001
33. Gast-Bray, A., "Materials in hot dip zinc pots", DOE-OIT Project: Development of Improved Materials for Pot Hardware, Kickoff Meeting, Pittsburgh, PA, May, 2001

34. Chang, K.-M., “Dross in hot-dipping bath”, DOE-OIT Project: Development of Improved Materials for Pot Hardware, Progress Meeting, Mississauga, Ont., August, 2001
35. Liu, X., “Corrosion testing overview”, DOE-OIT Project: Development of Improved Materials for Pot Hardware, Progress Meeting, Mississauga, Ont., August, 2001
36. Sikka, V., “ORNL Progress report”, DOE-OIT Project: Development of Improved Materials for Pot Hardware, Progress Meeting, Mississauga, Ont., August, 2001
37. Chang, K.-M., “Dross in hot-dipping bath”, DOE-OIT Project: Development of Improved Materials for Pot Hardware, Progress Meeting, Charleston, WV, December, 2001 174
38. Sikka, V., McElroy, S., Santella, M., Babu, S., Howell, R., “Material selection”, DOE-OIT Project: Development of Improved Materials for Pot Hardware, Progress Meeting, Charleston, WV, December, 2001
39. Chang, K.-M., “WVU Progress report on liquid metal corrosion testing”, DOEOIT Project: Development of Improved Materials for Pot Hardware, Progress Meeting, Oak Ridge, TN, June, 2002
40. Liu, X., “WVU Progress report on liquid metal corrosion testing”, DOE-OIT Project: Development of Improved Materials for Pot Hardware, Progress Meeting, Charleston, WV, December, 2002
41. Sikka, V., McElroy, S., Ott, R., “Long-term corrosion tests and second generation of materials for corrosion and wear testing”, DOE-OIT Project: Development of Improved Materials for Pot Hardware, Progress Meeting, Charleston, WV,

December, 2002

42. Liu, X., “WVU Progress report on liquid metal corrosion testing”, DOE-OIT Project: Development of Improved Materials for Pot Hardware, Progress Meeting, Morgantown, WV, May, 2003
43. Sikka, V., McElroy, S., Ott, R., “ORNL Progress report on development of materials for pot hardware”, DOE-OIT Project: Development of Improved Materials for Pot Hardware, Progress Meeting, Morgantown, WV, May, 2003
44. Liu, X., “WVU Progress report on liquid metal corrosion testing”, DOE-OIT Project: Development of Improved Materials for Pot Hardware, Progress Meeting, Roanoke, WV, October, 2003 175
45. Sikka, V., McElroy, S., “ORNL Progress report on development of materials for pot hardware”, DOE-OIT Project: Development of Improved Materials for Pot Hardware, Progress Meeting, Roanoke, WV, October, 2003
46. Sikka, V., McElroy, S., “Microstructural analysis of wear tested specimens”, DOE-OIT Project: Development of Improved Materials for Pot Hardware, Progress Meeting, Roanoke, WV, October, 2003
47. Liu, X., Barbero, E., Loth, J., Kang, B., Damiani, T., Gopalakrishnan, B., Irwin, C., Sikka, V., Goodwin, F. E., “WVU Progress Report”, DOE-OIT Project: Development of Improved Materials for Pot Hardware, Progress Meeting, Morgantown, WV, October, 2004
48. Irwin, C., Barbero, E., Sikka, V., Goodwin, F. E., Final Project Report, DOE-OIT Project: Development of Improved Materials for Pot Hardware, June, 2005
49. Barbero, E., Liu, X., Kang, B., Loth, J., Snider, J., Sikka, V., Goodwin, F. E.,

"Performance Evaluation of Current Hot-Dip Pot Hardware Materials", 2003 Galvanizer's Association Proceedings, Monterrey, Mexico

50. Snider, J., Loth, J., "Empirical Wear Rate Modeling of Zinc Pot Bearing Materials Using the WVU Small Scale Tester", Galvatech 2004 Conference Proceedings, Chicago, IL, pp. 595-604 176
51. Liu, X., Barbero, E., Sikka, V., "Corrosion of Several Alloys in Industrial Hot Dipping Baths", Galvatech 2004 Conference Proceedings, Chicago, IL, pp. 629-636
52. Parthasarathy, V., Kang, B., Krishnaswamy, A., Barbero, E., Chang, K.-M., Irwin, C., Goodwin, F. E., "Long Time Performance of Pot hardware in Continuous Galvanizing Line", Galvatech 2004 Conference Proceedings, Chicago, IL, pp. 637-656
53. Loth, J., "Zinc Pot Bearing Design Modification for Increased Life", Galvatech 2004 Conference Proceedings, Chicago, IL, pp. 657-666
54. Yao M.X., Wu.J.B.C., Liu.R., "Microstructural characteristics and corrosion resistance in molten Zn-Al bath of Co-Mo-Cr-Si alloys", Materials Science and Engineering A 407 (2005) 299-305.